Porcine Neonatal Heart Extracellular Matrix as a Regeneration Platform

A Dissertation Submitted to the Graduate School of the University of Texas at Arlington in Partial Fulfillment of the Requirements for the Degree of Doctor of Philosophy

Arlington, Texas

August 2021

By Karla L. Perez

Porcine Neonatal Heart Extracellular Matrix as a Regeneration Platform

By

Karla L. Perez

Approved:

_____

Jun Liao (Primary Advisor)

_____

Yi Hong (Co-Advisor)

_____

Kytai Nguyen (Committee Member)

_____

Zui Pan (Committee Member)

_____

Matthias Peltz (Committee Member)

_____

Georgios Alexandrakis (Graduate Advisor)

DEDICATION

To my friends and family who have made it possible for me to complete this dissertation.

To my parents Lucia and Uriel, your support has always got me through.

ACKNOWLEDGEMENTS

I would like to express my gratitude to many people, for which without their support, this accomplishment would not have been possible. Dr. Jun Liao, my principal advisor, has been a source of guidance through my dissertation project. I am grateful to be part of his Tissue Biomechanics and Bioengineering Lab. I would also like to acknowledge Dr. Kytai Nguyen and Dr. Yi Hong, who have made it possible for me to complete my degree here at UTA. Dr. Kytai Nguyen selected me for the NIH Fellowship, which has fully funded my studies for the last two years. This fellowship has not only supported me financially, it also allowed me to grow and learn from varied workshops and trainings that have fully enriched my time in the program. As my Co-advisor, Dr. Yi Hong has also been a source of guidance in my research. He has provided resources and insights that have significantly aided my research, in particular with cardiac patches. I am grateful for his expertise and support with my dissertation research. I would also like to extend my thanks and appreciation to the other members of my committee – Dr. Zui Pan, and Dr. Matthias Peltz who have provided knowledge and resources that were all a vital part of in my dissertation completion.

Moreover, I want to express my deepest gratitude to Dr. Michael Cho, our department chair, for his support since I started the program. When I transitioned from my full-time job in the Aerospace industry to becoming a full-time student pursuing a PhD in Bioengineering, Dr. Cho provided me with funding my first two years through the STEM

fellowship and since has worked tirelessly to solve any issues that have risen while providing much support during my time in the program. I am truly grateful.

I would also like to acknowledge and express my deepest appreciation for all of my colleagues who have supported me along the way. I would like to thank Dr. Fatemeh Hassanipour and Diana Alatalo for allowing me to use their rheometer at UT Dallas. I also want to thank my collaborators here at UT Arlington because they have been a source of support, guidance, and knowledge, in particular to Sadia Naz, Alan Taylor, Sara McMahan, Uday Chintapula, Jiazhu Xu, Victoria Messerschmidt and Tam Nguyen. Thank you for all your help. I attribute much of my success in the program to your support.

Lastly but certainly not least, I want to thank my family for their support through my time back as a graduate student. As I embark on different journeys throughout my life, knowing I always have a place to land is invaluable. Thank you.

TABLE OF CONTENTS

LIST OF FIGURES

LIST OF TABLES

ABSTRACT

Each year, an estimated 620,000 Americans have new heart attack and suffer from myocardial infarction (MI) that results in massive heart cell death and decrease in heart function. Various therapeutic strategies, such as pharmacological treatments and reperfusion strategies, have greatly improved short-term MI survival. However, these strategies do not restore normal cardiac function due to the permanent loss of cardiomyocytes. As a promising strategy, cardiac cell therapy delivers repairing cells to damaged areas (scar tissues) to revitalize the infracted heart. However, a key challenge in cardiac cell therapy, i.e. the extremely low survival and engraftment rate of transplanted cells, must be overcome before the tremendous power of cell therapy can be successfully exploited.

Biomaterials, such as polymeric/tissue-derived cardiac patches and injectable hydrogels, have been investigated as a means to provide mechanical supporting for MI, as well as to serve as a platform that triggers favorable cellular behavior and cardiac regeneration. Adult porcine myocardial scaffold as patch material and adult porcine myocardial extracellular matrix hydrogel as an injectable vehicle all showed potential in MI treatment. Recently, our *in vivo* neonatal pig model research demonstrated that the piglets would lose the fully regenerative potential by 7 days after birth, but greatly preserve the regenerative potential within 1 day of birth, pointing out the importance of biomechanical and biological cues of neonatal heart ECM in guiding cardiac full regeneration. We hence hypothesized that the 0-day neonatal heart extracellular matrix (ECM) microenvironment has biomechanical and biological cues that promote heart muscle regeneration, and the porcine neonatal heart ECM (nhECM) can be used as a biomaterial platform for MI treatment. Three aims were thus pursued to better understand the essential

properties of nhECM and design two novel nhECM-based biomaterials. **Aim 1**: Structural and biomechanical characterizations of the acellular porcine neonatal heart ECM (nhECM). **Aim 2**: Porcine nhECM-based nanofibrous cardiac patch via electrospinning technique. **Aim 3**: Fabricating and characterizing porcine nhECM-based hydrogel as a cardiac injection material.

In Aim 1, we performed histological, compositional, and mechanical assessments to determine the structural-mechanical relationship of the nhECM. Histological observation and compositional quantification were carried out to understand ECM microstructure and composition. Biaxial mechanical testing, uniaxial mechanical testing, stress relaxation, and shear testing were performed to reveal a thorough biomechanical behavior of the porcine nhECM.

In Aim 2, we developed a novel nhECM-electrospinning protocol to engineer porcine nhECM-based nanofibrous cardiac patch. The concentration of nhECM, solvent, electrospinning parameters, and patch stabilizing crosslinking were investigated and optimized. The structure, mechanical properties, and biocompatibility of nhECM nanofibrous patch were assessed via SEM, biomechanical testing, and cell culture, respectively.

In Aim 3, we developed an effective protocol to reliably fabricate nhECM-based hydrogel. Structural and rheological tests were performed to determine the structure and porosity of nhECM hydrogel and its gelation kinetics. Additionally, cytotoxicity assessment and cell proliferation assay were carried out to assess the biocompatibility and cell growth potential of the nhECM hydrogel.

KEY WORDS: Cardiac biomechanics, cardiac regeneration, myocardial infarction, extracellular matrix, neonatal heart ECM, injectable hydrogel, cardiac patch.

CHAPTER I

I. Introduction

1.1 Myocardial Infarction

Heart disease is the leading cause of death in the United States.[1] Approximately 800,000 people suffer a heart attack each year, placing a heavy financial and personnel burden on the health care industry.[2] A heart attack occurs once the coronary artery is blocked or other oxygen restriction takes place, which lead to the death of downstream cardiomyocytes in the ventricular wall and hence myocardial infarction (MI).[3-7] The death of cardiomyocytes starts the inflammatory response that leads to scarring and eventually left ventricular remodeling. [8-11] Post-MI remodeling often involves an expanded infarcted region, scar tissue formation, left ventricular wall thinning and dilation, significant loss of pumping functionality, and eventually heart failure (HF). [12-19]

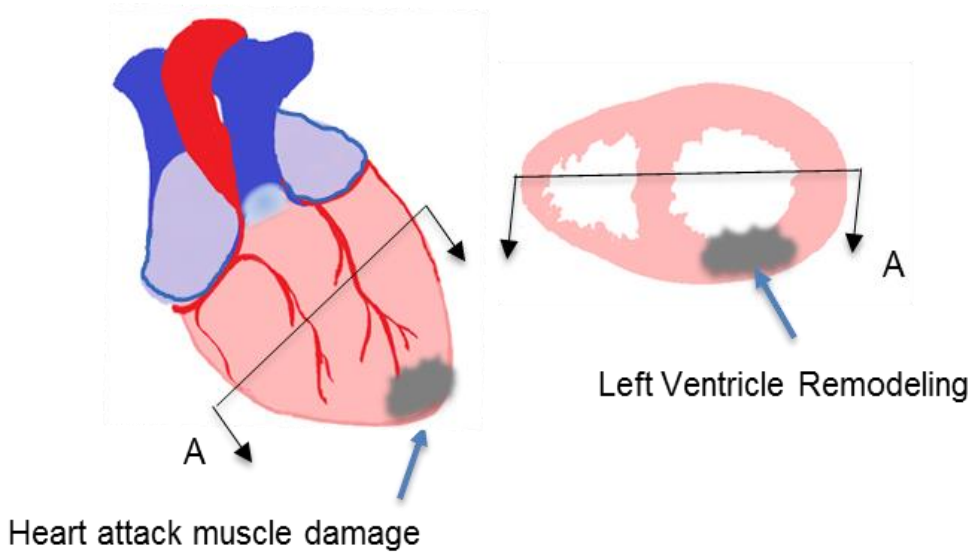

Figure 1: Schematic illustration of myocardium damage after a myocardial infarction (MI), which leads to post-MI left ventricle remodeling.

1.2 Current Treatments and New Therapeutic Efforts

Common treatment options for MI include reperfusion strategies and pharmacological therapies, as well as heart transplant for patients that develop heart failure (HF). Reperfusion strategies and pharmacological therapies have greatly improved short-term MI survival. However, those conventional strategies do not restore normal cardiac function due to permanent loss of cardiomyocytes and poor regenerative potential of heart muscles.[20] Heart transplants remain the gold standard for patients with HF. Unfortunately, they are not readily available to the majority of HF patients due to donor shortage and immune compatibility. In order to overcome the challenge of donor heart shortage, medical devices such as left ventricular assist device (LVAD) are used to help HF patients in heart failure while waiting for a donor match. However, these devices are associated with risky complications such as infection, bleeding, thrombosis, and even stroke. Other treatments currently being explored are stem cell therapies and direct injection of reprogramming factors to induce the production of cardiomyocytes.

Although advances have been made, clinical trials of stem cell injection show minimal effects on cardiac function.[21] The results could be attributed to low cell retention, poor cell engraftment, insufficient cell dosage, and ineffective delivery route. New methods and biomaterials are being explored to address these challenges. For example, Figure 2 depicts the types of ECM materials that are being explored for MI treatment. Cardiac patches have been developed to apply to the surface of the heart, where the fibrotic tissue has replaced the healthy myocardium. These patches can be made of different materials such as synthetic polymers and natural tissue-derived materials such as acellular collagen scaffolds. There have been studies [22-25] suggesting that cardiac patches prevent infarct wall thinning and improve heart function.

Hydrogels are another type of biomaterial that are being investigated as potential therapies for MI [26-28]. Hydrogels are delivered as injectable materials. The most common are, collagen, alginate, chitosan, and tissue ECM derived hydrogel. The study and development of these injectable biomaterials creates an opportunity to translate these therapies into lifesaving treatments for MI patients.

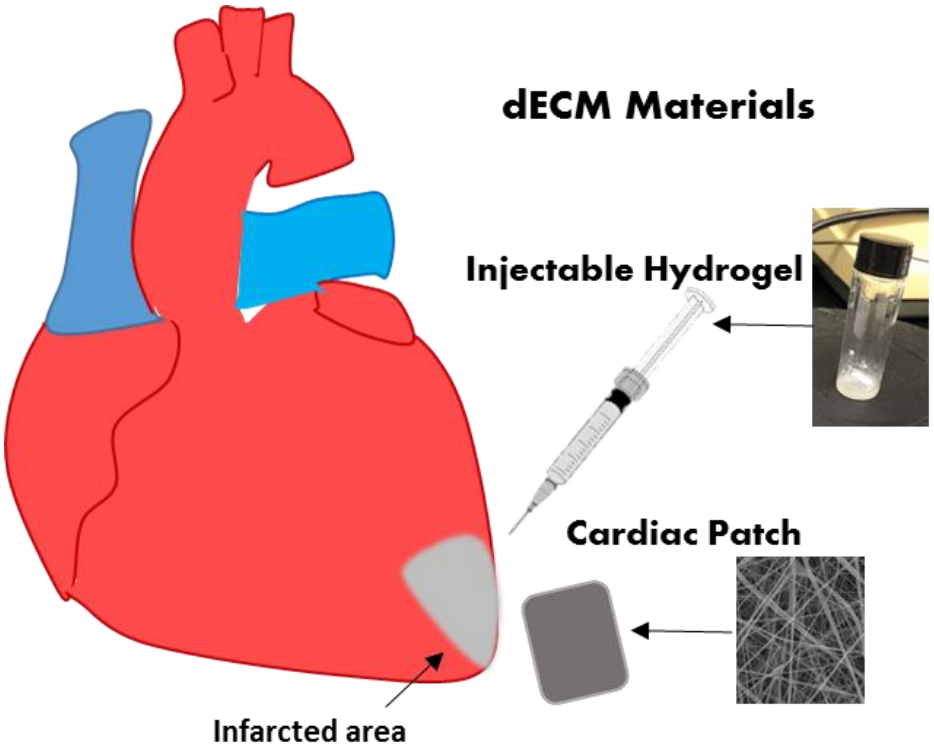

Figure 2: Main terminologies to differentiate applications of decellularized ECM (dECM).

1.3 Cardiac Regeneration and its Implication in Therapeutics

Patients who have suffered an MI event are unable to restore normal cardiac function due to the permanent loss of cardiomyocytes and fibrotic scarring. Thus, cardiac regeneration becomes an area of major interest when investigating potential treatments and therapies that aim to restore cardiac function. Several studies have shown that heart regeneration is possible on zebrafish and mice [8, 11, 21, 29-34]. Adult zebrafish are able to fully regenerate after ventricular apex resection. Using a ventricular apex resection model, Aurora et al demonstrated that the zebrafish heart is able to keep the regenerative potential even in adulthood because cardiomyocytes in this organism are mononucleated and remain proliferative into adulthood [8]. Neonatal mice are also able to regenerate resected apex, but only within their first seven days [8, 29, 35, 36]. The capacity to regenerate in the neonate mouse is likely in part due to the proliferative capacity of the cardiomyocytes at that stage. It was noted that mammals are born with proliferative, mononucleated cardiomyocytes but undergo a final round of replication without cell division which makes the cardiomyocyte population binucleated [8, 31].

Studies have been conducted to understand the underlying mechanisms, in which the cardiac ECM of neonatal rats and mice regulate cardiomyocyte proliferation and prevents ventricular remodeling [37-39]. The developmental stages examined by Williams et al [37]were fetal, neonatal, and adult, and cardiac ECM of sprague dawley rats was used as the substrate for cell study. They found that fetal cardiac ECM provided the highest cardiomyocyte proliferation after 5 days of culture. Fetal and neonatal cardiac ECM had significantly higher cardiomyocyte density when compared to adult cardiac ECM. Although cell attachment was lowest in fetal cardiac ECM, cell proliferation was highest in this group. What the he study suggests is that proliferation may

be the principal contributor of cardiomyocyte expansion in young ECM at fetal and neonatal stages. Using an *in-vivo* mouse MI model, Wang et al [38] demonstrated that neonatal mouse cardiac ECM prevents negative ventricular remodeling. The article reported less fibrosis and wall stiffening, as well as better ejection fraction after a single treatment with the neonatal mouse cardiac ECM.

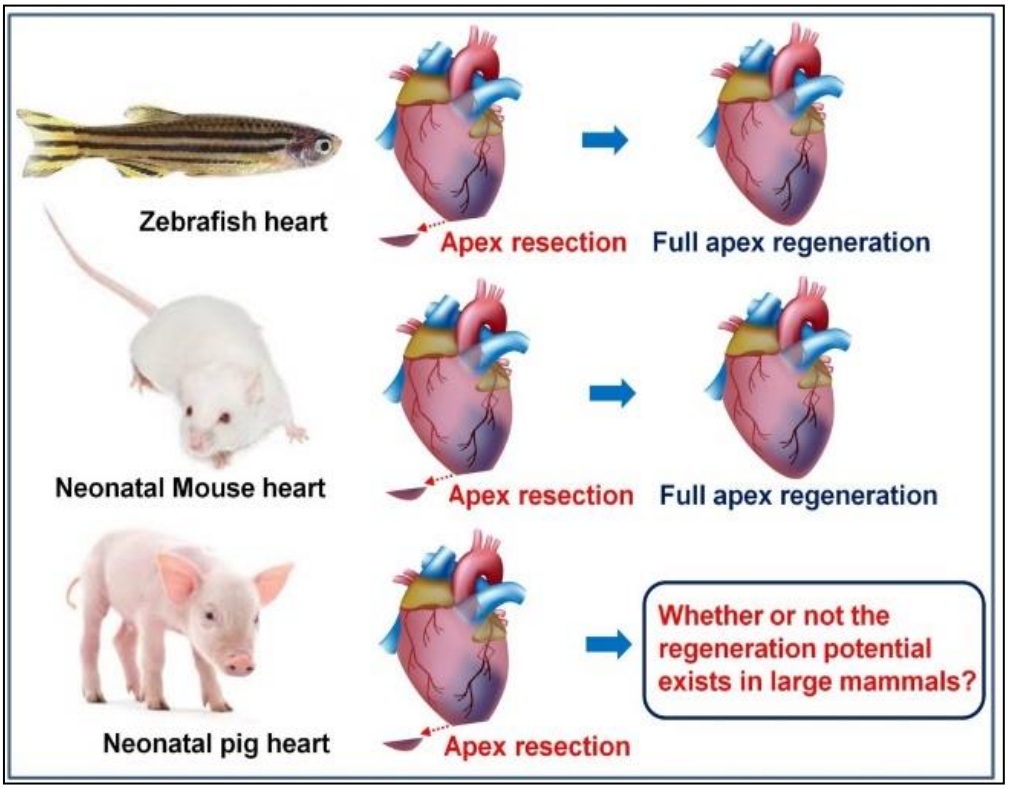

Figure 3: The reported full apex regeneration capability in zebrafish and mouse heart, and the research question about cardiac regenerative potential in large mammals.

Recently, we conducted a study using a neonatal pig model (Figure 3) to investigate if the full cardiac regenerative potential exists in large mammals. The study was performed on 0-day old and 7-day old neonatal pigs to investigate the regenerative potential after a partial apex resection. We found that the piglets would lose their full regenerative capacity 7 days after birth

but preserve regenerative potential within 1 day of birth. This finding aligns with previously reported timeframe of cardiac regenerative potential in mouse model. [8, 29]. At the apex resection injury site of the 0-day old piglet heart, we observed that cells were actively dividing and differentiating towards young cardiomyocytes, further suggesting the neonatal heart ECM microenvironment has factors that promote heart muscle regeneration. Our observations support the hypothesis that full cardiac regeneration is preserved in 0-day porcine neonatal hearts. It is this premise that led us to examine the bomechanical, structural, and compositional cues in the neonatal heart extracellular matrix (nhECM) and explore the feasiblity of nhECM as a biomaterial for MI treatment.

1.4 The Essential Role of the Heart Extracellular Matrix (ECM)

The extracellular matrix (ECM) is a complex structure that provides physical and biochemical cues to cells, and modulates signals and communication between cells and ECM to maintain a homeostatic environment. ECM is often comprised of collagen, glycosaminoglycans, elastin and other proteins, all directly affecting cell fate and tissue development. [26, 40]

Natural tissue-derived ECM materials have been investigated as potential scaffolds. The major advantage of using a decellularized ECM is its ability to simulate the environment of the native tissues. A study by Ott et al found that a decellularized intact rat heart was able to actively beat again by recellularizing with cardiac and endothelial cells and supporting the heart with a flow loop/electrical simulations. [41] Decellularized ECM materials present an opportunity to regenerate tissue and minimize negative remodeling due to scarring.

Biomechanical properties of ECM, often determined by the ECM composition and organization, play an important role in mediating cell fate. Engler et al [42] showed that varying the stiffness of the ECM substrate could cause human MSCs to differentiate into multiple independent lineages. Engler et al also demonstrated the stiffness of the ECM can have an effect on cardiomyocyte behavior. [42] Cardiomyocytes in a matrix with a stiffness mimicking scar tissue lacked striated myofibrils and stopped beating. However, matrices with a stiffness range of 11-17 kPa promoted striation and cardiomyocyte beating.[42] They thus conclude that the best scaffolds for cardiac tissue regeneration should have a modulus between tens of kPa and one MPa.[40, 42] These findings provide insight on how important it is to know the biomechanical properties of the nhECM when trying to develop it into MI therapeutic materials.

Faizan et al conducted a study that characterized the biomechanical properties of the neonatal porcine ventricle. The study reported the maximum stiffness of neonatal porcine left ventricle is in the range of 5 to 6 kPa, [43] different from the adult ventricle that had a stiffness ranging 10-20 kPa. To our knowledge, there is no detailed biomechanical, structural, and compositional characterizations for nhECM. Therefore, in order to bridge this knowledge gap, we set our Aim 1 to better quantify and understand the properties of porcine nhECM.

1.5 Cardiac Patches for MI Treatment

Poor retention and survivability of stem cell therapy limits its efficacy as a therapeutic treatment for MI.[24] Cardiac patches, without or with cells, have emerged as a potential therapeutic system to target cardiac repair after MI, and it is widely seen as a promising technology. In the last ten years, there has been exponential growth in the number of publications looking into

feasible materials to develop a cardiac patch. Cardiac patches have been developed and designed to be applied to the surface of the heart where the fibrotic tissue has replaced the healthy myocardium.

Studies suggest that cardiac patches prevent infarct wall thinning and improve heart function. Electrospinning is a popular fabrication technique to manufacture cardiac patches with flexibility that fits different applications. It is a fiber production method that uses electric force to draw charged threads of polymer solutions or polymer melts up to fiber diameters, in the order of some hundred nanometers. The nanoscale fibers are then deposited to a collector plate to form an electrospun mat.[44] One of the advantages of this technique is that the deposited fibers highly mimic the structure of fibrous ECM, which makes it an attractive technique for cardiac patch fabrication. As we know, a major challenge for cardiac patch construct is to fully simulate the complex anatomical structure of heart tissue. A fully integrated patch should be biocompatible, biodegradable, mimic the tissue microstructure, and provide conductivity while minimizing the immune response.[23, 25, 26, 45]

Common materials for cardiac patches include synthetic polymers like PCL, and recently there has been reported that PEO was utilized for electrospinning ECM fibers [46]. Synthetic polymers provide the ability to tune the mechanical properties of the electrospun mat and make a more stable and easy to working material. However, cardiac patches made of purely synthetic polymers tend to lack biocompatibility and bioactivity with the living system. Natural materials like chitosan and collagen have been widely used in electrospinning because of their biocompatibility. However, these materials lack mechanical strength. Thus, combinations of synthetic and natural polymers have been studied to overcome the limitations that one material

alone cannot provide. [24, 47, 48] For instance, a gelatin/PCL scaffold was developed and showed good biocompatibility and excellent tensile strength when compared to natural polymer alone. [49] Unfortunately, a dense layer of fibers on the scaffold prevented cell migration. [49]

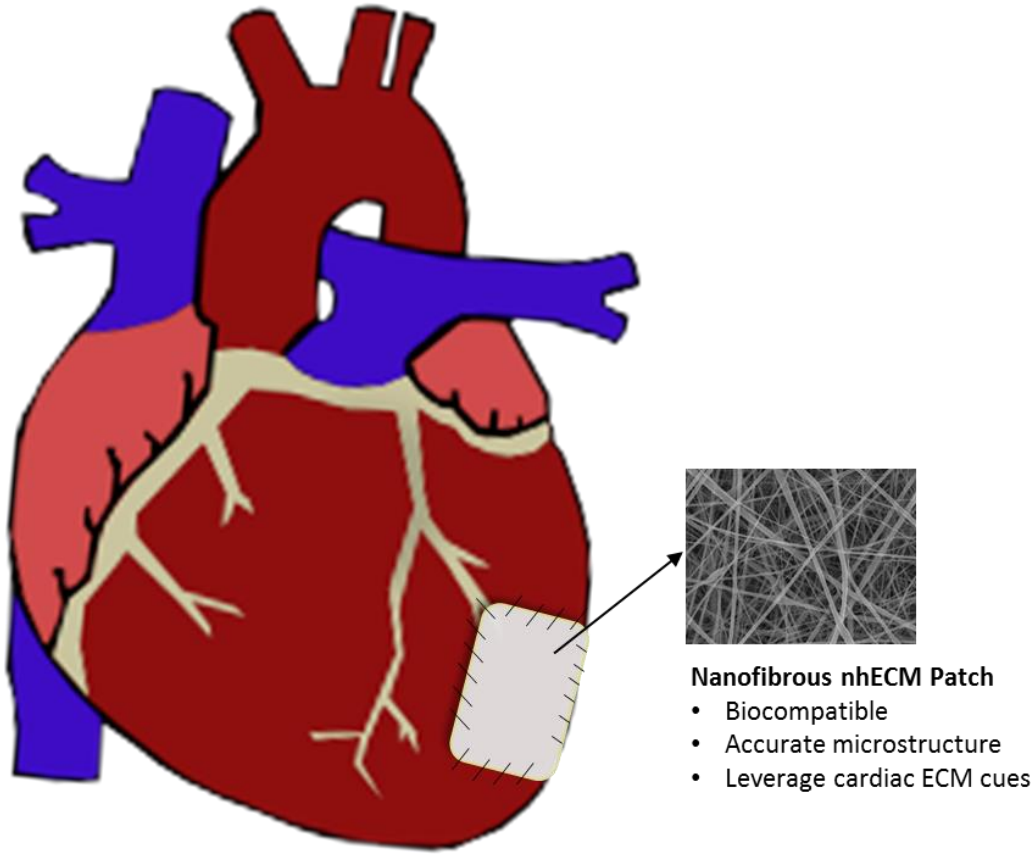

Figure 4: Working principle of cardiac patch and the requirements that need to be addressed.

The electrospinning of pure ECM presents has the benefit of incorporating natural biomechanical, structural, and compositional cues. However, a major challenge of this approach is being difficulty to handle, along with risk to rupture and the inability to maintain fibrous microstructure when coming in contact with water-based liquid. [23, 46] The limited studies on the ability to electrospin pure ECM [49] presents a great scientific challenge, i.e., whether it is

feasible to fabricate a cardiac patch out of pure nhECM. Our Aim 2 is thus to develop a stable and easy to handle patch that preserves the biocompatibility and bioactivity that are preserved in the nhECM, while provide structural integrity and mechanical strength.

1.6 Injectable Hydrogels for MI Treatment

Hydrogels have emerged as a promising option for cell culture and cell therapy because they mimic the microstructure of the ECM. For MI treatment, injectable hydrogels can be delivered to scar region with minimally invasive procedures, such us catheter delivery, which makes it particularly interesting in cardiac therapies. Different synthetic and natural materials are being explored as potential hydrogels for translational application. Synthetic polymers like polyethylene glycol (PEG) has been used in several applications because its mechanical properties can be tuned to the desired capability in an easier manner than natural polymers. However, PEG hydrogels alone are unable to provide the ideal environment for cell survival. [50] Poly(N-isopropylacrylamide) (PNIPAAm) is another polymer that has been used in cardiac constructs as a hydrogel. This material is thermosensitive, and it is of interest because its reversible behavior at solution-to-gelation transition point.

To overcome limitations of synthetic polymers, chemical conjugation with natural polymers have been actively investigated. Natural polymers are of great interest because of their biocompatibility. Collagen, chitosan, gelatin, alginate, and Matrigel are natural polymers that have been studied and applied as potential hydrogels for cardiac repair. These natural polymers preserve biochemical and biological properties that allow for high biocompatibility and increased

cell proliferation. However, natural polymers do not exhibit desirable mechanical strength/properties, and they experience longer gelation time and rapid degradation. [23, 50]

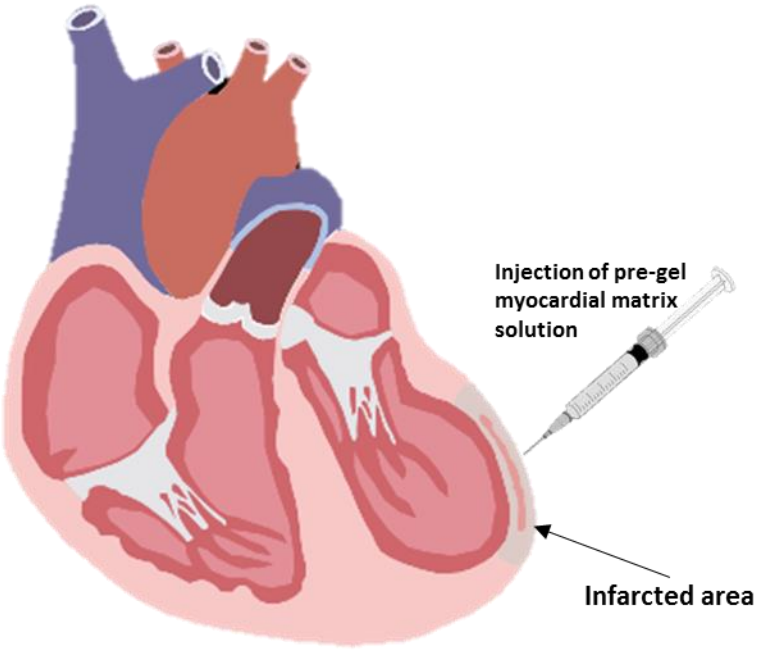

Figure 5: Schematic illustration of injectable hydrogel at the infarct site for MI treatment.

Another option that has been gaining attention is the use of decellularized ECM materials for the development of an injectable hydrogel. ECM scaffolds closely mimic the biophysical properties presented in the native tissue microenvironment. Singelyn et al developed an adult porcine myocardial matrix hydrogel that maintained a complex composition and was able to self-assemble to form a nanofibrous gel. [51] Subsequent animal studies of this hydrogel have shown to reduce negative LV remodeling and prevent cardiac function declination in rat and pig models when delivered 2 weeks post-MI. [28] The hydrogel-injected infarcted myocardium showed a reduced death rate of cardiomyocytes and enhanced infarct neovascularization with lower

hypertrophy and fibrosis. [28] Traverse et al reported the first human subject study of cardiac ECM hydrogel for MI treatment. The study concluded that the transendocardial injection of the VentriGel was safe and feasible. While efficacy evaluation needs further verification, this small scale clinical study did show improvements in patients with an increased distance in 6-min walk test. [27]

As reported in several studies, adult cardiac ECM hydrogel has demonstrated benefits in the treatment of MI [26, 27, 52]. To our knowledge, there has no study to develop nhECM-based hydrogel to harness the excellent regenerative potential of nhECM. In Aim 3, we intended to bridge this gap by developing injectable porcine nhECM hydrogel that could possibly provide biomechanical and biological cues to promote cardiac regeneration.

1.7 Proposed Research and Significance

Although much progress has been made in understanding the mechanisms for heart regeneration, there are still many unknowns and no direct translational approach has been widely implemented. The challenges to create an effective therapy that overcomes the above mentioned hurdles in pharmacology and other conventional treatments are still not being met. A treatment that addresses the underlying cause, which is the loss of cardiomyocytes and the fibrotic scarring is needed.

In this dissertation research, we propose to better understand the structural and biomechanical properties of the porcine nhECM and explore its applications in cardiac regeneration via a cardiac patch approach and hydrogel formation. The understanding and applications of porcine

nhECM is a logistic step to harness the regenerative potential of the neonatal heart ECM environment evidenced by the previous studies. Our ***hypothesis*** is that the 0-day neonatal heart ECM microenvironment has biomechanical and biological cues that promote heart muscle regeneration, and the porcine nhECM can be used as a biomaterial platform for MI treatment. Our research goals are therefore set as (i) performing structural and biomechanical assessments on porcine nhECM, (ii) engineering cardiac patch made of porcine nhECM via electrospinning, and (iii) fabricating porcine nhECM hydrogel as an injective therapeutic means.

These novel research efforts will be carried out via three research aims. First, we aim to characterize the structural and mechanical properties of the decellularized porcine neonatal heart ECM. The obtained knowledge will serve as a foundation for understanding the beneficial microenvironment of nhECM in favor of cardiac regeneration, as well as biomimicking. Second, we aim to harness the regenerative potential of nhECM and develop a nanofibrous cardiac patch made of nhECM via electrospinning technique. We anticipate that the electrospun, crosslinking-stabilized, nhECM nanofibrous cardiac patch has the biomimicking structural and biomechanical properties that benefit cardiomyocyte proliferation and later regeneration. Third, we aim to develop an injectable nhECM hydrogel that builds on the premise that adult heart ECM hydrogels being able to prevent left ventricular negative remodeling after MI, while expanding the applications of the hydrogel to add the mechanical and compositional cues of the nhECM.

1.8 Specific Aims

Aim 1: Structural and Biomechanical Characterizations of the Acellular Porcine Neonatal Heart ECM (nhECM).

In this Aim, we performed histological, compositional, and mechanical assessments to determine the structural-mechanical relationship of the nhECM. Histological observation and compositional quantification were carried out to understand ECM microstructure and composition. Biaxial mechanical testing, uniaxial mechanical testing, stress relaxation, and shear testing were performed to obtain a thorough biomechanical dataset of the porcine nhECM.

Aim 2: Engineering Porcine nhECM-based Nanofibrous Cardiac Patch via Electrospinning Technique.

A novel nhECM-electrospinning protocol was developed to engineer porcine nhECM-based nanofibrous cardiac patch. The concentration of nhECM, solvent, electrospinning parameters, and patch stabilizing crosslinking were investigated and optimized. The structure, mechanical properties, and biocompatibility of nhECM nanofibrous patch were assessed via SEM, biomechanical testing, and cell culture, respectively.

Aim 3: Fabricating and Characterizing Porcine nhECM-based Hydrogel as a Cardiac Injection Material.

We developed an effective protocol to reliably fabricate nhECM-based hydrogel. Structural and rheological tests were performed to determine the structure and porosity of nhECM hydrogel and its gelation kinetics. Additionally, cytotoxicity assessment was performed along with cell proliferation assay to determine the biocompatibility and cell growth potential of the nhECM-based hydrogel.

CHAPTER II

II. Structural and Biomechanical Characterizations of the Acellular Porcine Neonatal Heart ECM (nhECM)

2.1 Introduction

Damaged myocardium from an MI event presents irreversible damage to the heart tissue. Cardiac cell therapy has been investigated as a potential treatment but still experiences major challenges such as extreme low survival and poor engraftment rate after cell transplantation. Biomaterials, such us polymeric/tissue-derived cardiac patches and injectable hydrogels, have been investigated as a means to support the weakened MI tissue and assist cell engrafting and retention, with a hope to better trigger favorable cellular behavior and cardiac regeneration.

Specifically, natural tissue derived scaffolds have been investigated and show promising results in MI treatment.[23, 26, 38, 53] The key benefit of the acellular tissue scaffold is that the mechanical and biological cues of the ECM can be well preserved, and those cues have the potential to support cell proliferation and cell differentiation.[38, 46] For instance, adult porcine myocardial scaffold as patch material and adult porcine myocardial matrix hydrogel as an injectable vehicle all showed potential in MI treatment. [27, 50, 51, 54-60]

Recently, our *in vivo* neonatal pig model research demonstrated that the piglets would lose the fully regenerative potential by 7 days after birth, but greatly preserve the regenerative potential within 1 day of birth. Our histological study showed that, at the apex resection injury site of the 0-day old piglet heart, mesenchymal origin cells had actively dividing and differentiating towards young cardiomyocytes, further suggesting the neonatal heart ECM microenvironment has factors that promote heart muscle regeneration. This finding in neonatal pig heart model also aligns with previously reported timeframe of cardiac regeneration in mouse apex resection

model. [8, 29] The main hypothesis of this dissertation was thus formed, and we aimed to better understand the 0-day nhECM and explore its potential as a biomaterial platform for MI treatment.

Understanding the intrinsic biomechanical, structural, and compositional properties of the nhECM will allow for a more accurate design of biomimicking materials aiming to replicate those features. To our knowledge, there is no mechanical and structural characterizations for porcine nhECM. Therefore, in order to bridge this gap in knowledge, we performed histological, compositional, and mechanical assessments to determine the structural-mechanical relationship of the nhECM. Histological observation and compositional quantification were carried out to understand ECM microstructure and composition. Biaxial mechanical testing, uniaxial mechanical testing, stress relaxation, and shear testing were performed to reveal a thorough biomechanical behavior of the porcine nhECM.

2.2 Materials and Methods

2.2.1 Sample Preparation

Neonatal porcine hearts were obtained from 0-day old pigs from a local Mississippi farm (Prestage Farms of Mississippi, Inc., West point, MS). The piglets' hearts were harvested at Mississippi State University, placed in 1X PBS, and then shipped overnight in ice-cooled boxes to the University of Texas at Arlington, where the hearts were dissected and prepared for decellularization and testing. The neonatal heart samples were dissected with orientation of the circumferential and longitudinal direction labeled by placing a suture on the upper left corner of the tissue (Figure 6B). Each ventricle was visually inspected to avoid any anomalies prior to

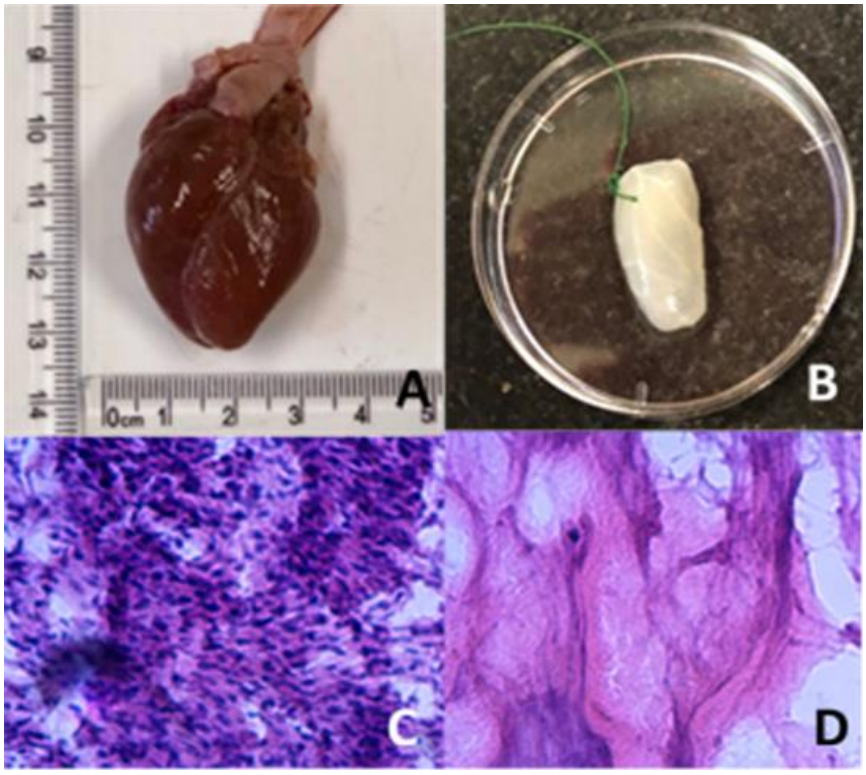

Figure 6: (A) Porcine neonatal heart. (B) Neonatal ventricle strip after decellularization. H&E staining of (C) neonatal ventricle wall and (D) acellular neonatal ventricle strip.

dissection and decellularization. The left ventricle and right ventricle samples were further divided into posterior and anterior sections. For longitudinal direction, the samples were categorized as left anterior ventricle (LAV), left posterior ventricle (LPV), right anterior ventricle (RAV), and right posterior ventricle (RPV). For circumferential direction, samples were dissected as the left ventricle (LV) and right ventricle (RV) only, without distinguishing anterior and posterior due to dimension limitation.

After dissection tissue strips were set in a pin supported structure (Figure 7) and then placed in a 50 ml tube filled with 1% SDS solution. The tubes were placed in a rotational shaker for continuous stirring until the tissue appeared a completely whitish color, a sign of full decellularization of collagenous scaffold. The solution was changed every 24 hours. After 5 to 7 days, the tubes were rinsed and the samples were then placed back in the tube filled with DI water. The samples were placed back in the shaker for 48 hours and the DI water was changed

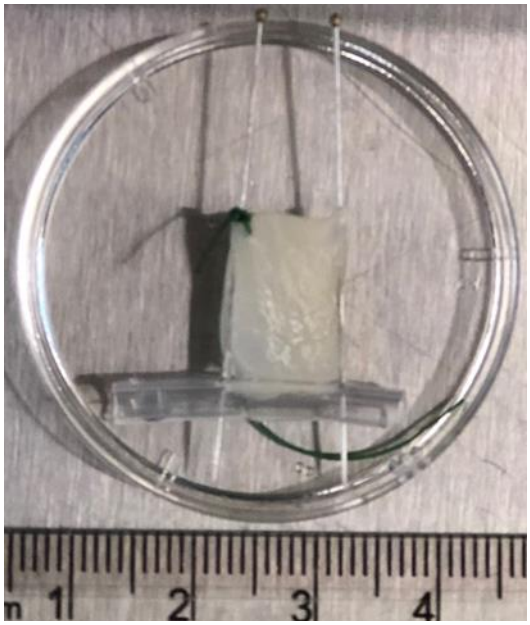

Figure 7: Frame supporting system to preserve structural integrity of acellular scaffold

every 12 hours. To confirm the tissue was successfully decellularized, H&E stain was performed as a verification (Figure 6C,D).

2.2.2 Biaxial Mechanical Testing

Four groups, LAV, LPV, RAV, and RPV, were subjected to biaxial mechanical characterization using a custom-built biaxial testing system (Figure 8A). The dissected and decellularized ECM samples described above were trimmed into a square shape approximately 10 mm X 10 mm, with one edge aligned along circumferential direction and the other edge aligned along longitudinal direction. The measurements were averaged for each ECM sample to obtain an accurate thickness dimension. The samples were then mounted onto the biaxial testing machine using 000 polyester sutures and completely immersed in 1X PBS during the testing. Tests were conducted at a strain rate of 0.5 mm/s. The applied forces were measured with two load cells, and the sample deformation was measured via a video camera, tracking 4 markers placed in square pattern on the center of the sample. After 10 cycles of preconditioning, an equibiaxial tension protocol of $T_{CD} : T_{LD}$ = 20 N/m : 20 N/m was performed to capture biaxial behavior.

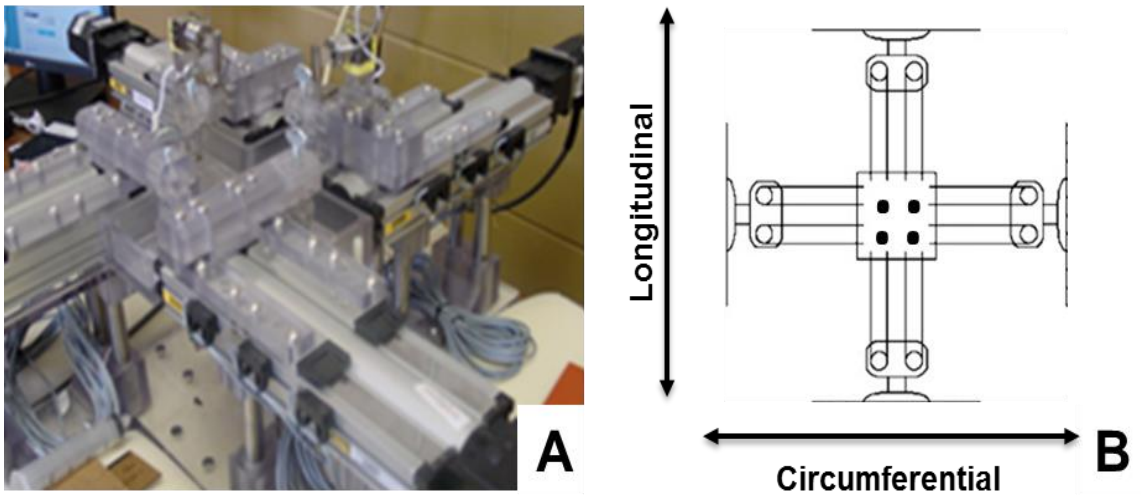

Figure 8: (A) Biaxial mechanical testing system. (B) Biaxial loading directions that were physiologically relevant.

2.2.3 Uniaxial Mechanical Testing

Uniaxial testing was performed using a universal testing system (Test Resources, MN). Samples were dissected and measured for length, width, and thickness and averaged using a digital caliper. The samples were gripped between toothed clamps aligned vertically as shown in Figure 9. Samples were fully submerged in 1X PBS to create a physiologically accurate environment. Preconditioning on all samples was performed by implementing 10 cycles of 10% strain using a continuous sawtooth waveform. After preconditioning, the samples (n = 5) were subjected to stress relaxation test and failure mechanical test. Stress relaxation was performed by applying a tensile load of 35 g at 60 mm/min ramping rate. After the desired load was reached, the motor was stopped in order to maintain the achieved constant strain. Stress decay was continuously monitored for 15 minutes while the sample under this constant strain.

Following stress relaxation, failure test was performed. Samples were loaded at a ramping rate of 10 mm/s until reaching failure. Note that all uniaxial testing was started with a tare load of 0.5 g. Engineering stress was calculated by normalizing the applied force to the original cross-sectional area, and engineering strain was calculated by normalizing the amount of sample deformation to the initial gauge length (reference length).

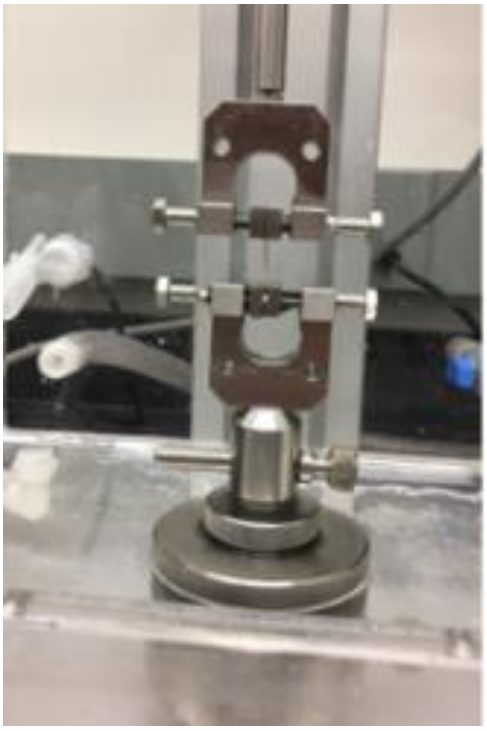

Figure 9: Sample mounted between the vertical clamps during tensile mechanical testing

2.2.4 Shear Mechanical Testing

In order to conduct this testing, the acellular tissue sample was cut into a square shape and mounted between a pair of custom-made shear plates that were mounted on the TestResouces machine and submerged in 1X PBS (Figure 10). Note that samples were placed between the plates using minimal cyanoacrylate. The shear load was applied along the longitudinal direction of the acellular tissue.

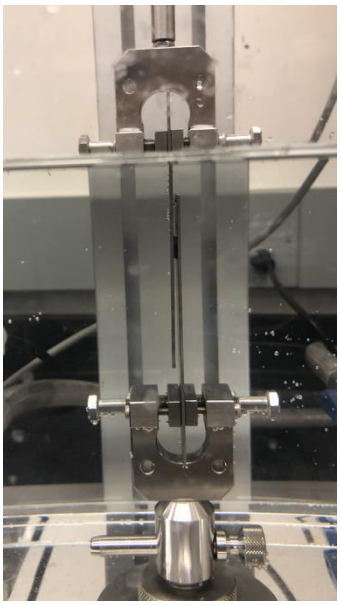

Figure 10: Shear testing setup with custom-made shear plates.

2.2.5 Histological and Compositional Analyses

Histology. The left ventricle was selected for histological analysis. The samples for the native and the decellularized tissue were included. Samples were fixed for 24 hours in 10% neutral buffered formalin prior to staining to preserve the tissue structure. Samples were embedded in wax, sectioned into 5 µm slices, and mounted on histological slides. Masson's Trichrome to reveal the tissue's ultrastructure, heart muscle red and collagen blue. The histological slides were then imaged under white field light using a light microscope.

Collagen Assay and GAG Assay for Compositional Assessments.

For porcine neonatal heart ECM (nhECM) composition analysis, collagen assay and glycosaminoglycan (GAG) assay were performed and compared to the porcine adult heart ECM

(ahECM). The collagen contents were quantified by a Hydroxyproline assay kit (Sigma) following manufacturer's protocol. In brief, Hydroxyproline standards for colorimetric detection were diluted in Hydroxyproline standard solution with 90 μL of water to prepare a 0.1 mg/mL standard solution. Adding 0, 2, 4, 6, 8, and 10 μL of the 0.1 mg/mL hydroxyproline standard solution into a 96 well plate generated 0 (blank), 0.2, 0.4, 0.6, 0.8, and 1.0 μg/well standards. For sample preparation, sample was added to a centrifuge tube. A 100 μL of concentrated hydrochloric acid (HCl, ~12 M) was then added, and the sample was capped tightly, and hydrolyzed at 120°C for 3 hours. Additionally, 4 mg of activated charcoal was added, mixed, and centrifuged at 10,000 × g for 3 minutes. 10–50 μL of supernatant was then transferred to a 96 well plate. Reagents were prepared, Chloramine T/Oxidation Buffer Mixture and DMAB Reagent. For each well, add 50 μL of DMAB Concentrate to 50 μL of Perchloric Acid/Isopropanol Solution and mix well. 1. Add 100 μL of the Chloramine T/Oxidation Buffer Mixture to each sample and standard well. Incubate at room temperature for 5 minutes. Next add 100 μL of the Diluted DMAB Reagent to each sample and standard well, and incubate for 90 minutes at 60°C. Finally, measure the absorbance at 560 nm (A_{560}).

For the GAG content analysis, the acellular heart ECM was digested and tested with a Blyscan Sulfated Glycosaminoglycan assay following previous described method [61]. In brief, 10 mg of sample was added to 500 mL of Papain solution. Tubes were incubated at 60°C for 18 hours. After incubation vortex samples for several minutes. Dimethylmethylene (DMMB) solution will be prepared along with Chondroitin Sulfate (ChS) standards. Mix standards and sample with DMMB dye solution and set UV-vis to be read at 525 nm.

2.2.6 Statistical Analysis

Data were reported as the mean ± standard deviation (SD), where a p-value less than 0.05 was considered as statistically significant. One way ANOVA with post-hoc Tukey test were performed for group-wise comparison.

2.3 Results

2.3.1 Biaxial Testing

Biaxial testing demonstrated that the circumferential direction was stiffer than the longitudinal direction in nhECM. Figure 10 shows the stress-stretch curve for the circumferential and longitudinal direction among all 4 groups (RAV, LAV, RPV, and LPV). Moreover, the nhECM at LV wall (Figure 10B,D) was found stiffer than the nhECM at RV wall (Figure 10A,C) in overall

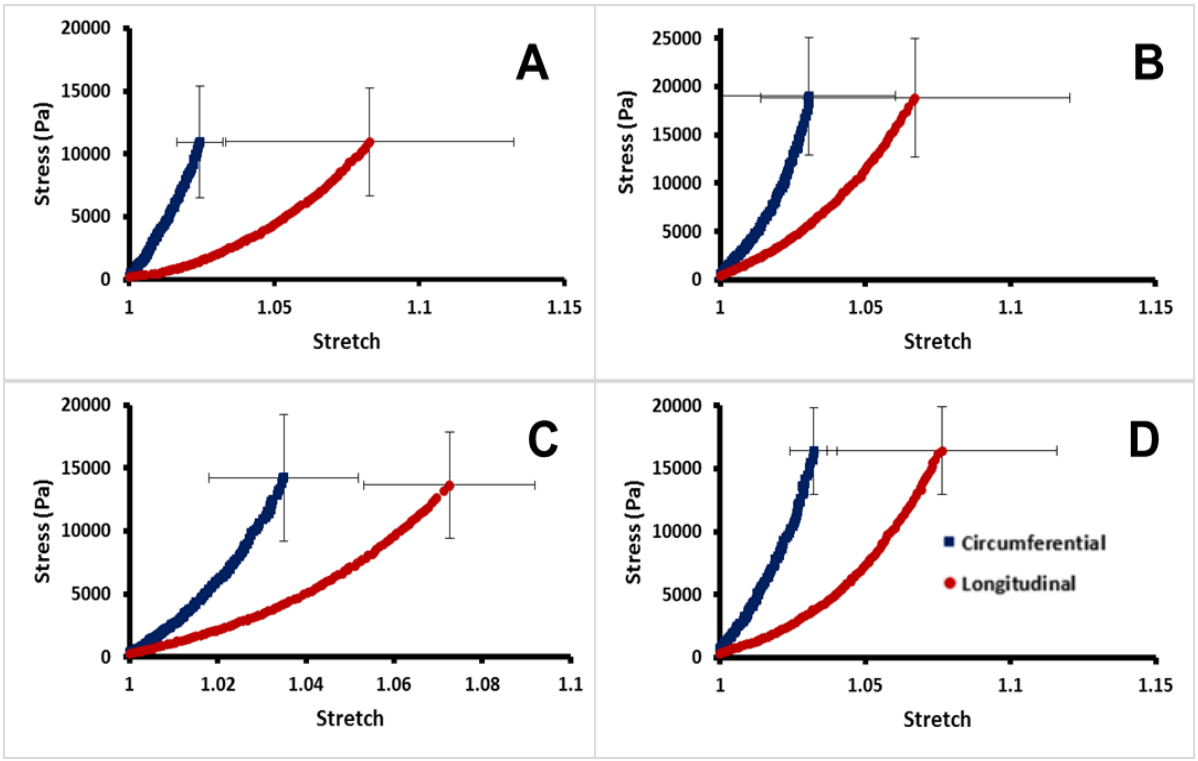

Figure 11: The biaxial mechanical behavior of the nhECM obtained from (A) RAV, (B) LAV, (C) RPV, and (D) LPV.

biaxial behavior. We also noticed that nhECM showed an overall biaxial characteristic (non-linear, anisotropic) similar to the porcine native neonatal myocardial tissue reported by Faizan et al,[43] indicating nhECM's essential role in neonatal heart passive mechanical properties.

2.3.2 Stress Relaxation

Neonatal heart ECM in the longitudinal (Figure 11) and circumferential (Figure 12) direction all exhibited a typical stress-relaxation curve of soft tissues. It was also observed that the acellular LAV relaxed faster and more than the acellular RAV, while RPV and LPV had similar stress relaxation. The LV and RV in the circumferential direction followed a similar pattern.

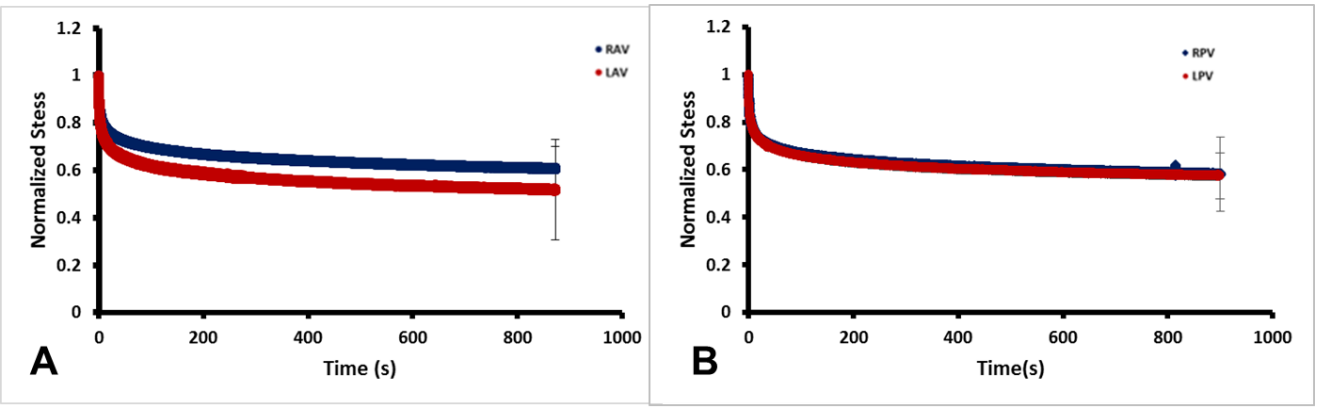

Figure 12: The longitudinal direction stress relaxation of the nhECM obtained from (A) RAV and LAV and (B) RPV and LPV.

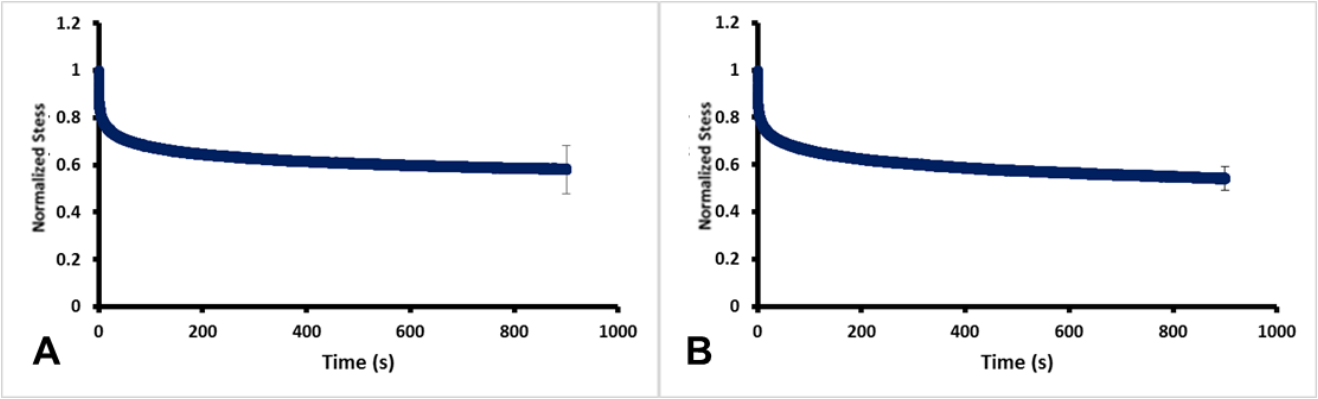

Figure 13: The circumferential direction stress relaxation of the nhECM obtained from (A) RV and (B) LV.

2.3.3 Failure Testing

In Figure 13A, we found that, along longitudinal direction, the nhECM from LAV and LPV were stiffer and had greater mechanical strength than the nhECM RAV and RPV; the failure stress and failure strain of the LAV nhECM had the highest values. In Figure 14B, along circumferential direction, nhECM from LV also showed a stiffer and more extensible behavior when compared to the nhECM from RV. A comparison between the nhECM and the native neonatal myocardium were also performed (Figure 15), with the maximum failure stress summarized in Table 1. We found that the nhECM was significantly stiffer than the native neonatal myocardium and this trend was consistent in LAV, RAV, LPV, and RPV locations (Figure 15). The higher stiffness in the nhECM was expected due to the fact that the acellular tissue became a scaffold made predominantly of collagen, while cardiomyocyte component was being fully removed (Figure 17).

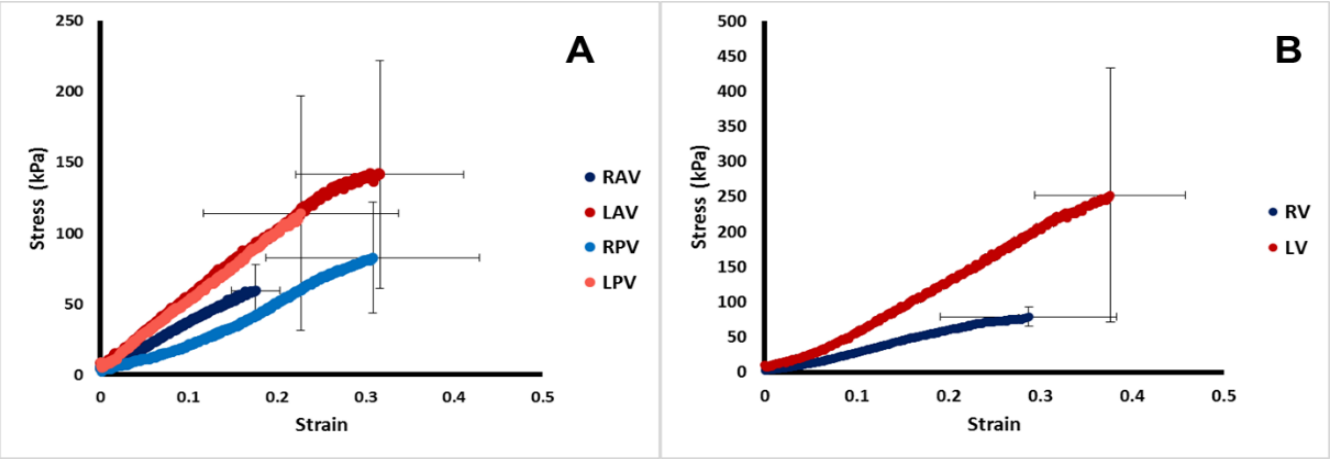

Figure 14: Failure stress-strain curves for the nhECM. (A) nhECM of RAV, LAV, RPV, and LPV in the longitudinal direction. (B) nhECM of RV and LV in the circumferential direction.

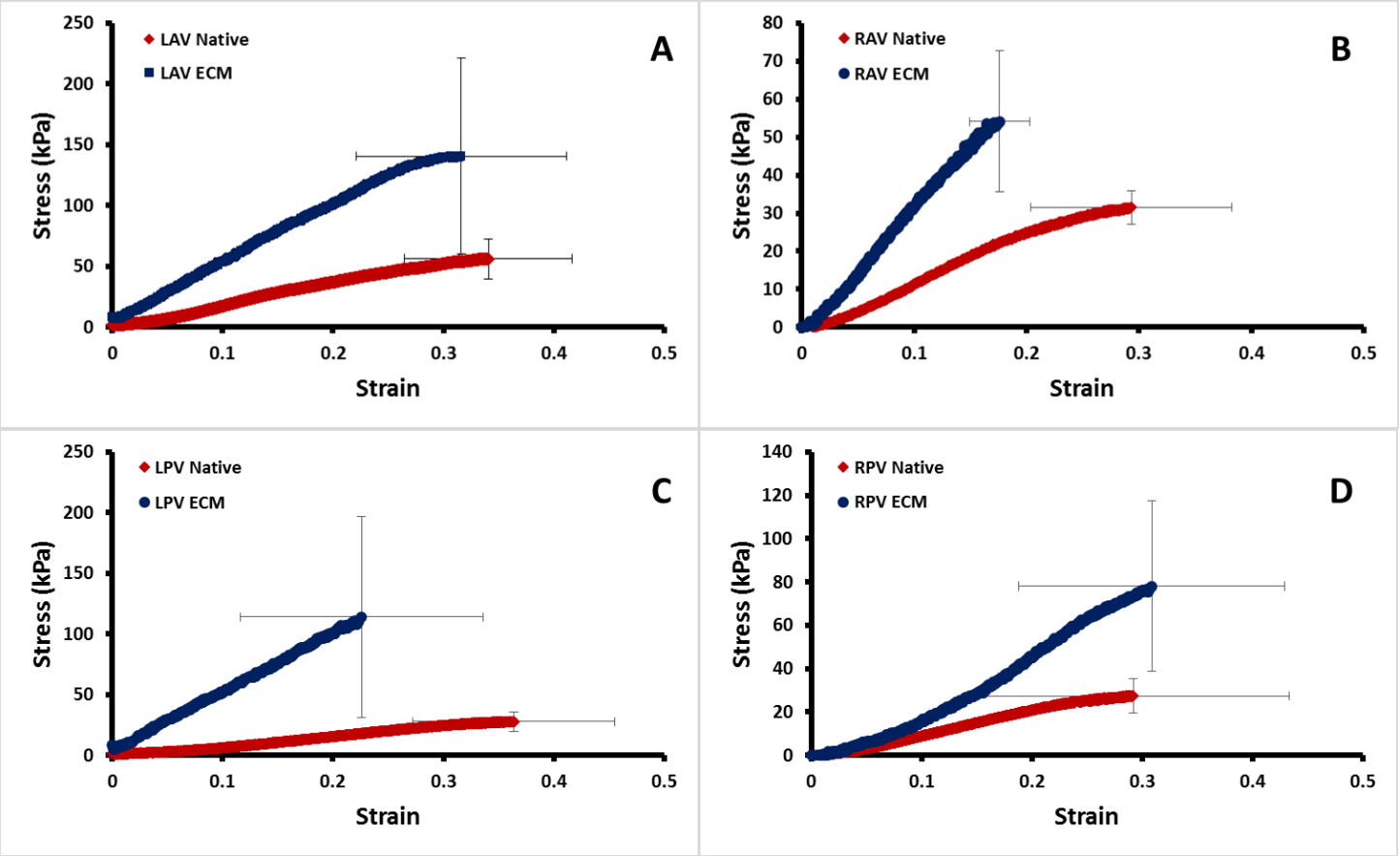

Figure 15: Failure stress-strain curves for the nhECM and the corresponding native neonatal myocardium. (A) LAV, (B) RAV, (C) LPV, and (D) RPV.

Table 1: Failure stress comparison for the nhECM and the corresponding native neonatal myocardium.

Failure Stress (kPa)				
	Native	**Std Dev (+/-)**	**ECM**	**Std Dev (+/-)**
LAV	56.12*	16.50	140.44*	80.51
LPV	27.87*	8.10	114.08*	82.83
RAV	31.59*	4.40	54.13*	18.60
RPV	27.35*	7.92	78.06*	39.43

2.3.4 Shear Testing

Figure 16 showed the average shear behavior measured from LAV nhECM samples. In the range of 0 to 0.5 strain, shear modulus of the nhECM was much weaker than that reported by Wang et al in the adult acellular porcine myocardial scaffold.[62]

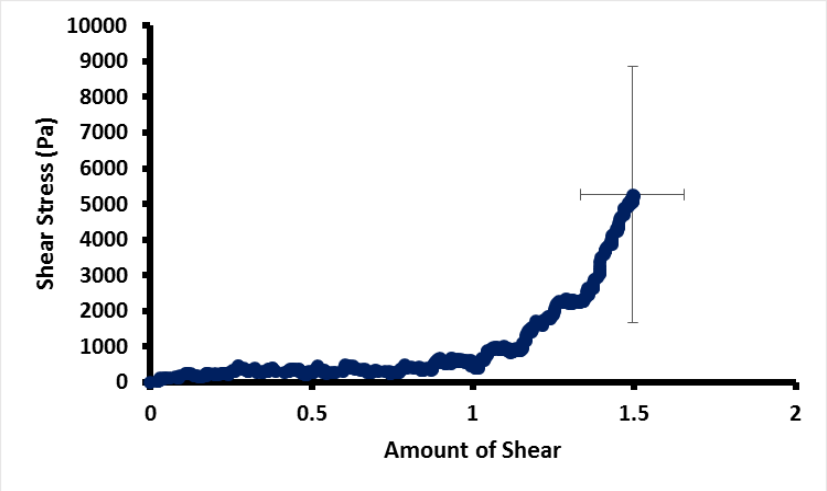

Figure 16: Average shear behavior measured from the LAV nhECM.

2.3.5 Histological and Compositional Analyses

Mason Trichrome staining showed that thorough decellularization was achieved in nhECM (Figure 17). We found that the nhECM had higher amount of GAG when compared to the ahECM (GAG assay, Figure 18), and the nhECM had lower collagen content when compared to the ahECM (Collagen assay, Figure 19).

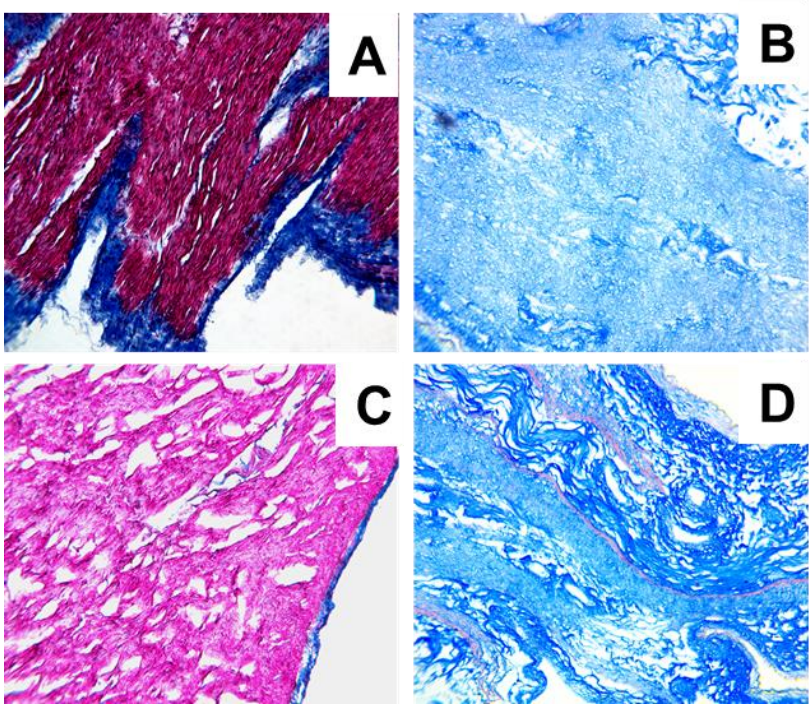

Figure 17: Histology of Masson's trichrome stain at 20x magnification (heart muscle: red, collagen: blue). (A) Native neonatal myocardium, longitudinal direction. (B) nhECM, longitudinal direction. (C) Native neonatal myocardium, circumferential direction. (D) nhECM, circumferential direction.

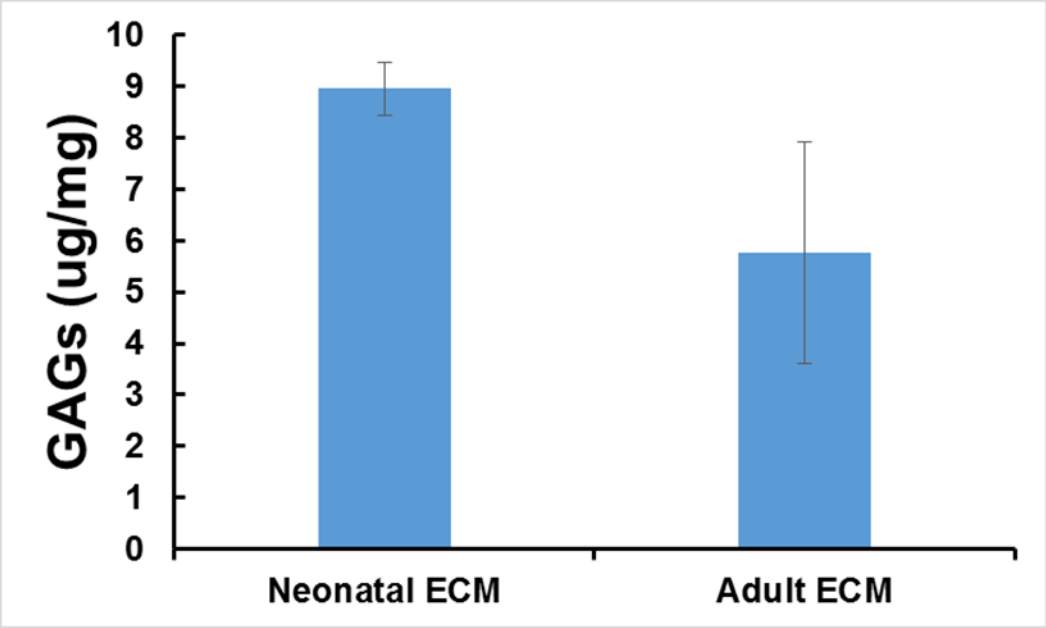

Figure 18: Glycosaminoglycan content of nhECM and ahECM.

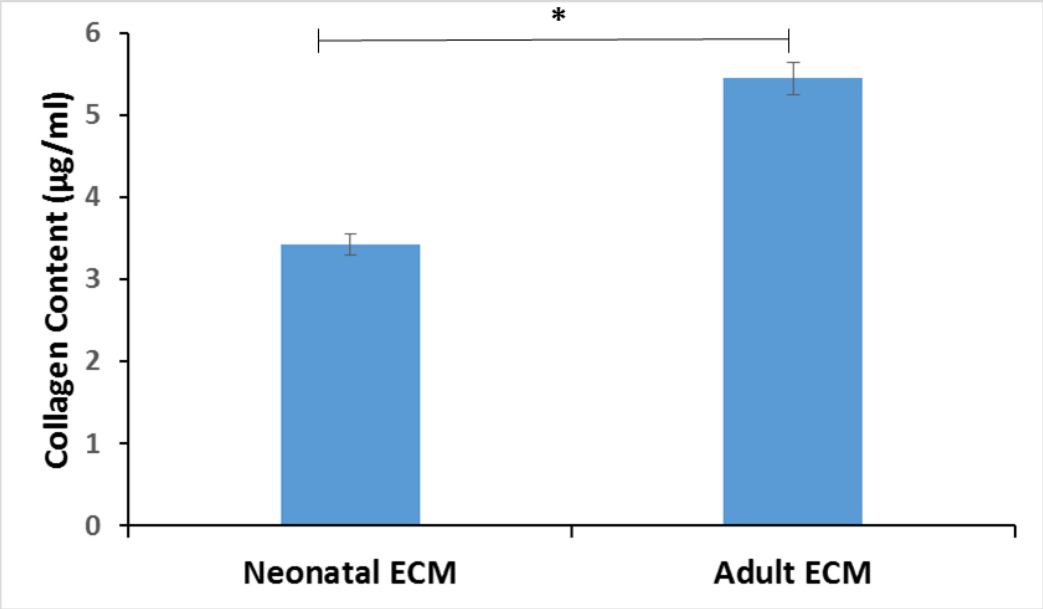

Figure 19: Collagen content of nhECM and ahECM.

2.4 Discussion

In this chapter we thoroughly characterized the nhECM scaffold that was decellularized using 1% SDS solution. We developed a pin based support structure to maintain the structural integrity of the nhECM scaffold and prevent structural collapse after removing all cell components. Full decellularization was verified by H&E staining.

Testing results showed that the nhECM had a non-linear, anisotropic, and viscoelastic behavior. Biaxial mechanical testing demonstrated that the circumferential direction was stiffer than the longitudinal direction supported by other studies.[43, 62] Moreover, the LV nhECM was found stiffer than the RV nhECM in overall biaxial behavior. The failure stress-strain curves showed that the acellular LAV and LPV were stiffer and had greater mechanical strength than the acellular RAV and RPV, and the failure stress and failure strain of the acellular LAV had the highest values. The native neonatal myocardium and the acellular neonatal ECM scaffold where both tested up to failure for comparison. The overall peak stress in the acellular tissue was significantly higher in than in the native tissue. Stress relaxation testing was also investigated and it was also observed that the acellular LAV relaxed slightly faster, while the acellular RAV, while RPV and LPV had similar stress relaxation trend. Shear modulus of the nhECM was very low when compared with ahECM data in literature.[62]

We found that the porcine ahECM had 60% higher collagen content than the porcine nhECM. In a study by Wang et al, they found that the collagen content in the acellular adult mouse heart ECM have 50.7% more collagen than the acellular neonatal mouse heart ECM [38]. This result

aligns with our finding in collagen contents when comparing porcine nhECM and ahECM. In our GAG assessment, we found 55.4% more GAG content in the porcine nhECM when compared to the porcine ahECM. This finding is also supported by the previous finding in mouse model. In the study by Wang et al, they reported 154% higher concentration of GAG in the acellular neonatal mouse heart ECM when compared to the acellular adult mouse heart ECM. [38] The differences in collagen and GAG contents often have influence on various cellular behavior. The observed differences in ECM compositions support the theory that nhECM is drastically different from the ahECM (adult heart extracellular matrix), supporting our hypothesis that the nhECM provides its unique cues that likely promote cardiac tissue regeneration.

2.5 Conclusion

We were able to decellularize the neonatal porcine myocardium and maintain its structure after decellularization. Moreover, we have successfully accomplished the mechanical, structural, and compositional characterizations of the nhECM. Our study demonstrated that the nhECM had a non-linear, anisotropic, and viscoelastic behavior. We also noticed that the nhECM showed an overall biaxial characteristic (non-linear, anisotropic) similar to the porcine native neonatal myocardial tissue, which signified nhECM's essential role in governing the passive mechanical properties of neonatal heart. Failure testing showed that the nhECM was significantly stiffer than the native neonatal myocardium. The higher stiffness in the nhECM could be attributed to the pure collagen scaffold makeup after removing soft cardiomyocyte components. Moreover, shear modulus of the nhECM was very low when compared to the ahECM. We found that the porcine ahECM had 60% higher collagen content than the porcine nhECM, while there was 55.4% more GAG content in the porcine nhECM when compared to the porcine ahECM. In short, when

comparing the nhECM to the ahECM, we observed drastic differences in biomechanical, structural, and compositional properties, which strongly supports our hypothesis that the nhECM has its unique cues that likely promote cardiac tissue regeneration. The results from this chapter allow us to better understand nhECM's intrinsic properties, which in turn could help better design our novel biomimicking materials in Chapter 3 and 4.

CHAPTER III

III. Engineering Porcine nhECM-Based Nanofibrous Cardiac Patch via Electrospinning Technique.

3.1 Introduction

Cardiac patches are increasingly investigated as a potential therapeutic treatment after an MI event. They have also been investigated as a treatment for patients with congenital heart defects. Since the early 2000s, there has been an increase in publications in the cardiac patches.[22, 23, 54, 63, 64] Cardiac patches have shown in animal studies to reduce infarct size and improvement on contractile function of the left ventricle.[22, 23, 54, 63, 64] Naturally derived ECM has been used in many cardiac applications including cardiac patches yielding promising results.[54, 55] In 2019, the first ECM patch (Cor^{TM} Patch), which was developed from porcine small intestinal submucosa, was approved by the FDA for epicardial tissue support,.[65-67]

Electrospinning has been a widely used technique in the development of cardiac patches because of it is a simple, effective, and scalable method to fabricate nanofibrous scaffolds that present similar morphology to cardiac ECM.[44, 49, 68, 69] Electrospinning allows for the modification of properties such us fiber diameter or scaffold structure.[48, 70, 71] A majority of electrospun scaffolds for cardiac patches are fabricated by combination of synthetic and natural polymers to leverage the mechanical properties of synthetic polymers and the biocompatibility of natural polymers. Electrospinning pure natural polymers such as collagen or cardiac ECM presents its unique challenges. Electrospun natural polymers are unstable and disintegrate when coming to contact with water based solution if the material is not previously cross-linked.[72-75]

In current literature, the majority of studies that have been conducted for electrospinning natural polymers including cardiac ECM involve a co-polymer in order to preserve the elasticity of the scaffold, as well as to provide mechanical support. [46, 74, 76] There are limited studies that fabricate pure ECM electrospun scaffolds. In a study by Schoen et al, [46] a scaffold was developed via electrospinning using adult porcine cardiac ECM. In their study, the ECM was electrospun with a solution that included poly(ethylene oxide) (PEO) in order to obtain a viscoelastic solution that was able to be deposited by electrospinning. In their study, they state that the PEO was removed from the scaffold after electrospinning by performing several washes with an aqueous medium. Their approach did not require cross-linking.[46]

In this study, we used pure porcine neonatal ECM (nhECM) as the basis of our cardiac patch. We developed a novel approach to dissolve pure nhECM in a solvent to create a viscous solution that was able to be electrospun. In order to stabilize the ECM we further developed a cross-linking protocol. Several cross-linking agents have been investigated to stabilized the natural polymers after electrospinning specially EDC and Genipin.[72, 73, 77, 78] In a study by Akhshabi et al,[79] they studied the use of the EDC carbodiimide with NHS to crosslink a collagen electrospun mat. The results after crosslinking showed that the collagen was stabilized and remained biocompatible. Fiber swelling after cross-linking is another challenge when stabilizing a natural polymer electrospun scaffold. In a study by Campiglio et al,[80] they explored how solvent selection could affect the fiber morphology after cross-linking treatment. They showed that a non-swelling solvent, acetonitrile, can better preserve fiber morphology of the scaffold after cross-linking.

In this chapter, we reported a novel electrospinning fabrication and cross-linking technique to create an nhECM cardiac patch that harnesses the regenerative potential of the nhECM. To assess its feasibility as a patch material, we further characterized the structure, mechanical properties, and biocompatibility of nhECM nanofibrous patch via SEM, biomechanical testings, and cell culture.

3.2 Materials and Methods

3.2.1 Sample Preparation

Harvested neonatal hearts were collected and received as described in section 2.2.1. The left and right ventricle were dissected and cut into thin slices, which were then prepared for decellularization. The tissue was rinsed in DI water for 3 hours, and the DI water was changed every one hour. 1% SDS solution was prepared, and the rinsed tissue was placed in the solution to achieve decellularization. The tissue was constantly stirred in the 1% SDS solution for 4 to 5 days until completely turning into a whitish appearance that often associated with pure ECM scaffolds. The solution was changed after 8 hours the first day and every 24 hours after that. The tissue was then rinsed in DI water for 24 hours with DI water being changed at least 5 times. The obtained tissue was frozen overnight and then lyophilized. The nhECM was digested in 1 mg/ml of HCL/pepsin solution as described by Syngelyn et al.[51] The mixture was then neutralized with NaOH frozen overnight and was lyophilized again.

3.2.2 Scaffold Fabrication using Electrospinning Technique

The digested, lyophilized nhECM was dissolved in 1,1,1,3,3,3 hexafluoro-2-propanol (HFIP) under constant stirring for 2 hours. HFIP has been widely used as a solvent for electrospinning.[81, 82] Figure 20 illustrates the electrospinning process showing the syringe pump, the syringe setup, and the circular collection plate where the fibers were deposited. The solution was electrospun using a +15 kV electric field and a deposition rate of 0.5 mL/hr, with a total of 4 mL of solution used per scaffold. Different concentrations of the solution were tested in order to determine the needed concentration to obtain high quality nanofibers without the formation of defective beads. Fiber morphology of the dried scaffold was then assessed by scanning electron microscopy (SEM).

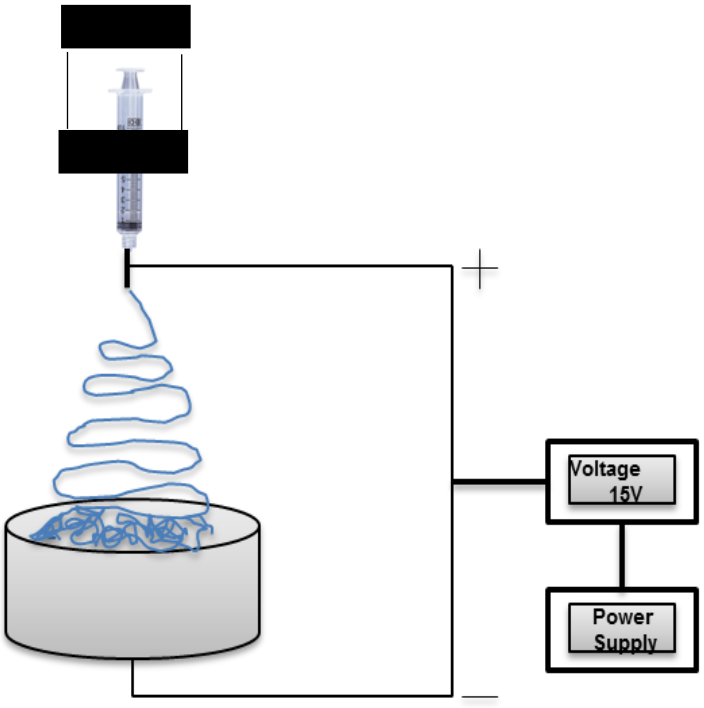

Figure 20: Electrospinning Setup depicting collector plate, syringe with polymeric solution attached to the syringe pump and the voltage and power supply setup

3.2.3 Cross-linking of the Electrospun Scaffold

As we mentioned above, electrospinning of natural polymers has experienced great technical challenges, and only a few attempts succeeded by adding a synthetic polymer as co-spinning material. Electrospinning of pure ECM has been rarely reported in literature.[46] Moreover, it was reported that the electrospun Type II collagen scaffolds did not have the ability to maintain its fiber microstructure upon hydration.[72] EDC was used as a cross-link agent for natural polymer scaffolds and was able to stabilize collagen scaffolds; however, EDC failed to maintain fiber morphology post cross-linking.[72, 79] Genipin (GP), a natural cross linker, had been used in electrospinning with a goal to retain fiber morphology.[73, 78] We thus also explored a GP cross-linking protocol modified form Luo et al.[83]

Electrospun samples were cut from the mat using a biopsy tool with 8 mm diameter. GP cross-linking and EDC cross-linking, along with types of solvents (ethanol and acetonitrile), were tested and compared to investigate which cross-linking agent and solvent combination best preserve fiber morphology integrity of the electrospun nhECM scaffold. For GP cross-linking, 30 mM GP cross-link solution in 100% ethanol was used. Samples were incubated in 30mM GP-100% ethanol solution for 24 hour in a centrifuge tube at 37°C. Sample was rinsed 5 times with 100% ethanol for 15 min to quench unreacted GP. Sample was then air dried for 24 hours prior to SEM images. For EDC crosslinking, 50mM EDC cross-link solution was prepared with a 100% concentration of the solvent used. Note that we first used 100% ethanol as the solvent, but fibers showed aggressive swelling after the treatment. We hence tested acetonitrile as the solvent for EDC to avoid fiber swelling. Lastly, samples were cross-linked in EDC-acetonitrile for 2, 4 and 6 hours to assess best cross-linking time.

3.2.4 Morphological Characterization

For structural analysis of the unseeded electrospun scaffold was characterized using scanning electron microscopy (SEM) (Hitachi S-4800 II FE-SEM). The samples were cut with a 8 mm biopsy punch tool and mounted onto a metal disk. Samples were sputter coated with a Hummer VI sputtering system (gold/platinum) for one minute prior to SEM imaging. Fiber diameter in the electrospun scaffold was measured from the SEM images using ImageJ. The diameter measurements were taken by tracking diameter lines perpendicular to the long axis of the fiber (100 measurements per field).

3.2.4 Fourier-Transformed Infra-Red Spectroscopy (FTIR)

In order to better understand the effects of cross-linking on the nhECM electrospun scaffold, we performed FTIR. Infra-red spectra of the nhECM electrospun scaffold before and after cross-linking was measured for comparison. Samples were prepared with an 8-mm biopsy tool. The tests were done using a FTIR spectrometer (Thermo Nicolet 6700 FTIR Spectrometer) from a range of 4000 to 650 wavelength (cm^{-1}).

3.2.5 Mechanical Testing

Uniaxial failure mechanical testing of the electrospun nhECM groups were carried out pre and post cross-linking, following methods described in 2.2.3. Briefly, the electrospun acellular nhECM scaffold was rehydrated by submerging in 1X PBS bath at 37^{o}C prior to dissection and

testing. The scaffold was mounted onto a universal testing system (Test Resources, MN). Samples were dissected and measured for length, width, and thickness using a digital caliper and averaged to obtain the dimension. For each test, the scaffold sample was gripped and aligned vertically between two pairs of toothed clamps. The clamp ramp speed was 10 mm per second.

3.2.6 Contact-Angle Test

Contact angle was measured to determine the wettability of the scaffold surface. A high contact angle refers to a hydrophobic surface and a low contact angle refers to a hydrophilic surface. Contact angle of the electrospun nhECM scaffold was measured by a video contact angle system (Water High Resolution Camera and Fta32 video software) on dry samples [84]. Water was used as the testing liquid. The droplet size was set at 4 µl for each tested sample (n=4). The measurement was taken at 0, 15, 30, and 45 seconds for each sample. The average and standard deviation of the contact angles were reported for each time point.

3.2.7 Swelling Ratio Measurement

Swelling ration testing was performed to assess the change in fiber morphology after rehydrating the scaffold. Swelling ratio testing was conducted as described by Hoveizi et al.[85] The nhECM cross-linked scaffold samples were cut with an 8-mm biopsy tool, and each sample was placed in a 1.5 ml centrifuge tube. Each sample was fully submerged in 1X PBS and incubated for 24

hours at 37°C. The dimension of the sample was then measured and compared with the original dimension to calculate the swelling ratio.

3.2.8 Cytotoxicity Test

Cell culture was performed using HL-1 cardiomyocytes. The cardiomyocytes will be cultured in prepared Claycomb media as previously described [86] until approximately 90% confluency.
The experiment was performed using 50 mg/ml EDC-cross-linked nhECM scaffold. Circular samples were cut with an 8-mm biopsy tool. The samples were then sterilized via UV light in cell culture hood for 30 minutes. After sterilization, the samples were placed in a 96-well plate with 200 µl of 1X PBS and placed in the incubator at 37°C with 5% CO_2 overnight. The HL-1 cardiomyocytes were then passaged per protocol to prepare them for scaffold seeding. 1X PBS was removed from each well, and the HL-1 cells were seeded at a density of 10k cells/well. Cell growth and viability was assessed using live/dead assay (Invitrogen) and MTS assay (Promega) at Day 1 and Day 5 time points.

3.2.9 Statistical Analysis

Statistical analysis of all values were reported as the mean ± standard deviation (SD), where a p-value less than 0.05 was considered as statistically significant. One way ANOVA with post-hoc Tukey test were performed for group-wise comparison.

3.3 Results

3.3.1 Scaffold Fabrication

Fiber morphology of the nhECM scaffold was viewed by SEM. Figure 21 shows how electrospun fibers were formed at different nhECM concentrations (26 mg/ml, 33 mg/ml, and 50 mg/ml). The lowest nhECM concentration we tried was 20 mg/ml. This concentration did not gather a thick enough mat to analyze the fiber morphology. A lot of beads were observed on the mat for 26 mg/ml concentration protocol (Figure 21A). The two higher concentrations at 33 mg/ml and 50 mg/m had good fiber deposition and morphology (Figure 21B,C). The 50 mg/ml was selected as the concentration to continue because this concentration yielded the best fiber composition. Interestingly, at 50 mg/ml concentration we observed two set of randomly dispersed fibers (thicker and thinner), which were consistent with the adult ECM electrospun fibers and collagen type I scaffolds.[46] The average fiber diameter of the 50 mg/ml mat was 190 nm +/- 0.11. A higher concentration of 75 mg/ml was attempted but it presented a lot of undissolved nhECM in HFIP. Therefore, it was deemed not feasible for electrospinning.

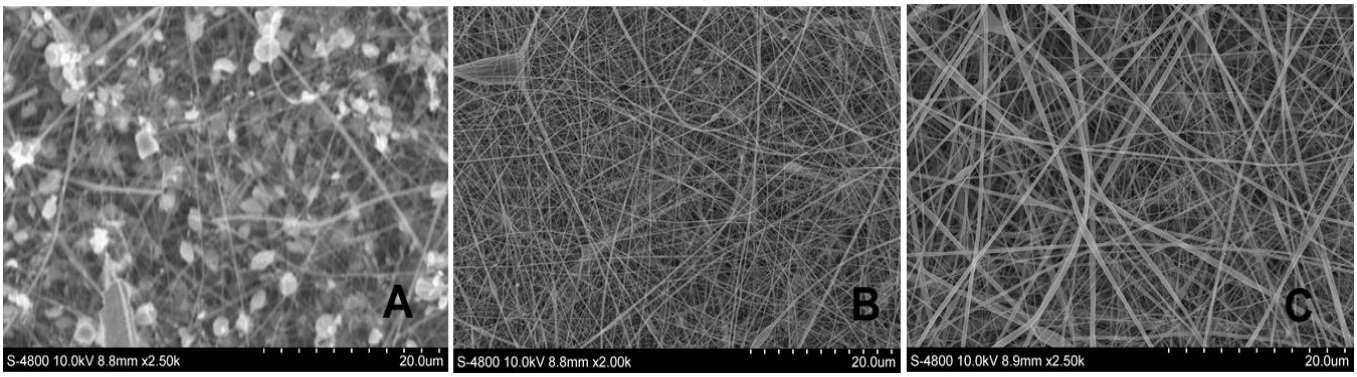

Figure 21: Scanning electron images of electrospun fibers consisting of pure nhECM at (A) 26 mg/ml, (B) 33 mg/ml, and (C) 50 mg/ ml.

3.3.2 Effectiveness of Cross-Linking

The nhECM electrospun samples were evaluated for the effectiveness of cross-linking. Figure 22 shows the sample of electrospun mat pre cross-linking and post cross-linking with EDC and GP after a 24 h incubation at 37ºC for GP cross-linking and 2 hour at room temperature for EDC cross-linking. Upon evaluation of the scaffolds via SEM, it was observed that the fiber

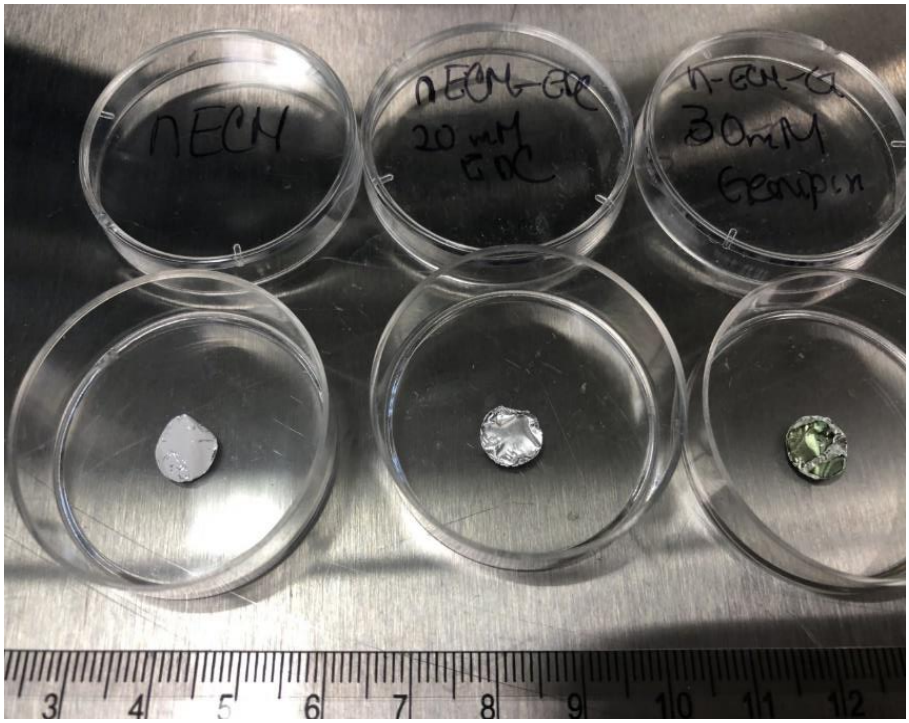

Figure 22: Samples of electrospun mats for nhECM pre and post cross-linking with EDC and Genipin.

morphology dramatically changed after cross-linking (Figure 23). Figure 23A shows the fiber morphology before cross-linking and Figure 23B and Figure 23C show the scaffold morphology after crosslinking with EDC and GP, respectively using 100 % ethanol as the solvent. We observed the loss of fiber after the cross-linking process. This phenomenon could be attributed to the nature of ethanol as a solvent because it tends to cause swelling.[80] In a study by Campiglio et el, it was found that cross-linking with Acetonitrile, instead of ethanol, could better

preserve fiber morphology.[80] We hence switched to acetonitrile as the cross-linking solvent to test whether this new solvent generated effective cross-linking, as well as preserve the desirable fiber morphology.

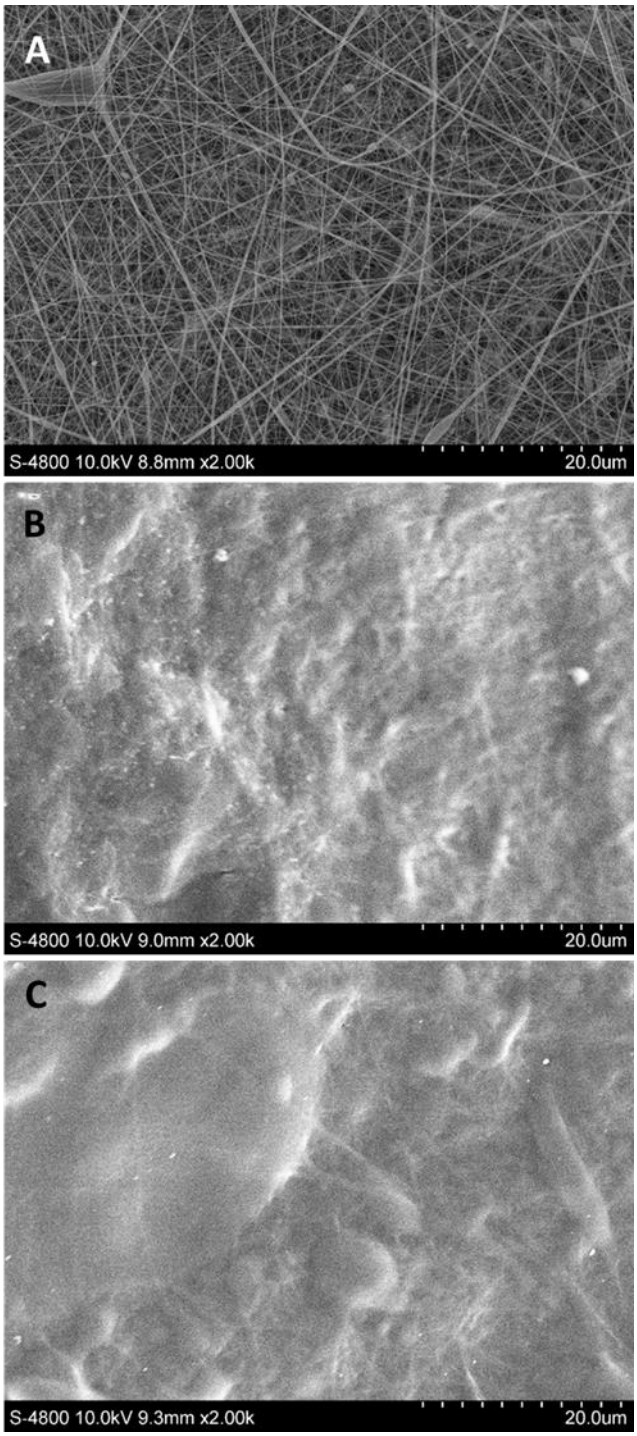

Figure 23: Samples of nhECM electrospun mats at statuses of (A) pre cross-linking, (B) post EDC cross-linking with 100% ethanol as solvent, and (C) post Genipin cross-linking with 100% ethanol as solvent.

With undesirable fiber morphology associated with 100% ethanol solvent, we changed our approach and experimented with acetonitrile as the new solvent candidate, which was less prone to causing swelling. Figure 24 showed SEM images of the fiber morphology after cross-linking the scaffold with 50 mM EDC in 100 % acetonitrile and 30 mM GP in 100 % acetonitrile at different time points (2 hours, 4 hours, and 6 hours). We found that, using acetonitrile as solvent, the fiber morphology was overall maintained for both GP cross-linking and EDC cross-linking at 2-hour and 4-hour treatment time points. However, at 6-hour time point, fiber morphology for both GP cross-linking and EDC cross-linking deteriorated largely and showed aggressive swelling. The best fiber morphology was shown in electrospun nhECM samples after 4-hour

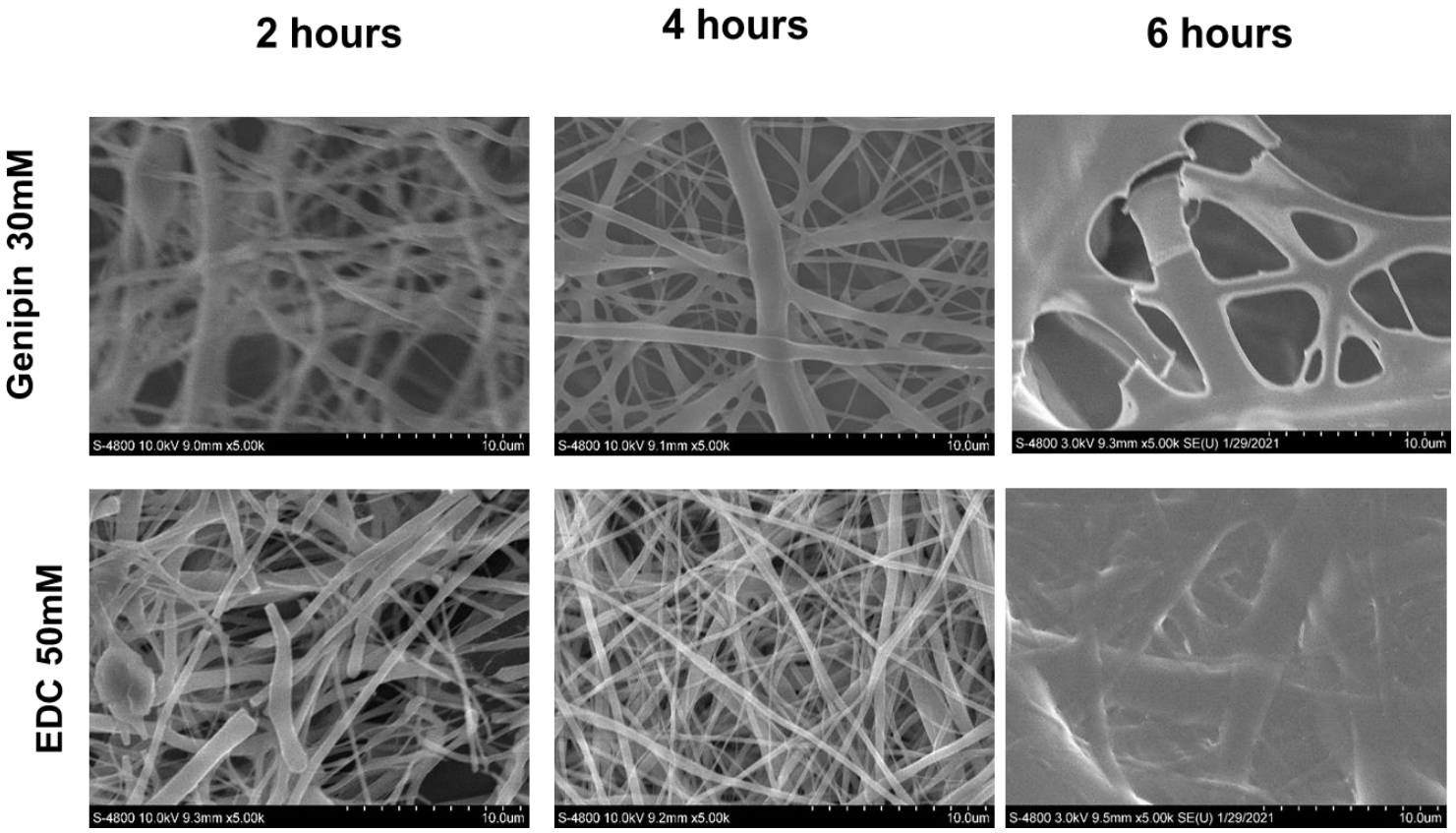

Figure 24: SEM images of electrospun nhECM after crosslinking with Genipin 30 mM and EDC 50 mM using 100% acetonitrile as a solvent at 2-hour, 4-hour, and 6-hour time points.

treatment using 50 mM EDC cross-linking in 100% acetonitrile solvent. We thus chose 4-hour

50 mM EDC-100% acetonitrile cross-linking protocol as the candidate to full characterizations reported in the following sections.

During the cross-linking protocol optimizing procedure, we observed that the use of acetonitrile as a solvent often caused considerable shrank in the electrospun nhECM scaffold (Figure 25). In order to prevent shrinkage and improve the repeatability of cross-linking protocols, a post cross-liking drying setup was designed. The setup consisted of two rods that supported each side of the scaffold while it was still wet. This way, the dried edges were constraint to the rods and prevented scaffold shrinkage. Silica beads were added to the closed container to absorb air humidity that could damage the water sensitive natural ECM fiber structure.[80] This novel setup was able to effectively prevent the scaffold from shrinking and from adhering to the petri dish, which was another challenge encountered when cross-linking with acetonitrile (Figure 26).

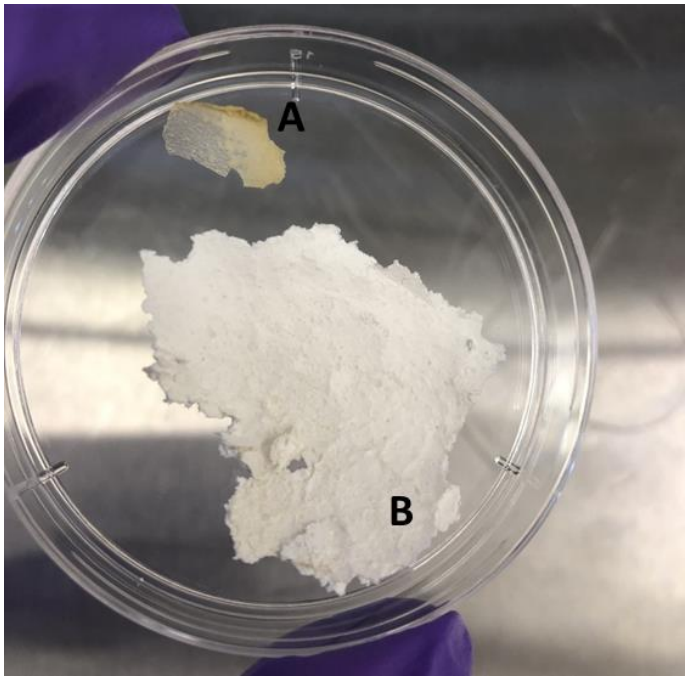

Figure 25: Size difference of scaffold after cross-linking on petri dish. (A) Electrospun nhECM after cross-linking and overnight air drying in petri dish. (B) Un-crosslinked nhECM electrospun mat.

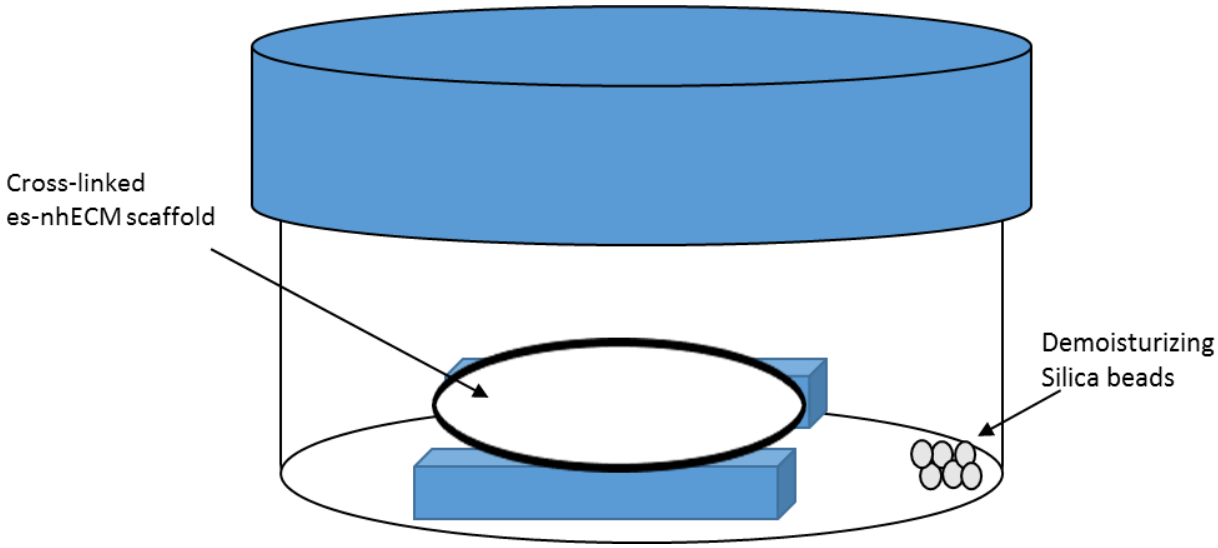

Figure 26: Post-crosslinking drying setup for preventing nhECM scaffold shrinkage.

3.3.3 Ultrastructure of nhECM Fibers

For ultrastructural analysis, the optimized electrospun nhECM scaffold (50 mg/ml) crosslinked with 50 mM EDC and 100% acetonitrile as a solvent was subjected to SEM observation. The SEM images and fiber diameter distributions of the nhECM scaffold pre and post cross-linking were presented in Figure 27. The nhECM scaffold showed high quality, randomly-aligned, and well meshed nhECM fibers (Figure 27A), and those fiber characteristics were well preserved after 50 mM EDC-crosslinked in 100% acetonitrile (Figure 27B), only with an 50% increase in average fiber diameter (Table 2), which were likely related to the physicochemical response of cross-linking stabilization. The analysis of the nhECM fibers demonstrated that the pre cross-

linking nhECM scaffold had an average fiber diameter of ~190 nm, and the post cross-linking nhECM scaffold had an average fiber diameter of ~300 nm (Table 2).

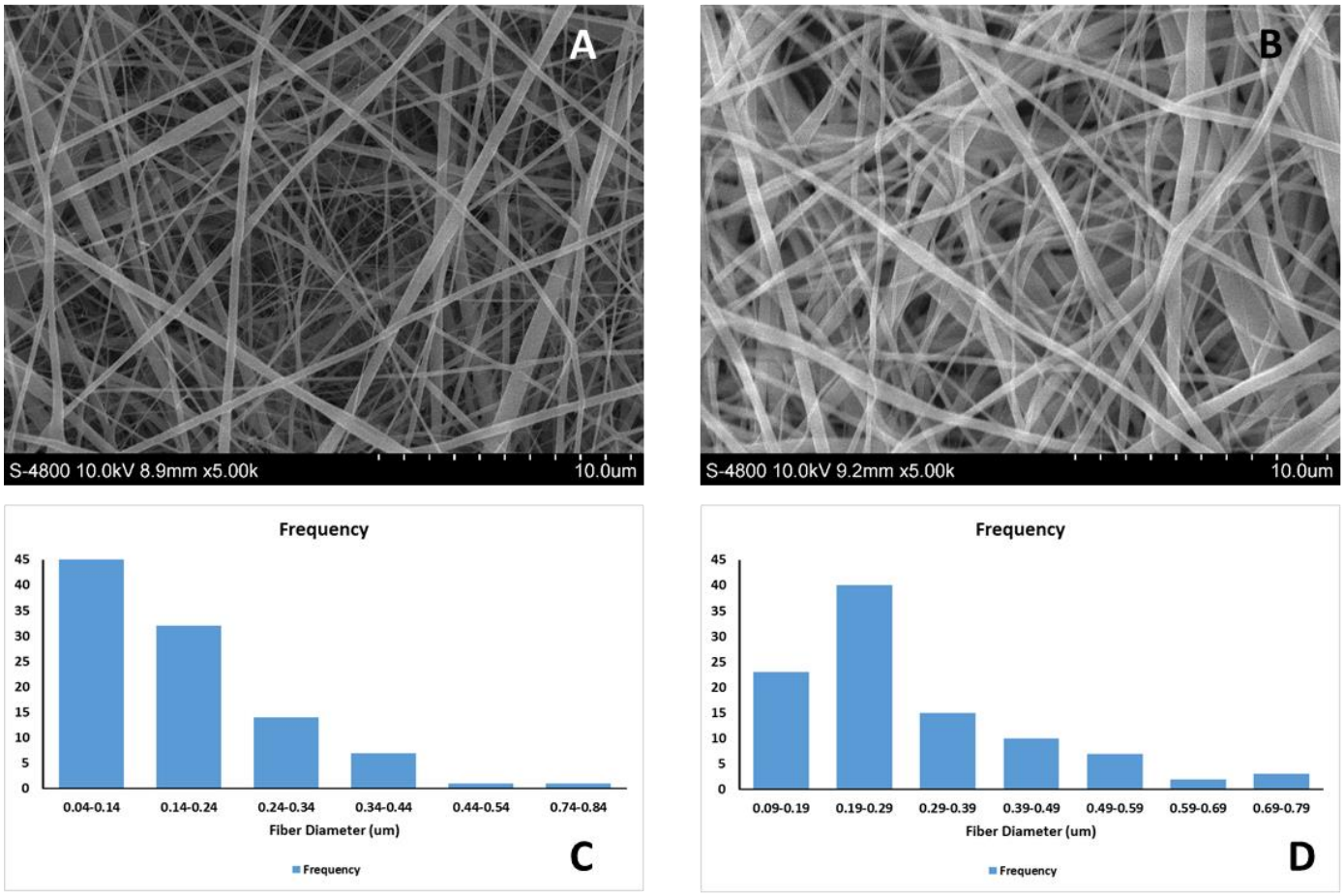

Figure 27: SEM images of the nhECM electrospun scaffold pre cross-linking (A) and post cross-linking (B). Fiber distributions of the nhECM electrospun scaffold pre cross-linking (C) and post cross-linking (D). Note that 50 mg/ml nhECM was treated via 50 mM EDC-100% acetonitrile cross-linking protocol.

Table 2: Average fiber diameter of pre and post cross-linking. Note that 50 mg/ml nhECM was treated via 50 mM EDC-100% acetonitrile cross-linking protocol.

nhECM scaffold	Diameter (μm)
Pre-crosslink	0.19 ± 0.11
Post-crosslink	0.30 ± 0.15

3.3.4 Fourier-Transform Infrared Spectroscopy pre and post Cross-Linking

Collagen is the main protein contained in the connective tissue ECM.[87-89]. The FTIR spectrum of the nhECM electrospun scaffold showed the typical characteristic of the FTIR spectra found in collagen. There have been several studies that show that collagen displays bands at around 3300 cm^{-1} for Amide A, 1610-1690 cm^{-1} which corresponds to the amide I, 1540-1555 cm^{-1} referring to amide II, and around 1235 cm^{-1} for amide III.[90-93] In Table 3, we summarized the peaks and transmittance value relate to the bands presenting in our cross-linked nhECM scaffold and uncross-linked nhECM scaffold, which all closely matched the amide peaks found in collagen. As shown by the FTIR spectra (Figure 28), both the cross-linked nhECM scaffold and uncross-linked nhECM scaffold demonstrated the feature characteristics of collagen. There was also a small difference between cross-linked nhECM scaffold and uncross-linked nhECM scaffold. A peak at 1150 cm^{-1} was reduced in the cross-linked sample when compared to the uncross-linked nhECM sample. The band at this value was attributed to the glycosidic bond [89] leading us to believe the bond was affected during the cross-linking process.

The integrity of the triple helix structure in the collagen could be analyzed with the ratio of absorbance from peak 1234 and 1450 cm-1. [89, 94] This ratio provided an assessment of the denaturation of the collagen, with a ratio around 0.5 suggesting denaturation while a value of 1 suggesting no denaturation. The ratio was calculated for the cross-linked nhECM scaffold and uncross-linked nhECM scaffold with 1.01 and 0.99, respectively which suggest that no collagen denaturation occurred in both cross-linked and uncross-lined nhECM scaffolds.

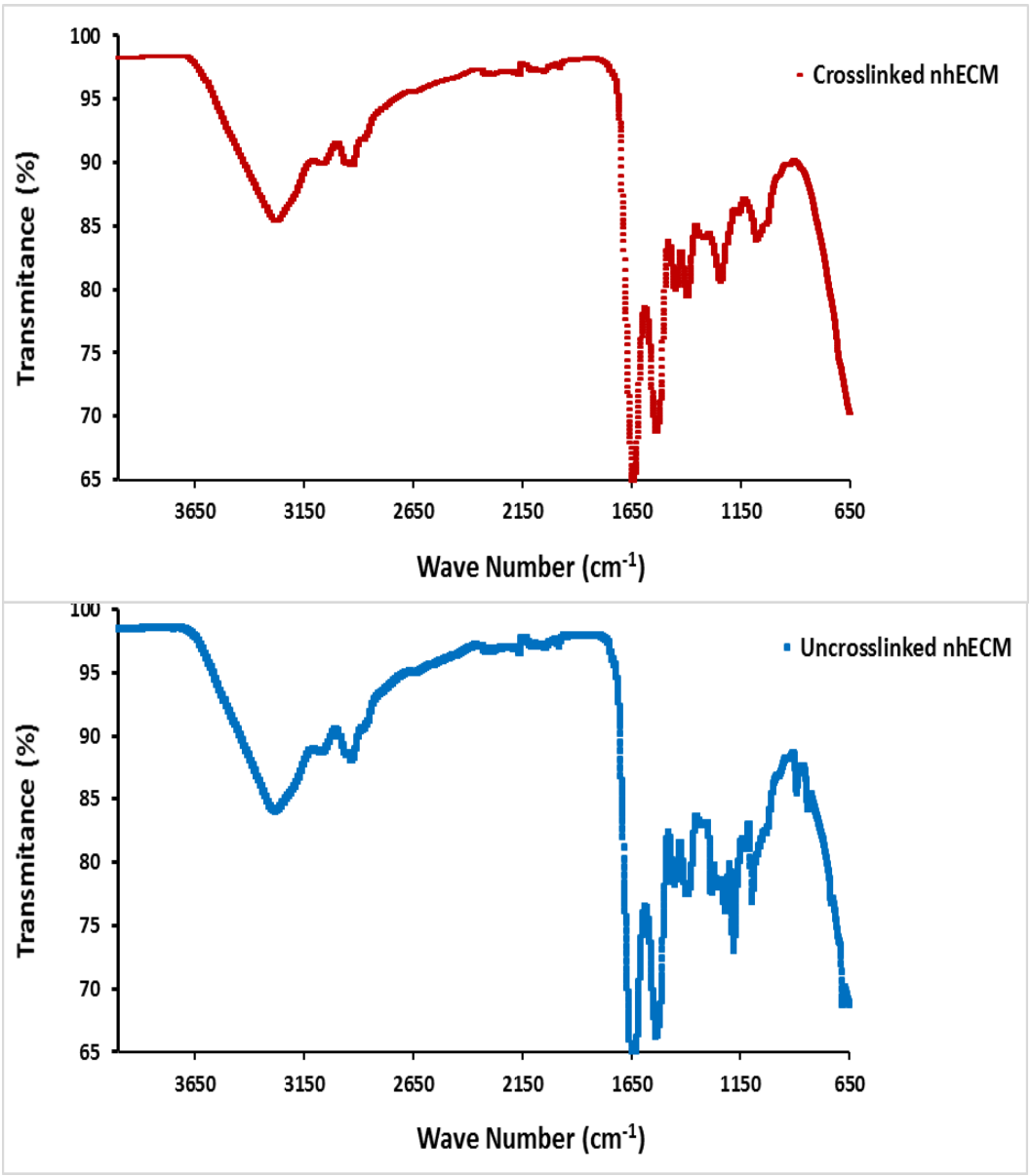

Figure 28: FTIR spectra for the cross-linked nhECM scaffold (A) and the uncross-linked nhECM scaffold (B). Note that 50 mg/ml nhECM was treated via 50 mM EDC-100% acetonitrile cross-linking protocol.

Table 3: FTIR peak band analysis for uncross-linked nhECM scaffold and the cross-linked nhECM scaffold

	Band Position (cm-1)			
Sample	**Amide A**	**Amide I**	**Amide II**	**Amide III**
pure nhECM	3279.9	1642.4	1536.5	1239.4
nhECM crosslinked	3279.2	1642.4	1536.4	1283.8

3.3.5 Mechanical Properties of the Cross-Linked nhECM

Uniaxial failure mechanical testing was performed and showed very positive results on the mechanical properties of the cross-linked nhECM. The 50 mM EDC cross-linking protocol produced great fiber morphology in the cross-linked electrospun nhECM scaffold. Interestingly, the dry, cross-linked nhECM scaffold had a fragile, paper-like quality and could be ruptured with minor handling. However, once the cross-linked nhECM scaffold was rehydrated, it gained both mechanical strength, stiffness, and extensibility, allowing it to be handled and subjected to failure test. The stress-strain curves of the rehydrated cross-linked nhECM scaffold exhibited an extensibility similar to the native neonatal myocardium and overall stiffness and mechanical strength that were smaller but quite close to the native neonatal myocardium (Figure 29). In Table 4, we summarize the failure stress and failure strain of the native neonatal myocardium and the rehydrated cross-linked nhECM scaffold.

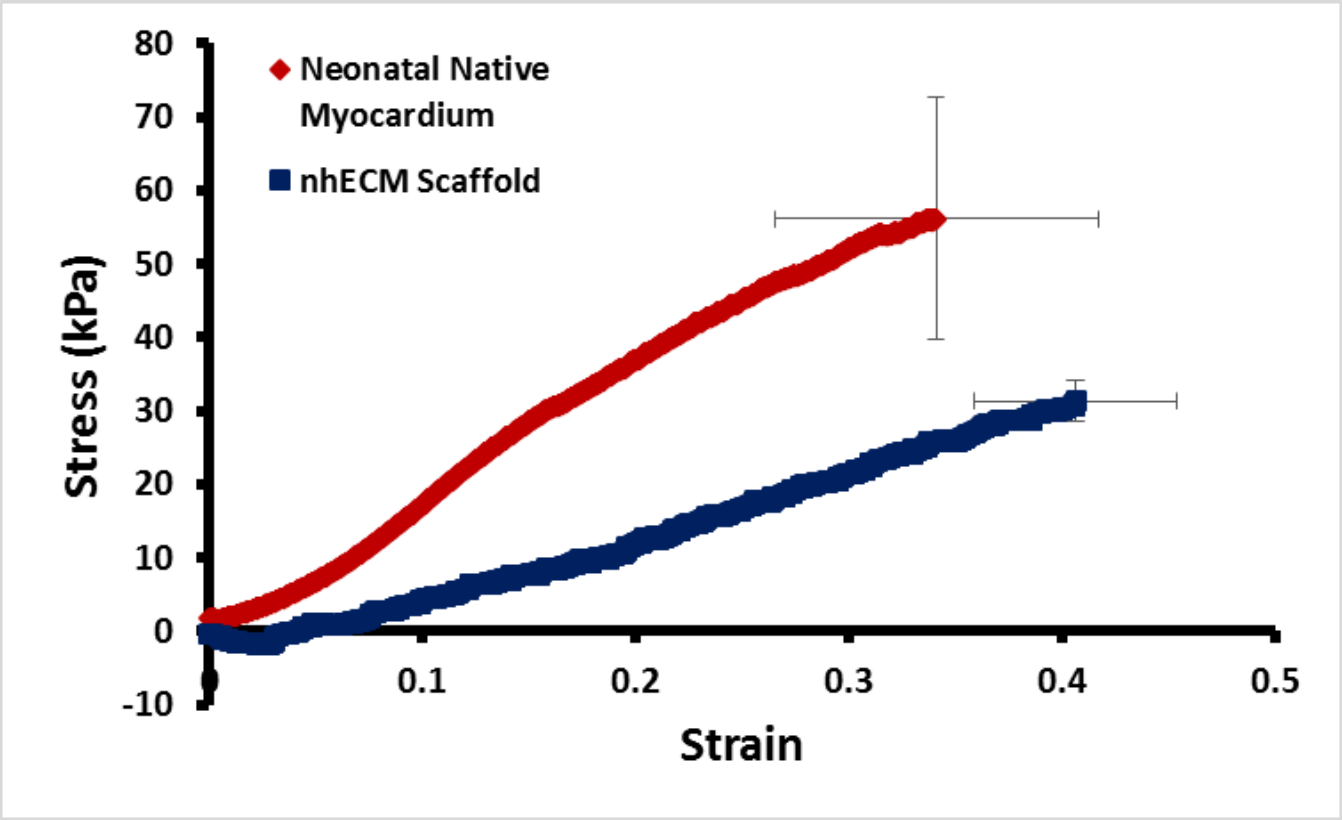

Figure 29: Failure stress-strain curves of the native neonatal myocardium and rehydrated cross-linked nhECM scaffold.

Table 4: Failure stress and failure strain values of the native neonatal myocardium and rehydrated cross-linked nhECM scaffold

	Strain	Std Dev (+/-)	Stress (kPa)	Std Dev (+/-)
Neonatal Native Myocardium	0.34**	0.08	56.12**	16.50
nhECM Cross-linked Scaffold	0.41**	0.05	31.32**	2.80

3.3.6 Contact Angle

Surface wettability is an important property for a biomaterial because it determines if the surface is hydrophobic or hydrophilic. A contact angle higher than 90^{o} indicates hydrophobic surface and less than 90^{o} a hydrophilic surface.[76] Contact angle of the electrospun nhECM scaffold was measured by a video contact angle system using water as the testing liquid. The measurement was taken at 0, 15, 30, and 45 and seconds for each sample. Figure 30A showed the progression of the shape of the water droplet on the cross-linked nhECM scaffold at different time points. We found that the water contact angle decreased rapidly, and it was less than 90^{o}, indicating the cross-linked nhECM scaffold was a hydrophilic material. The contact angle values with respect to various time points were plotted in Figure 30B.

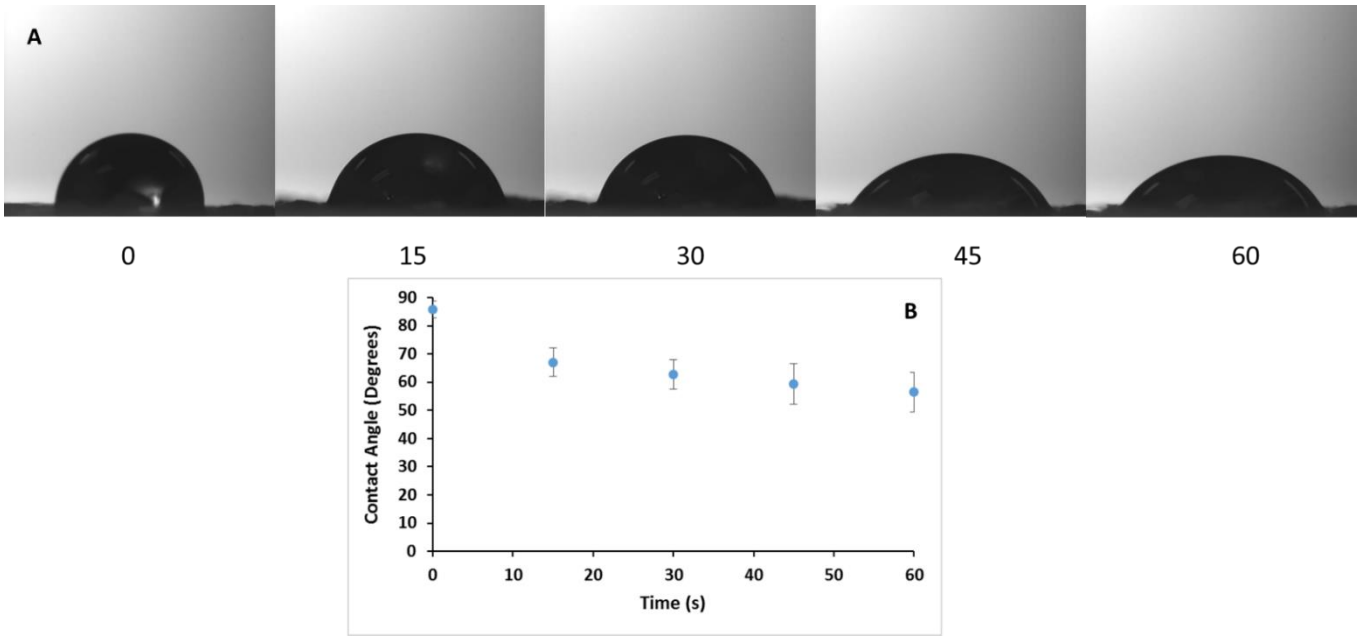

Figure 30: (A) Water droplet on the cross-linked nhECM scaffold from time 0 to 60 seconds (B) Contact angle values with respect to various time points.

3.3.7 Swelling Ratio

The morphological change in the cross-linked nhECM scaffold after it being submerged in PBS was visibly apparent. Figure 30 showed the dry cross-linked nhECM scaffold, which was whitish and opaque, and the rehydrated cross-linked nhECM scaffold, which showed rehydration-caused swelling and semi-transparent texture. The ultrastructural morphologies were also assessed using SEM and compared (Figure 31C,D). At ultrastructural level, the fiber structure greatly altered after rehydration (Figure 31D). The fibers after being rehydrated were thicker and present a morphology more similar to the morphology of a hydrogel. The swelling ratio with respect to diameter was a ~72% shrinkage, while the swelling ratio with respect to thickness was a ~318% increase.

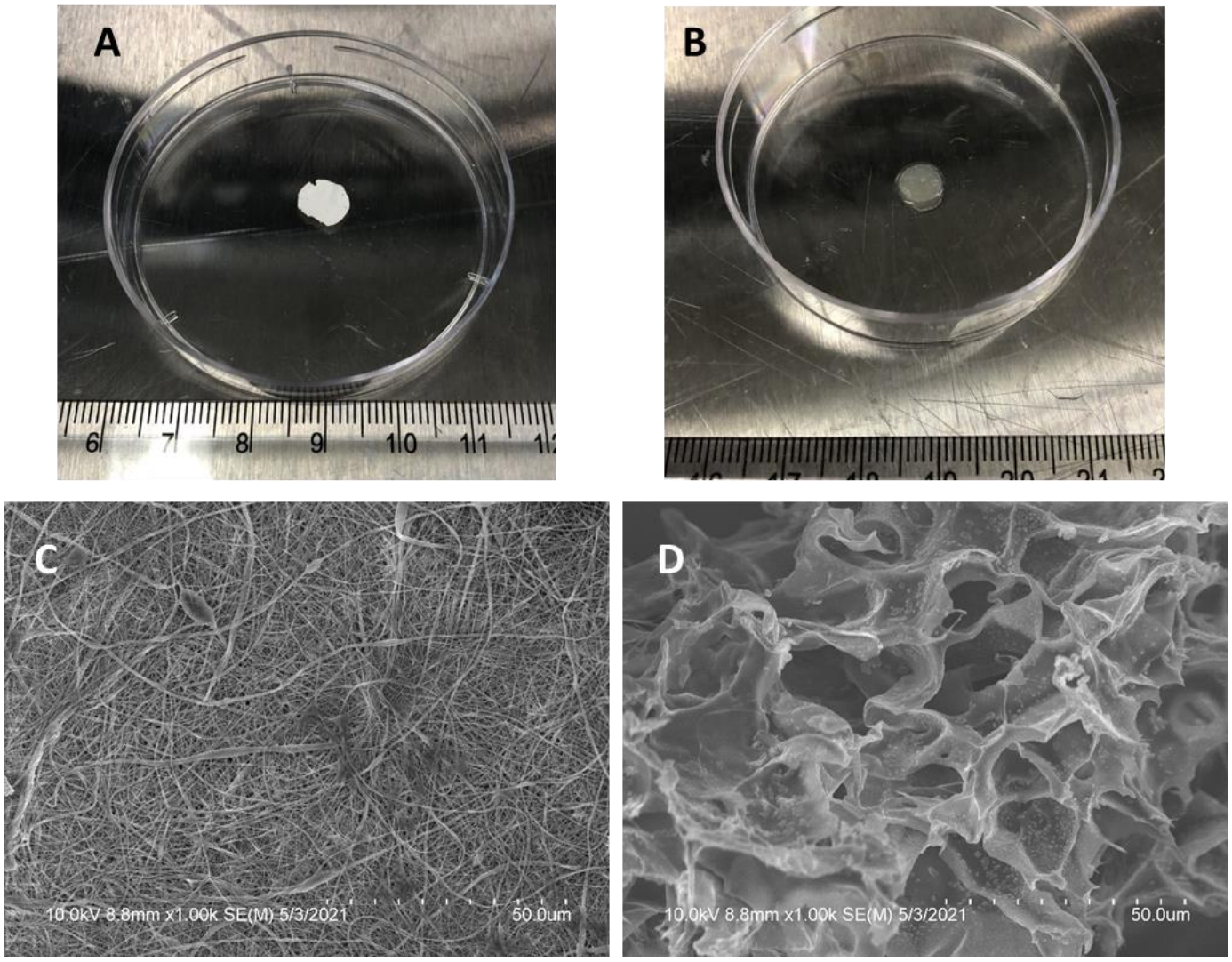

Figure 31: Morphology of the dry cross-linked nhECM scaffold (A) and the rehydrated cross-linked nhECM scaffold (B). SEM images of the dry cross-linked nhECM scaffold (C) and the rehydrated cross-linked nhECM scaffold (D).

3.3.8 Cytotoxicity of the Cross-linked nhECM scaffold

The results of our cytotoxicity study showed that the cross-linked nhECM scaffold was in favor of survival and proliferation of the HL-1 cardiomyocyte cells. The cell viability was assessed using live/dead assay (Promega). In Figure 31 showed that the growth of live cells (green) from

Day 1 to Day 5. Figure 32 reported the results from the MTS assay from Day 1 to Day 5. The average absorbance from Day 1 to Day 5 increased from 0.12 to 0.37, indicating a ~216% increase.

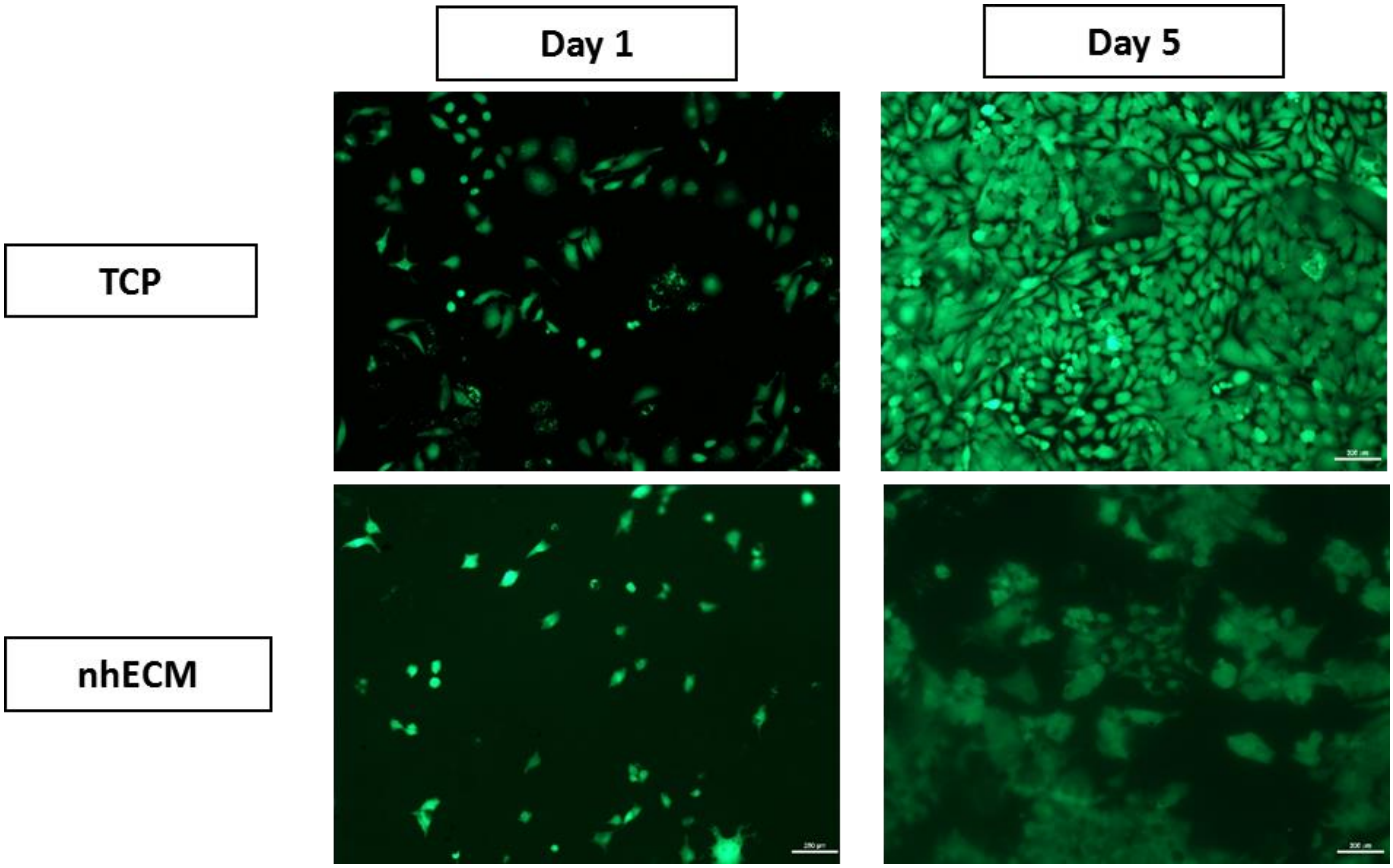

Figure 32: Live/dead assay imaging of HL-1 cardiomyocytes on TCP and the cross-linked nhECM scaffold for Day 1 and Day 5. Note that 50 mg/ml nhECM was treated via 50 mM EDC-100% acetonitrile cross-linking protocol.

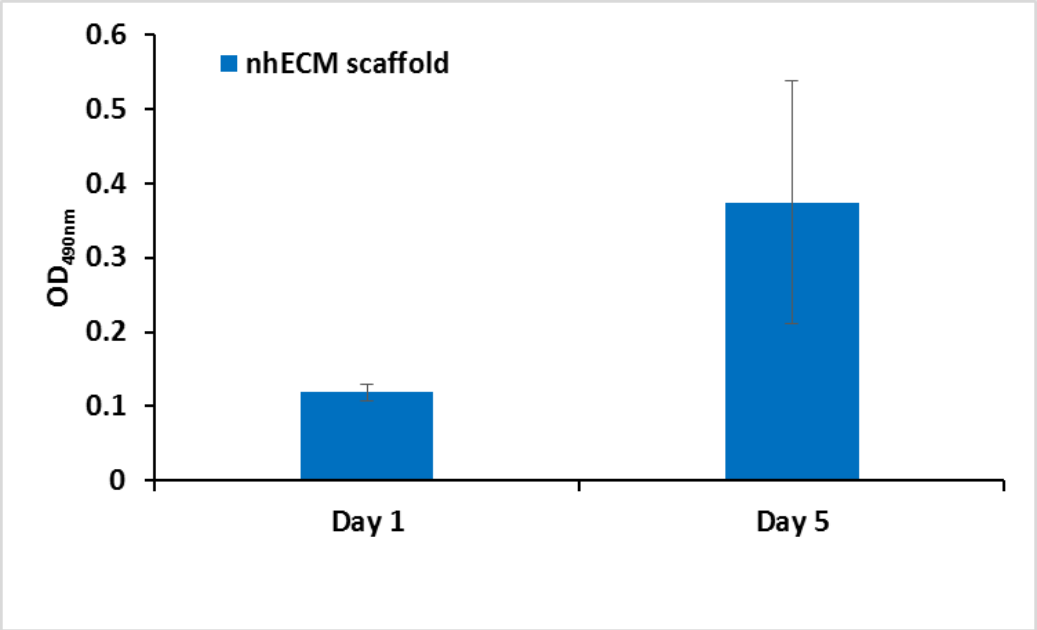

Figure 33: Cell proliferation results from HL-1 cells on the cross-linked nhECM scaffold from Day 1 and Day 5. Note that 50 mg/ml nhECM was treated via 50 mM EDC in100% acetonitrile cross-linking protocol.

3.4 Discussion

Decellularized cardiac ECM is a promising material for the treatment of MI.[22] However, developing a solution that can electrospin the pure cardiac ECM into biomaterial remains a challenge. The majority of electrospun cardiac ECM scaffolds in current literature had to include a polymer when creating the solution for electrospinning. In this study, we developed a novel procedure to digest pure nhECM and an effective cross-linking protocol that preserved fiber morphology and desirable biomaterial mechanical properties at hydrated condition. We showed how the solvent for cross-linking plays an important role in preserving fiber morphology.[80] The 50 mg/ml nhECM and the cross-linking protocol using 50mM EDC in 100% acetonitrile were able to generate best fiber morphology. Full characterizations of the cross-linked nhECM scaffold generated by this optimal protocol proved its effectiveness in many key aspects. We demonstrated the presence of non-denatured collagen in the cross-linked nhECM scaffold using FTIR analysis. We showed that the cross-linked nhECM had high quality, randomly-aligned, and well meshed fibers. Healthy adult myocardial fiber diameter has been reported to be between 10 μm to 25μm [95, 96]. Collagen fiber in the heart has been reported to measured 120 nm to 150 nm in diameter.[97, 98] It has been shown that the diameter and distribution of collagen fibrils play an important role to govern the ECM stiffness and the interaction with cells.[99] The fiber of the cross-linked nhECM scaffold have a diameter of ~300 nm, which is between the myocardial fiber diameter and the collagen fibril diameter and thus suitable as a scaffolding material. By analyzing the surface wettability of the cross-linked nhECM, we found that it had hydrophilic property.

By assessing the mechanical properties of the native neonatal myocardium and the cross-linked nhECM scaffold, we showed that the rehydrated cross-linked nhECM scaffold exhibited desirable mechanical behavior that mimicked the native neonatal myocardium, with similar extensibility and slightly smaller stiffness and mechanical strength. An interesting observation was the lack of mechanical properties of the dry cross-linked nhECM scaffold and the fact that the cross-linked nhECM scaffold could gain mechanical strength and properties after rehydration. As shown in the swelling ratio study, we observed the morphological swelling at macroscopic level and ultrastructural level in the cross-linked nhECM scaffold. The mechanism of this mechanical discrepancy between dry status and rehydrated status could possible relate to the morphological difference between the dry cross-linked nhECM scaffold and the rehydrated cross-linked nhECM scaffold, with later had a more gel-like ultrastructure. The swelling of individual fibers might make certain binding and chain interaction feasible and hence confer better mechanical behavior. The porous gel-like ultrastructure might also favor cell infiltration and proliferation, which was validated in HL-1 cardiomyocytes cytotoxicity experiment.

Future studies will involve fine-tuning the ultrastructural and mechanical properties of the rehydrated cross-linked nhECM scaffold, performing more detailed cell experiments, and testing the therapeutic function of the cross-linked nhECM cardiac patch using small animal model.

3.5 Conclusion

Our study demonstrated that cardiac patch scaffold could be fabricated by electrospinning technique using pure nhECM. **(1)** We have determined the concentration of nhECM that yielded a scaffold with intact nanofibers and was able to be effectively cross-linked. The optimal concentration for nhECM was 50 mg/ml and the best cross-linking protocol was 50 mM EDC in 100% acetonitrile solvent. **(2)** We successfully cross-linked the nhECM cardiac patch and analyzed fiber morphology and mechanical properties at dry status and rehydrated status. It was observed that, although the material had weak mechanical properties at dry status, upon rehydration the cross-linked nhECM scaffold could gain much desirable mechanical strength and properties, mimicking the native neonatal myocardium. **(3)** We also proved the cross-linked nhECM scaffold is composed of non-denatured collagen and is hydrophilic and biocompatible, as shown by active cardiomyocyte survival and proliferation after reseeding. We assessed the cell viability via live/dead assay and cell proliferation via MTS assay. Both studies concluded that there was significant growth of the HL-1 cells from Day 1 to Day 5. In short, our major findings established a solid foundation for engineering pure nhECM-electrospun cardiac patch for MI treatment. This proof-of-concept study will be further investigated, and the therapeutic function of the cross-linked nhECM cardiac patch will be tested by future *in-vivo* animal experiments.

CHAPTER IV

IV. Fabricating and Characterizing Porcine nhECM-Based Hydrogel as a Cardiac Injection Material

4.1 Introduction

Hydrogels have emerged as a promising option for the treatment of MI [27, 28, 50, 51, 100, 101]. Injectable hydrogels can be delivered to the injured heart with minimally invasive procedures, such us catheter delivery, which makes it an attractive approach due to its minimally invasive profile. In the past ten years, there have been many studies on the development and characterization of injectable hydrogels for treating various diseases. For instance, hydrogels were used as drug delivery systems for the cancer treatment [102]. Moreover, injectable hydrogels were used in bone and meniscus repair [101, 103, 104]. Most recently, injectable hydrogels were developed and delivered to MI scar tissue and reached to small animal validation (rodent model), large animal validation (pig and ovine model), and early clinical study. [27, 50, 51, 56-60]

In the area of cardiac tissue engineering there have been studies using hydrogels fabricated from pure cardiac ECM [26] or hybrid compositions with cross-linkers like genipin to induce endothelial differentiation from mesenchymal stem cells [105]. As we mentioned above, the feasibility of adult porcine cardiac ECM hydrogel has been studied both *in-vitro* and *in-vivo* with small and large animal models [57-60]. In 2019, the first *in-vivo* human study of an injectable hydrogel derived from porcine adult ECM, VentriGel, was conducted in patients that had suffered a MI [27]. The study was part of phase one clinical study for this injectable hydrogel. In the study, fifteen patients were treated with VentriGel. The first objective of the study was the study of the safety and feasibility of a single dose hydrogel delivery via transendocardial injections, and the second objective was to find out the efficacy of the treatment. The results proved the safety and feasibility of the hydrogel and showed improvements in 6-min walk test distance for patients [27].

Although further evaluation is still required to prove the safety and efficacy, this is an encouraging step in the research of cardiac ECM hydrogels for the treatment of MI patients.

Similar to the approach taken in the development of a porcine adult ECM injectable hydrogel, we further innovated the hydrogel design by focusing on the development of an injectable hydrogel based on porcine neonatal heart ECM (nhECM). This is a novel approach that has the potential to leverage the regenerative potential of the neonatal cardiac ECM, which has been verified in previous study and our recent neonatal pig model research.

The neonatal ECM has been proven to promote cardiomyocyte proliferation. In an *in vitro* study by Williams et al, [37] the team studied how the cardiac ECM regulated cardiomyocyte proliferation at various developmental stage. They analyzed the effects of fetal, neonatal, and adult ECM obtained from rats and found that the fetal and neonatal cardiac ECM had greater effect on cardiomyocyte proliferation. Furthermore, in an *in-vivo* study by Wang et al, [38] they investigated how the cardiac ECM derived from neonatal mouse could help prevent ventricular remodeling in adult rats. They observed significant improvement in cardiac function and scar limitation after applying neonatal cardiac ECM to MI when compared to adult cardiac ECM.

The above mentioned studies have been conducted using hearts from small animals like mice and rats. Our recent *in vivo* study on porcine neonatal heart regeneration further point out the importance of structural and mechanical cues of neonatal heart ECM in guiding cardiac full regeneration. As we mentioned in section 1.3, our in vivo neonatal pig model research demonstrated that the piglets would lose the fully regenerative potential by 7 days after birth, but

greatly preserve the regenerative potential within 1 day of birth. For these reasons, we hypothesized that the injectable hydrogel manufactured from nhECM could possibly provide biomechanical and biological cues that promote cardiac regeneration at the MI injury site. We hence proposed to develop an effective protocol to reliably fabricate nhECM-based hydrogel, so that the injectable hydrogel could leverage the benefits of neonatal heart ECM and better promote cardiac repairing. Structural and rheological tests, along with cell viability assays were performed to determine the structure and porosity of nhECM hydrogel, gelation kinetics, and the biocompatibility and cell growth potential.

4.2 Materials and Methods

4.2.1 Hydrogel Fabrication

Porcine neonatal hearts were harvested as described in section 2.2.1. The left and right ventricle were dissected and cut into thin slices. The slices were then prepared for decellularization. A 1% SDS solution is prepared. The tissue was first rinsed with DI water for 3 hours with DI water change every hour. The decellularization was performed under constant stirring in the 1% SDS solution for 4 to 5 days until the slices completely turned into translucent white color. The solution was changed after 8 hours the first day and every 24 hours after that. Once decellularization achieved, the acellular tissue was rinsed in DI water for 24 hours with the DI water being changed at least 5 times. The decellularized nhECM was frozen overnight and then lyophilized. The lyophilized, powdered nhECM was digested in a 1 mg/ml of HCL/pepsin solution as previously described.[51, 106] The mixture was then neutralized with 0.1 M NaOH and 10X PBS, and

brought to pH-7.4 value. Final concentration was achieved by adding 1X PBS. The digested solution is then placed in mold and store at 37 ^{o}C for 30 minutes for gel formation.

4.2.2 Morphological Characterization

In order to characterize the structure of hydrogel, SEM images were taken to assess porosity and surface topography. Three groups of hydrogels were prepared and compared, collagen (2mg/ml), nhECM (10mg/ml), adult heart ECM (ahECM) (10 mg/ml). Hydrogels were prepared as described in section 4.2.1. After the formation of hydrogels, they were submerged in liquid nitrogen and broken into smaller pieces while in frozen status. Immediately, they were placed in the lyophilizer. After achieving full lyophilization, the samples were prepared for SEM imaging. Samples were sputter coated by gold/platinum target using Hummer VI sputtering system for one minute prior to SEM imaging. Images were then taken using a scanning electron microscope (SEM) (Hitachi S-4800 II FE-SEM). Fiber diameters and pore sizes were measured using ImageJ (NIH).

4.2.3 SDS-Page

SDS-Page separates the proteins and allows them to migrate through the gel pad during electrophoresis. This procedure was conducted to assess the protein bands of collagen, nhECM, and ahECM hydrogel groups. Solubilized collagen, nhECM, and ahECM pre-gel solutions were analyzed by SDS-PAGE. The solutions were run on a polyacrylamide gel (Bio-Rad) in

Tris/glycine/SDS buffer and analyzed using gel electrophoresis. The gel was then stained with Coomassie Brilliant Blue and prepared for imaging.

4.2.4 Gelation Kinetics

The gelation properties of the hydrogels were evaluated turbidometrically. The pre-gel solutions for collagen (2 mg/ml), nhECM (10 mg/ml), and ahECM (10 mg/ml) were prepared and distributed in a 96-well plate maintained cold over ice. For each group, 100 µl pre-gel solution per well was added (n=6) and placed in the Infinite M200 plate reader (Tecan, UK). The spectrometer was pre-heated to 37^{o}C, and the absorbance was measured at 405 nm every two minutes for sixty minutes. The readings were normalized for absorbance. The normalized absorbance was then used in (Equation 1) [100, 101, 107]

$$NA = \frac{A - A_o}{A_{max} - A_o} \quad (1)$$

NA = Normalized Absorbance

A = Absorbance at a given time

A_o = Initial absorbance

A_{max} = Maximum absorbance

The time of half gelation ($t_{1/2}$) was defined as the time at 50% absorbance. Gelation rate was define as the slope of the linear region of the gelation curve. The lag time (t_{lag}) was defined as the intercept of the linear region of the gelation curve with 0% absorbance, obtained by extrapolating the linear fit. [107]

4.2.5 Rheological Properties

The mechanical properties of the hydrogels were assessed using a rheometer. Rheological and viscometric measurements were made using Anton Paar Rheometer with a 150 mm parallel plate system with a 0.5 mm gap. Three groups, collagen gel (2mg/ml), nhECM hydrogel (10 mg/ml), and ahECM hydrogel (10 mg/ml), were measured and compared. The pre-gel solution was prepared for each group as described in section 4.2.1. The rheometer plate was maintained at 8^{o}C when the pre-gel solution was loaded. Approximately 1.5 ml of pre-gel solution was loaded for each test. The gap to enclose the pre-gel solution into the parallel plate system was set to 0.5 mm, and the temperature was then set to 37^{o}C to allow for gelation, which took place in approximately 30 minutes. For each group (n=3), the storage modulus (G') and loss modulus (G'') were calculated by an amplitude sweep at a frequency of 1 rad/s or 0.16 Hz.

4.2.6 *In-vitro* Cell Culture

Cell culture was performed using HL-1 cardiomyocytes. The cardiomyocytes were cultured in prepared Claycomb media as previously described [86] until approximately 90% confluency. Pre-gel solution for each comparative group, i.e., TCP, Collagen (2mg/ml), nhECM (10mg/ml), ahECM (10 mg/ml), were added to 96-well plate (n=6) with an amount of 50 µl per well. The plate was incubated at 37°C and 5% CO overnight. After incubation, each well was washed with 1X PBS, and HL-1 cells were seeded on the hydrogels at a density of 10,000 cells per well.

Live/dead assay (Invitrogen) was performed at Day 1 and Day 5 to assess cell viability. MTS assay was used to assess cell proliferation at Day 1, Day 4, and Day 7.

4.2.7 Statistical Analysis

Data were reported as the mean ± standard deviation (SD), where a p-value less than 0.05 was considered as statistically significant. One way ANOVA with post-hoc Tukey test was performed to quantify the statistical significance for group comparison.

4.3 Results

4.3.1 Fabrication of nhECM hydrogel

The nhECM hydrogel was prepared from porcine neonatal heart ECM. The porcine neonatal hearts were obtained from a local farm in Mississippi and shipped overnight as described in the previous section. Figure 34 showed the major fabrication steps, covering native neonatal heart to dissection, to decellularization (with histological verification), to powderization, to gel formation.

After comparative analysis using different concentrations and determining which concentration provided highest cell viability, we identify that the nhECM hydrogel with a 10 mg/ml concentration was most promising and hence performed fully characterizations at this concentration. As shown in Figure 35, we examined the cell proliferation (HL-1 cardiomyocytes) at Day 1 and Day 5 for

three nhECM concentrations (5 mg/ml, 10 mg/ml, and 20 mg/ml), and found that the lower concentration at 5 mg/ml and the higher concentration at 20 mg/ml did not proliferate as good as 10 mg/ml nhECM. On the other hand, the 10 mg/ml nhECM had 116% cell proliferation after five days of culturing.

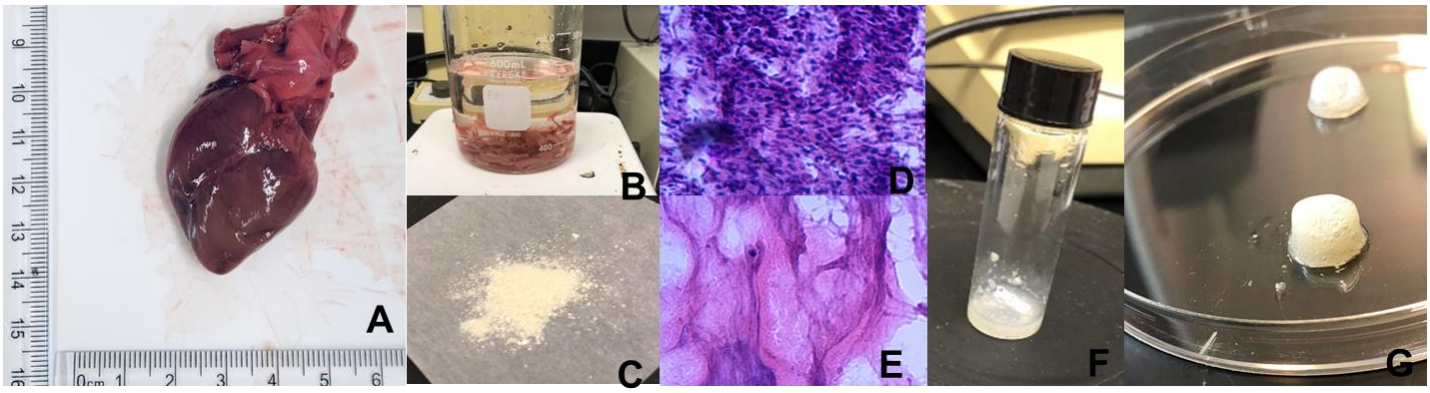

Figure 34: Fabrication of porcine neonatal ECM hydrogel. (A) Porcine neonatal heart. (B) Dissected porcine neonatal myocardium in 1% SDS solution. (C) Lyophilized nhECM Matrix. H&E staining of (D) native porcine neonatal myocardium and (E) acellular porcine neonatal heart ECM. (F) Digested pre-gel solution. (G) Formed nhECM hydrogel.

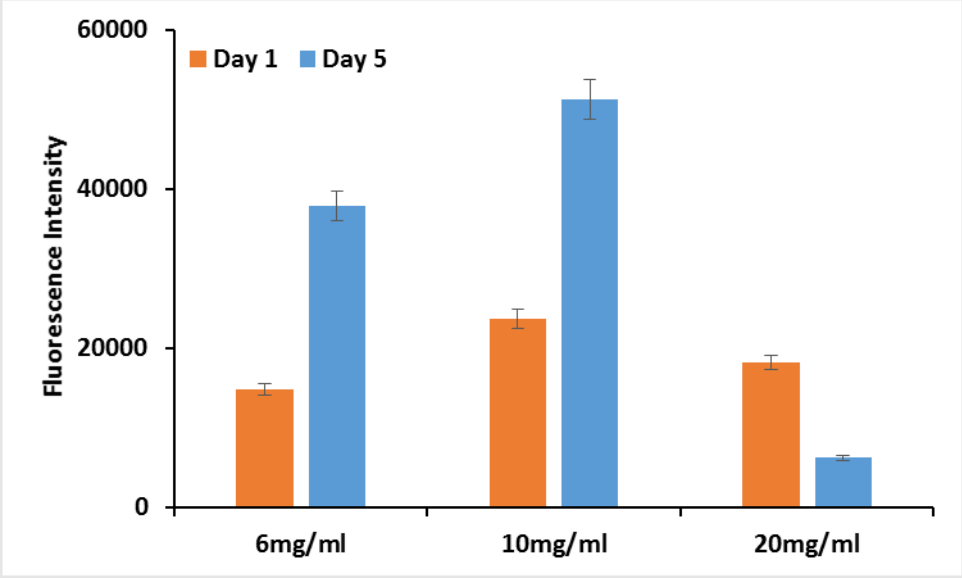

Figure 35: Cell proliferation results from HL-1 cells-seeded nhECM hydrogels at different concentrations to identify hydrogel protocol with optimal biocompatibility/cell proliferation support.

4.3.2 Morphological Characterization

The structure of the hydrogels was assessed via SEM imaging. The three groups, collagen, nhECM, and ahECM all showed a porous structure with interconnectivity. The fiber structure aligned with a random orientation and was formed from the reassembled collagen. Figure 36 showed the morphologies of all three groups at 1,000X and 10,000X magnification. Average diameter of the fibers on each group was presented in Table 5. The ahECM has the higher diameter at ~1 µm, closely followed by the nhECM at a diameter of ~0.97 µm. The collagen gel had the smallest fiber diameter at ~0.63 µm. Fiber diameter distribution for each group was shown in Figure 37.

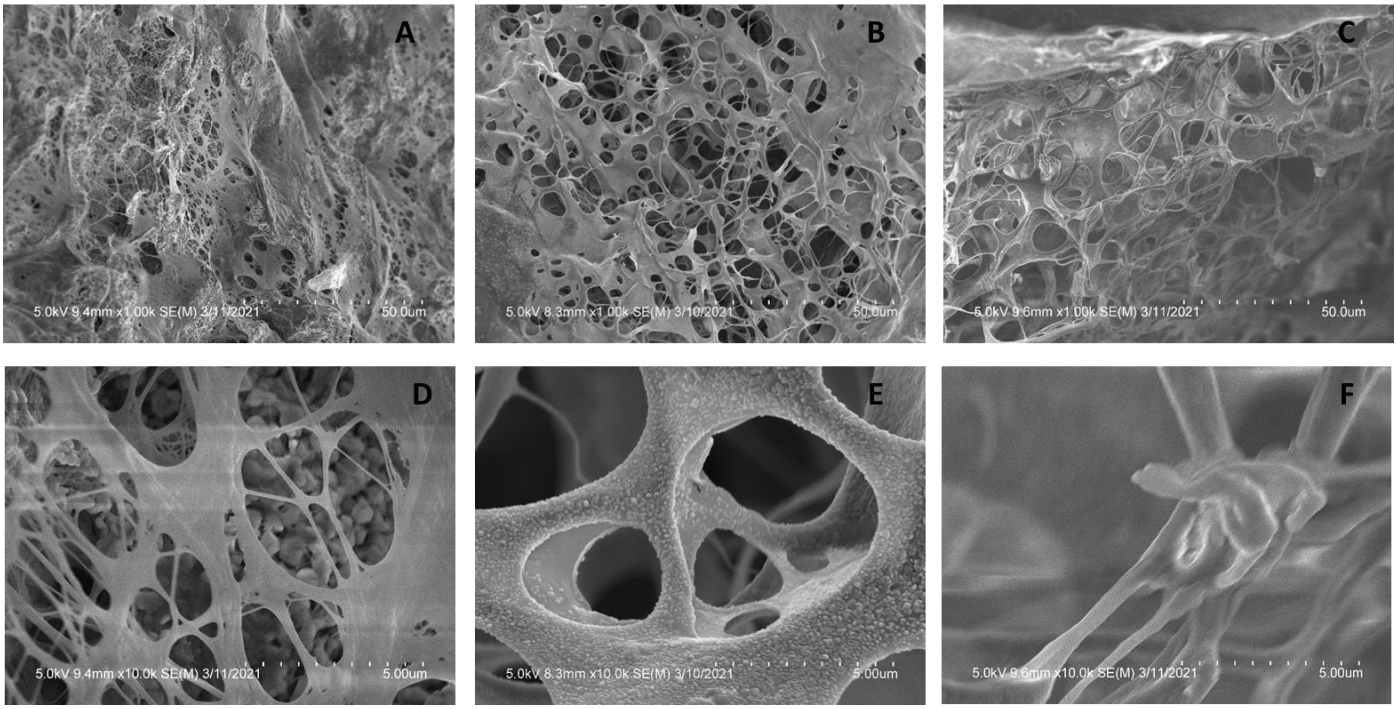

Figure 36: SEM micrographs of collagen hydrogel at 1,000X magnification (A) and 10,000X magnification (D), nhECM hydrogel at 1,000X magnification (B) and 10,000X magnification (E), and ahECM hydrogel at 1,000X magnification (C) and 10,000X magnification (F).

Table 5: Average fiber diameter of collagen, nhECM, and ahECM hydrogels

	Diameter (µm)	Standard Deviation (+/-)
Collagen	0.63	0.50
nhECM	0.97	0.53
ahECM	1.00	0.52

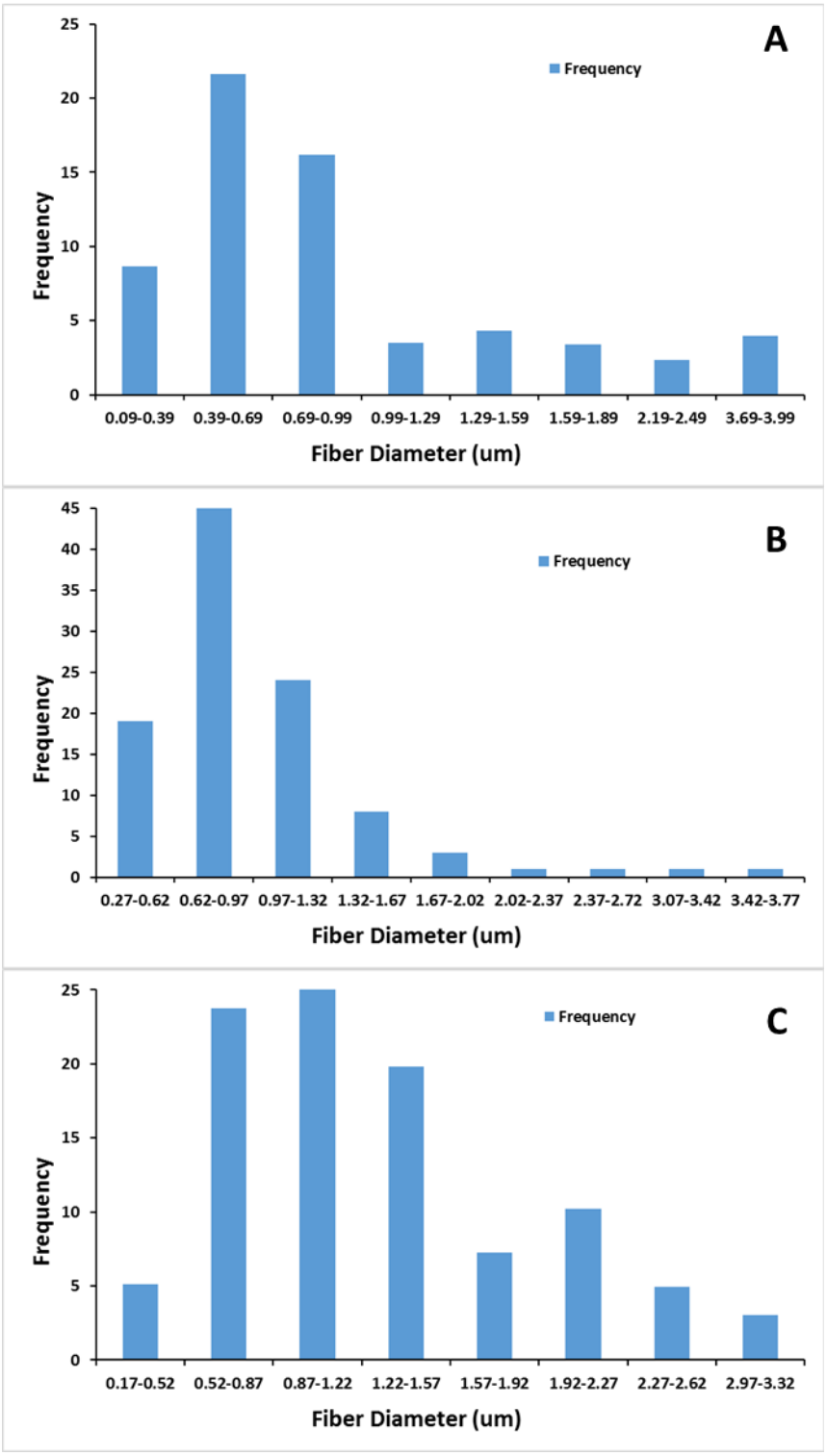

Figure 37: Fiber diameter distribution of (A) collagen hydrogel, (B) nhECM hydrogel, and (c) ahECM hydrogel.

3.3 Gelation Kinetics

The turbidimetric gelation kinetic of all three groups (collagen hydrogel, nhECM hydrogel, and ahECM hydrogel) all showed a sigmoidal shape (Figure 38A). We found that the collagen hydrogel had the smallest t_{lag} (4 min) when compared to the nhECM hydrogel (8 min) and ahECM hydrogel (10 min) (Figure 38B). The gelation rate was fastest for the collagen hydrogel, and the gelation rate of nhECM hydrogel was higher than the ahECM hydrogel (Figure 38C). However, the time to reach half maximum absorbance was not significantly different between nhECM hydrogel and ahECM hydrogel (Figure 38D).

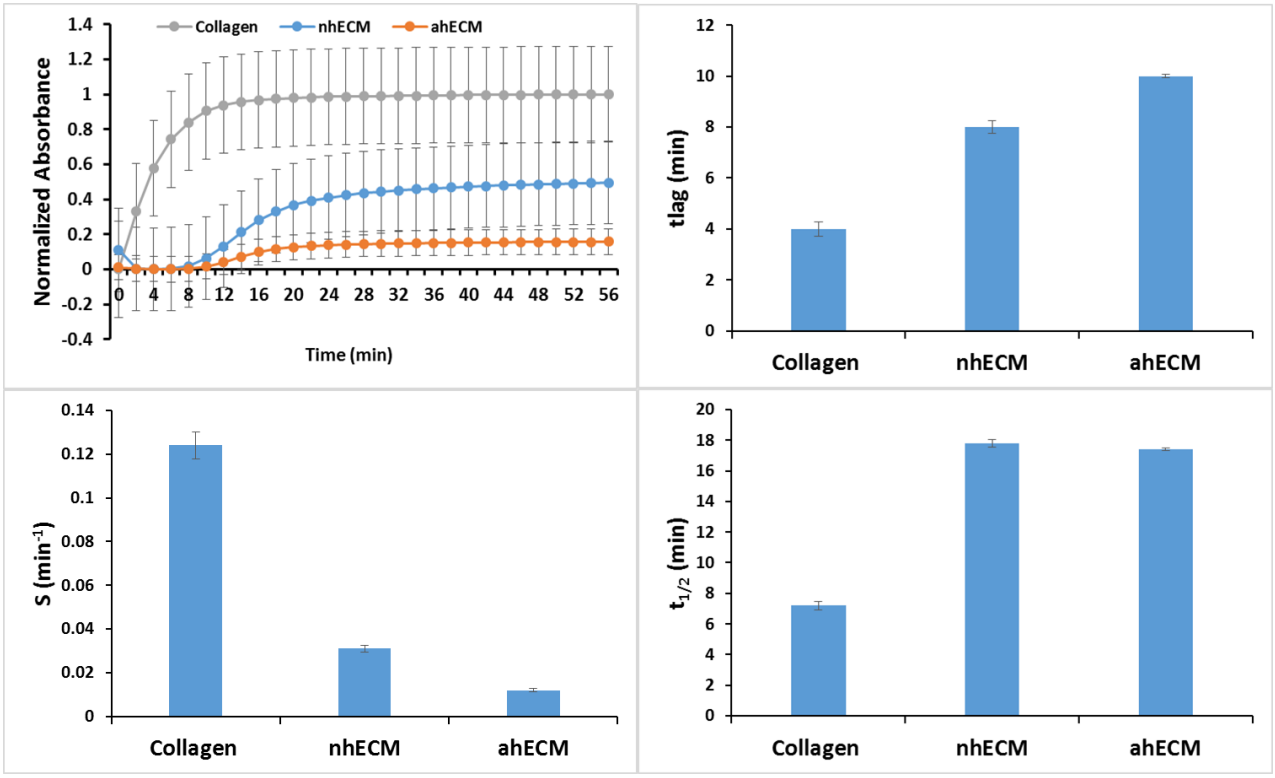

Figure 38: (A) Turbidimetric gelation curves of collagen hydrogel, nhECM hydrogel, and ahECM hydrogel. (B) Comparison of lag time, (B) gelation rate, and (D) time to reach half gelation.

4.3.4 SDS-Page

SDS-Page was conducted with the pre-gel solutions of collagen, nhECM, and ahECM. The collagen pre-gel solution had stronger protein concentration in the 200-100 kDA bands, which was expected from pure collagen. We also noticed that the nhECM hydrogel and ahECM hydrogel showed similar bands and band intensities (Figure 39).

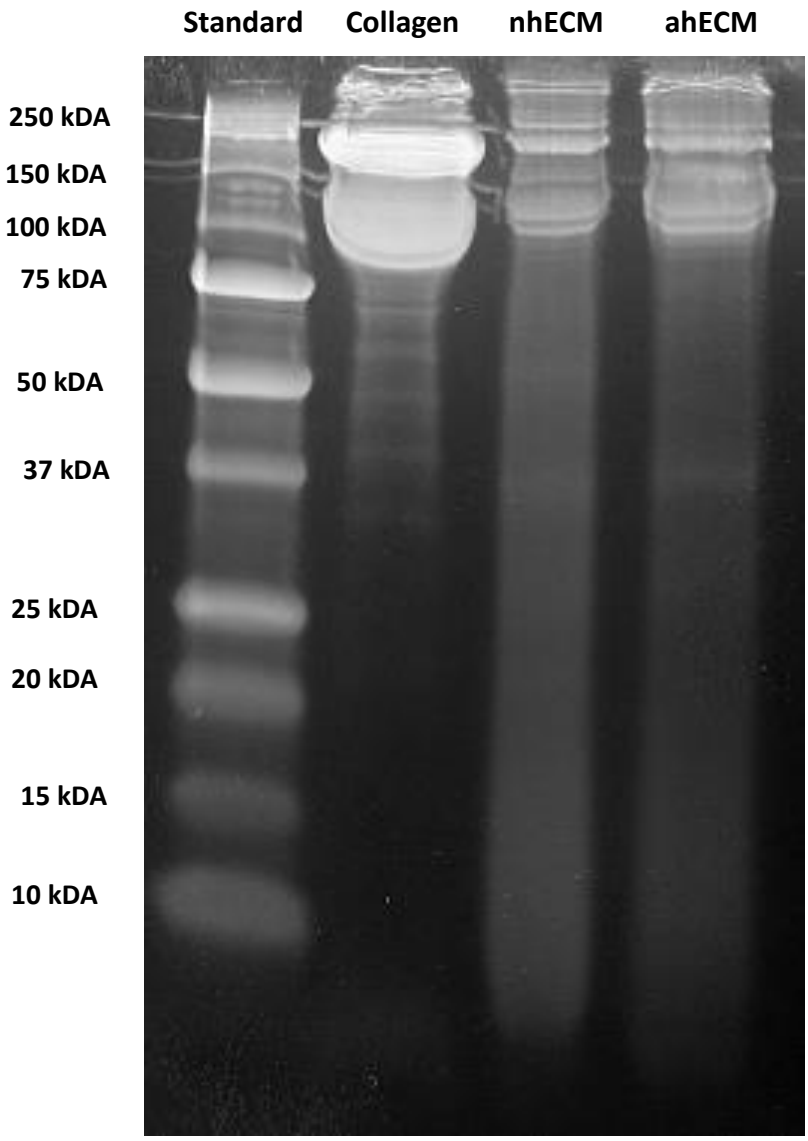

Figure 39: SDS-PAGE from pre-gel solution for collagen, nhECM, and ahECM hydrogels showing protein size and distribution.

4.3.5 Rheological Properties

Rheological results of collagen hydrogel (2 mg/ml), nhECM hydrogel (10 mg/ml), and ahECM hydrogel (10 mg/ml) were obtained using an Anton Paar Rheometer (Figure 40). An amplitude sweep at a constant frequency of 1 rad/s was conducted for all samples (n=3) to determine the storage modulus of the hydrogel. The hydrogels all exhibited a viscoelastic gel-like behavior. The linear viscoelastic region (LVER) was observed between 0.1 and 1% strain. For estimating the storage modulus value in LVER, we used a 0.5% strain across all groups. Figure 40 showed the relationships between the storage modulus and the shear strain for the three tested groups. Table 6 summarized the storage modulus (G') of all three groups in the LVER region. We found that the ahECM hydrogel had the largest storage modulus (~171.3 Pa), and the nhECM had a storage modulus (~12.7 Pa) lower than collagen (42.1 Pa), consistent with the fact collagen in nhECM might be still in early developmental stage (Table 6).

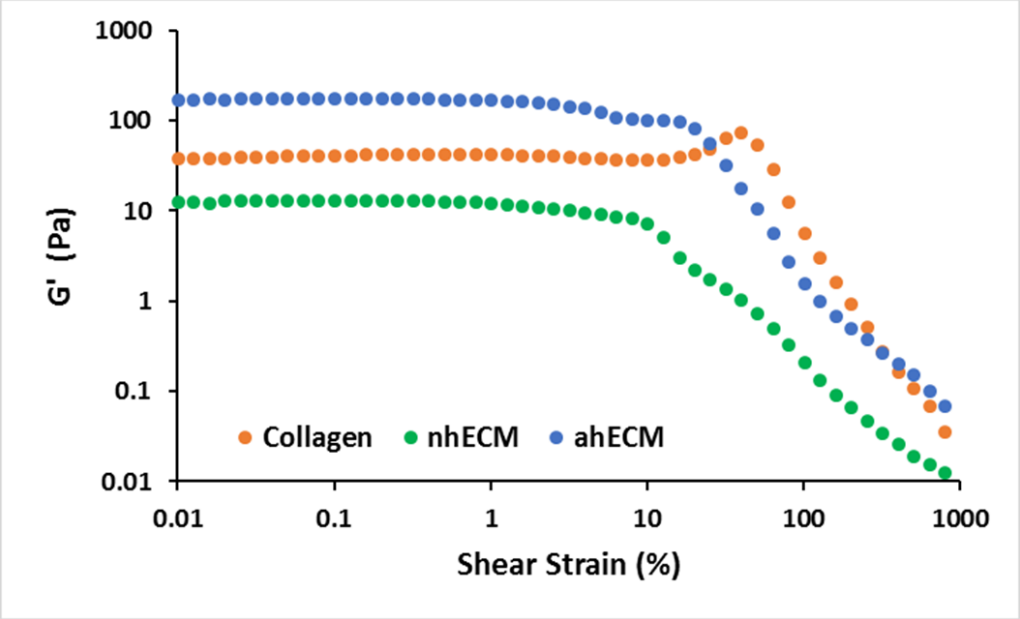

Figure 40: The relationships between the storage modulus and the shear strain for collagen hydrogel, nhECM hydrogel, and ahECM hydrogel.

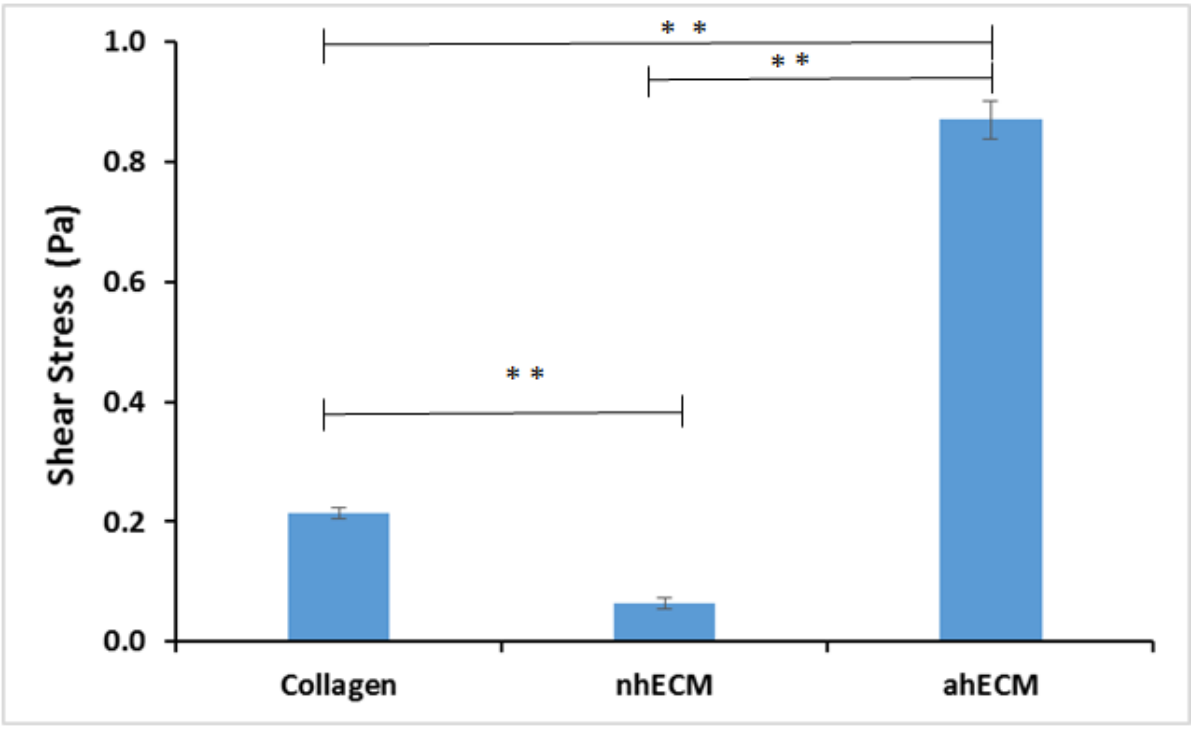

Figure 41: Shear stress (Pa) of collagen, nhECM, and ahECM hydrogels

Table 6: Storage modulus value for collagen hydrogel, nhECM hydrogel, and ahECM hydrogel at 5% strain in the LVER

	G' (Pa)	Standard Deviation (+/-)
Collagen	42.1	0.01
nhECM	12.7	0.01
ahECM	171.3	0.03

4.3.4 In-vitro cell culture assessment

The cell viability was assessed using live/dead assay (Invitrogen), and cell proliferation was assessed with MTS assay (Promega). We found that the nhECM hydrogel supported survival and proliferation of the HL-1 cardiomyocytes in our culture conditions. We first did a preliminary study to compare collagen hydrogel, nhECM hydrogel, and ahECM hydrogel at Day 1 and Day 5. We observed successful cell attachment and proliferation among all there hydrogel groups, as indicated by the live/dead assessment (Figure 42) and the MTS cell proliferation assay (Figure 43).

In order to further assess the nhECM hydrogel and compare with collagen hydrogel and ahECM hydrogel, we conducted a three time point study at Day 1, Day 4, and Day 7. The live/dead assay confirmed cell growth up to Day 7 (Figure 44). MTS cell proliferation assay showed that the nhECM hydrogel group had a significant growth trend from Day 1, Day 4, to Day 7 (Figure 45). Moreover, nhECM hydrogel was able to achieve an overall growth trend similar to collagen gel and slightly better than hem hydrogel at Day 7 (Figure 45).

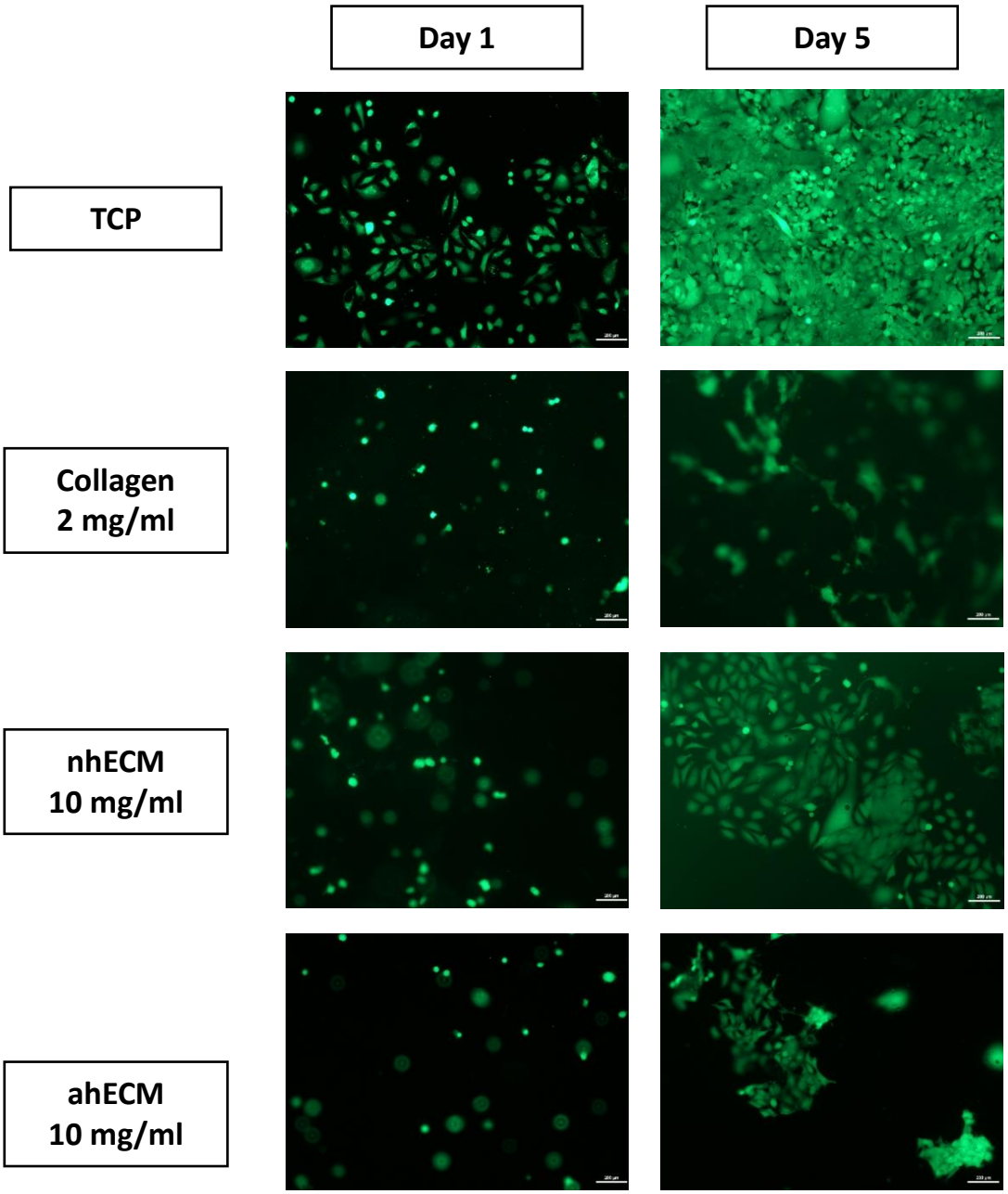

Figure 42: Fluorescent images of live/dead stain for TCP, collagen hydrogel, nhECM hydrogel, and ahECM hydrogel at Day 1 and Day 5.

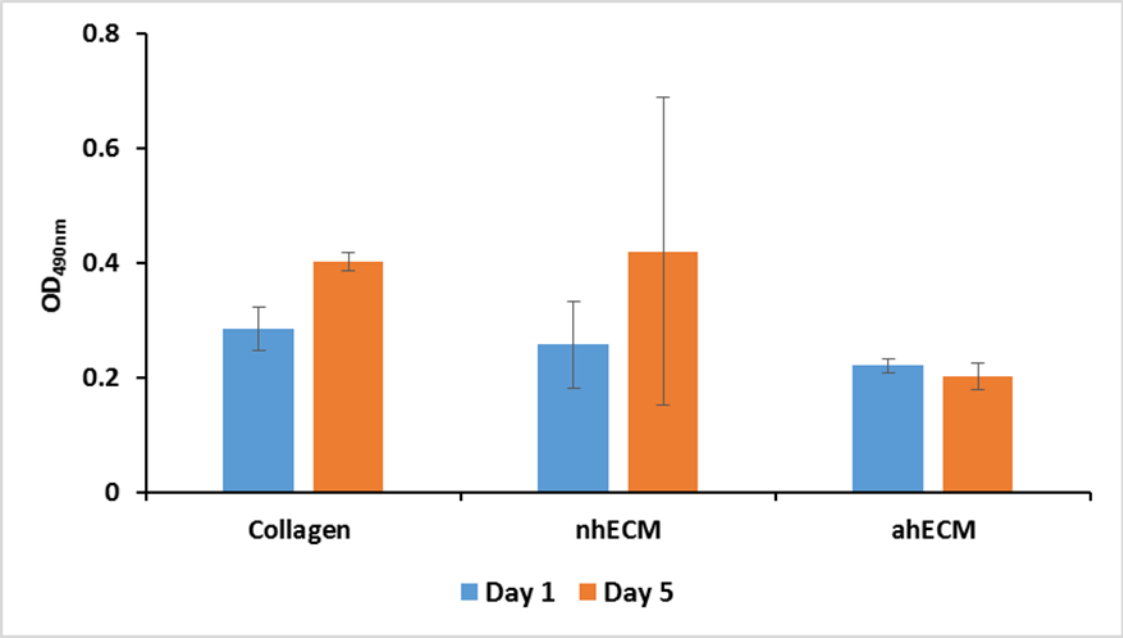

Figure 43: Cell proliferation results from HL-1 cells on collagen hydrogel, nhECM hydrogel, and ahECM hydrogel at Day 1 and Day 5.

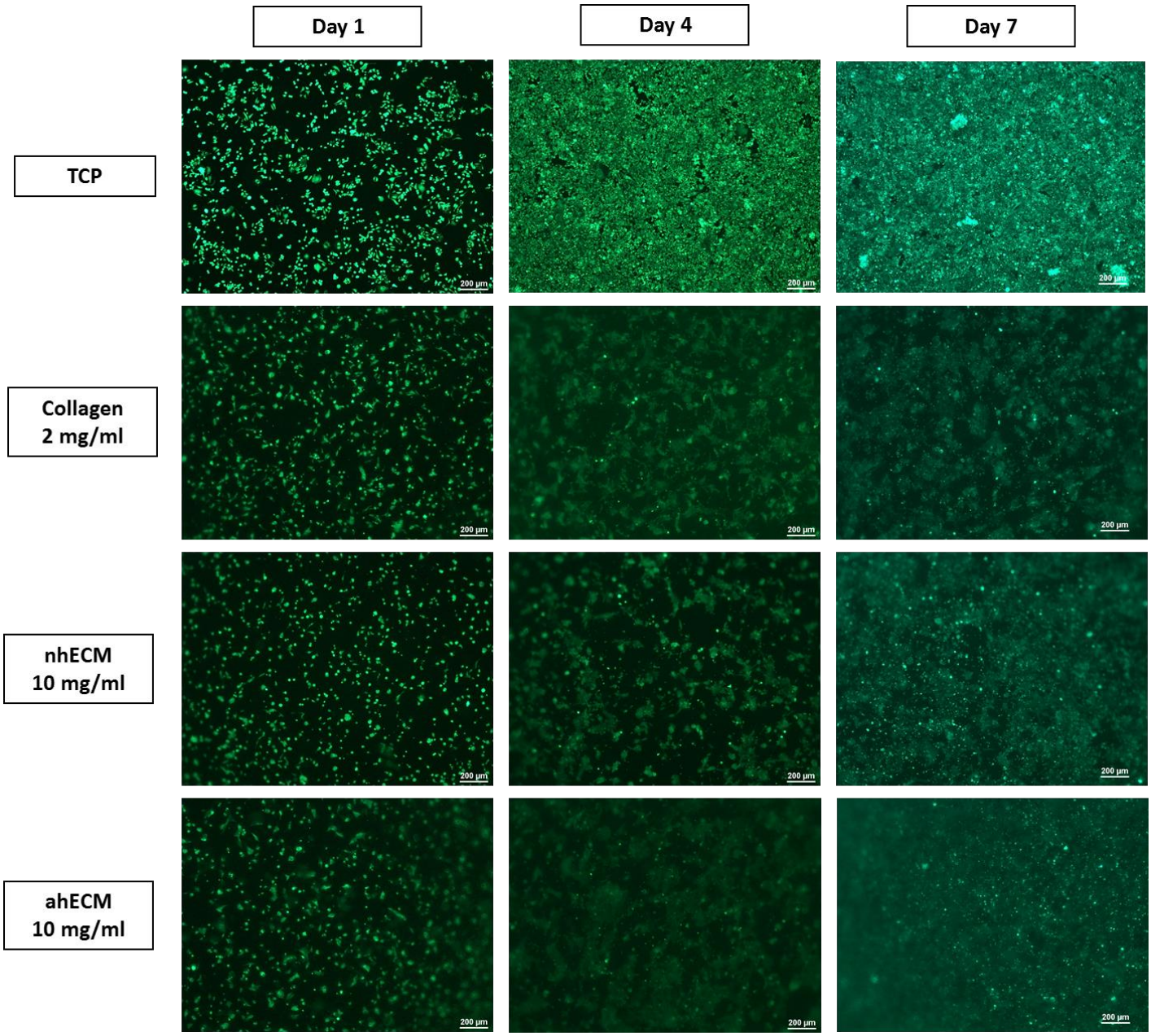

Figure 44: Fluorescent images of live/dead stain for TCP, collagen hydrogel, nhECM hydrogel, and ahECM hydrogel at Day 1, Day 4, and Day 7.

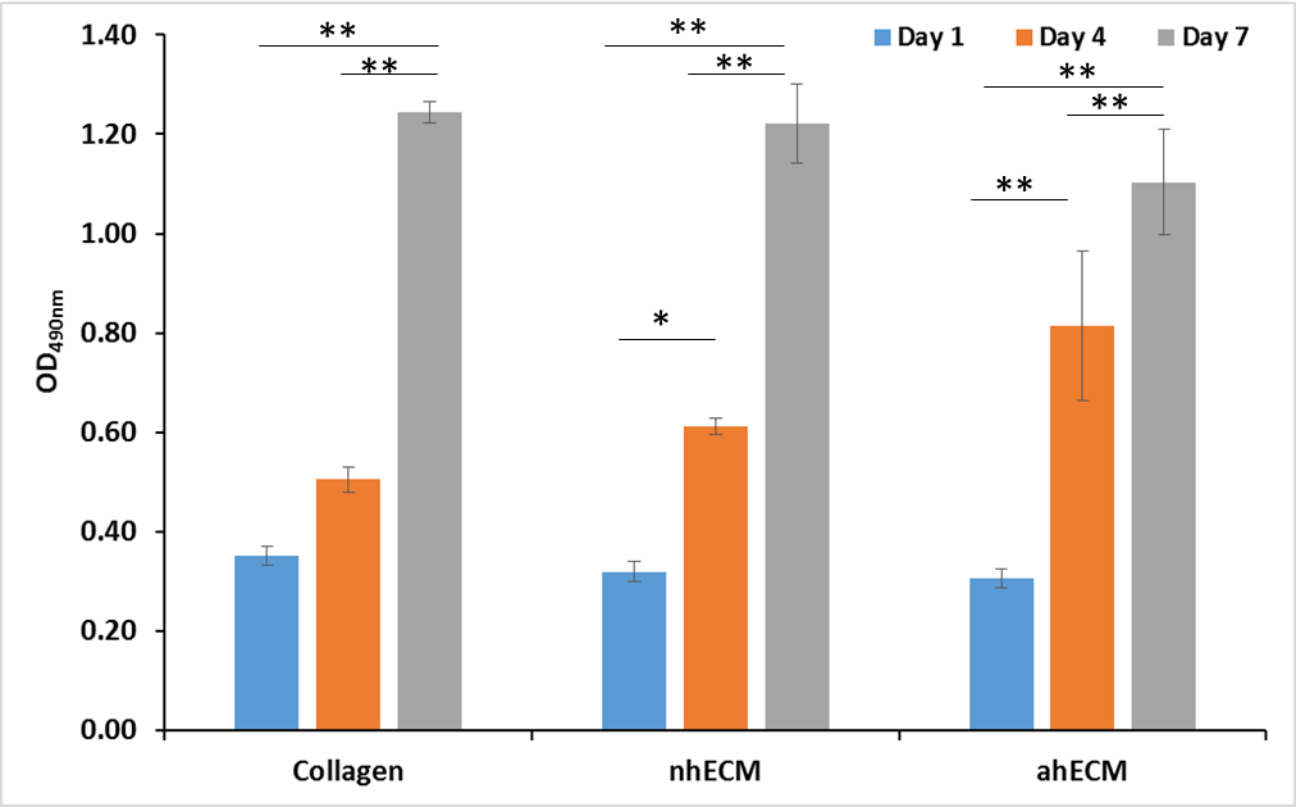

Figure 45: Cell proliferation results from HL-1 cells on collagen hydrogel, nhECM hydrogel, and ahECM hydrogel at Day 1, Day 4, and Day 7.

4.4 Discussion

In this study, we successfully fabricated nhECM hydrogel and performed full characterization on nhECM hydrogel with 10 mg/ml concentration. To better understand the performance of the nhECM hydrogel, collagen hydrogel (2mg/ml) and ahECM hydrogel (10mg/ml) were used as comparisons to test the hypothesis that the 0-day neonatal heart ECM microenvironment, with biomechanical and biological cues, could be used as a potential injectable hydrogel for MI treatment. Our experiments verified that we were able to establish a reliable protocol to fabricate nhECM hydrogel, which had excellent gel integrity, ultrastructure, rheological properties, and biocompatibility to support cell attachment and proliferation. All those results prove that the nhECM is a viable alternative for hydrogel-based MI treatment and is worthy of further exploration.

The observed differences among collagen hydrogel, nhECM hydrogel, and ahECM hydrogel provide insights and point future directions to improve the function of nhECM hydrogel. A major difference in our nhECM was the mechanical properties of this novel hydrogel when compared with the collagen hydrogel and ahECM hydrogel. Although all three groups exhibited a gel-like viscoelastic behavior, they did exhibit different storage modulus. From our rheological measurement, the storage modulus of nhECM hydrogel (12.7 Pa) was smaller than the collagen hydrogel (42.1 Pa), and much smaller than the ahECM hydrogel (171.3 Pa), which reflected the developmental stage of neonatal heart. In a study by Ramadan et al, [108] they reported a storage modulus of ~60 kPa for the porcine native myocardial tissue. As an interesting confirmation, it was reported that myocardial matrix hydrogel had a storage modulus of 5-10 Pa. [109] The storage modulus (12.7 Pa) we measured from nhECM hydrogel fell into this range (5-

10 Pa). [109] Nevertheless, during the treatment of MI, mechanical supporting can possibly be a factor and future fun-tuning of the hydrogel elasticity might be needed. It has been reported that the storage modulus can be increased with an increase in ECM concentration [110, 111]. Another way to improve the mechanical properties of the nhECM could be to include nanoparticles when fabricating the hydrogel.

The nhECM hydrogel was proven to be biocompatible and promoting cardiomyocyte proliferation. In our preliminary study on Day 1 and Day 5, we observed significantly more cardiomyocyte proliferation with the nhECM hydrogel when compared to the ahECM hydrogel. In Day 1, Day 4, and Day 7 study, this trend was further verified, i.e., the nhECM hydrogel showed higher growth from Day 4 to Day 7 when compared to the ahECM hydrogel. These results showed to be congruent with the findings from other studies, in which higher cell growth took place in neonatal scaffold when compared to adult scaffold. [38]

To the best of our knowledge, this is the first work that develops an ECM hydrogel from porcine neonatal heart ECM. Future developments will be to investigate the application of stem cells in nhECM hydrogel, which is more clinically relevant. The stem cell encapsulation, cell-nhECM hydrogel interaction, cell differentiation, repairing/remolding, and angiogenesis potential would be topics worthy of investigation. Moreover, as we mentioned above, hydrogels for MI treatment might experience functional challenge due to its low mechanical stiffness and strength. Other challenges are the inability to carrying electrical signals and scalable production with high reliability. Those challenges could be studied and addressed by the development of hybrid techniques that increase strength and conductivity via nanoparticle inclusion [27, 53, 112]

4.5 Conclusion

We have successfully developed an effective protocol to reliably fabricate nhECM hydrogel. The nhECM hydrogel showed a porous structure with interconnectivity and a fiber diameter (~0.97) μm closed to ahECM (~1 μm). From SDS-PAGE, we found that the nhECM hydrogel had protein bands and band intensities similar to the ahECM hydrogel. Gelatin kinetics showed that the gelation rate of nhECM hydrogel was higher than the ahECM hydrogel, while the time to reach half maximum absorbance was not significantly different from the ahECM hydrogel. The nhECM had a storage modulus lower than collagen hydrogel and ahECM hydrogel, consistent with the fact collagen in nhECM might be still in early developmental stage. We proved that the optimized nhECM hydrogel was biocompatible and promoting cardiomyocyte proliferation, with a better performance than ahECM hydrogel. All those results signify that the nhECM hydrogel could be a promising candidate for MI injectable hydrogel treatment. With all the strong proofs of porcine nhECM hydrogel as a potential injectable biomaterial, continued investigations such as fine-tuning hydrogel properties, stem cell-hydrogel interaction, and animal experiments would further build a solid foundation to move this novel nhECM hydrogel to translational applications.

CHAPTER V

V. Summary and Future Studies

5.1 Summary

We were able to decellularized the neonatal porcine myocardium and maintain its structure after decellularization. Moreover, we have successfully accomplished the mechanical, structural, and compositional characterizations of the nhECM. Our study demonstrated that the nhECM had a non-linear, anisotropic, and viscoelastic behavior. We also noticed that the nhECM showed an overall biaxial characteristic (non-linear, anisotropic) similar to the porcine native neonatal myocardial tissue, which signified nhECM's essential role in governing the passive mechanical properties of neonatal heart. Failure testing showed that the nhECM was significantly stiffer than the native neonatal myocardium. The higher stiffness in the nhECM could be attributed to the pure collagen scaffold makeup after removing soft cardiomyocyte components. Moreover, shear modulus of the nhECM was very low when compared to the ahECM. We found that the porcine ahECM had 60% higher collagen content than the porcine nhECM, while there was 55.4% more GAG content in the porcine nhECM when compared to the porcine ahECM. In short, when comparing the nhECM to the ahECM, we observed drastic differences in biomechanical, structural, and compositional properties, which strongly supports our hypothesis that the nhECM has its unique cues that likely promote cardiac tissue regeneration.

Our study demonstrated that cardiac patch scaffold could be fabricated by electrospinning technique using pure nhECM. (1) We have determined the concentration of nhECM that yielded a scaffold with intact nanofibers and was able to be effectively cross-linked. The optimal concentration for nhECM was 50 mg/ml and the best cross-linking protocol was 50 mM EDC in 100% acetonitrile solvent. (2) We successfully cross-linked the nhECM cardiac patch and analyzed fiber morphology and mechanical properties at dry status and rehydrated status. It was

observed that, although the material had weak mechanical properties at dry status, upon rehydration the cross-linked nhECM scaffold could gain much desirable mechanical strength and properties, mimicking the native neonatal myocardium. (3) We also proved the cross-linked nhECM scaffold is composed of non-denatured collagen and is hydrophilic and biocompatible, as shown by active cardiomyocyte survival and proliferation after reseeding. We assessed the cell viability via live/dead assay and cell proliferation via MTS assay. Both studies concluded that there was significant growth of the HL-1 cells from Day 1 to Day 5. In short, our major findings established a solid foundation for engineering pure nhECM-electrospun cardiac patch for MI treatment. This proof-of-concept study will be further investigated, and the therapeutic function of the cross-linked nhECM cardiac patch will be tested by future in-vivo animal experiments.

Lastly, we have successfully developed an effective protocol to reliably fabricate nhECM hydrogel. The nhECM hydrogel showed a porous structure with interconnectivity and a fiber diameter (~0.97) μm closed to ahECM (~1 μm). From SDS-PAGE, we found that the nhECM hydrogel had protein bands and band intensities similar to the ahECM hydrogel. Gelatin kinetics showed that the gelation rate of nhECM hydrogel was higher than the ahECM hydrogel, while the time to reach half maximum absorbance was not significantly different from the ahECM hydrogel. The nhECM had a storage modulus lower than collagen hydrogel and ahECM hydrogel, consistent with the fact collagen in nhECM might be still in early developmental stage. We proved that the optimized nhECM hydrogel was biocompatible and promoting cardiomyocyte proliferation, with a better performance than ahECM hydrogel. All those results signify that the nhECM hydrogel could be a promising candidate for MI injectable hydrogel treatment. With all the strong proofs of porcine nhECM hydrogel as a potential injectable biomaterial, continued

investigations such as fine-tuning hydrogel properties, stem cell-hydrogel interaction, and animal experiments would further build a solid foundation to move this novel nhECM hydrogel to translational applications.

5.2 Limitations and Future Work

Limitations of this study include sample variability from batch to batch due to variations in obtained 0-day neonatal porcine hearts. The obtained neonatal hearts varied in size and weight depending on the piglet size. Another limitation is the fact that this research is based on porcine model. Due to its close similarity to human heart in anatomy, mechanical properties, and ECM compositions, porcine model has been widely used for both basic research and translational applications, such as the use of porcine cardiac ECM hydrogel in human MI treatment. However, when we develop biomaterials from the porcine hearts and target translational application, there are always potential complications, such as immunogenicity and xenogeneic viral risk, which we will have to carefully address in future work.

For electrospun nhECM cardiac patch, future studies will involve fine-tuning the ultrastructural and mechanical properties of the rehydrated cross-linked nhECM scaffold, performing more detailed cell reseeding experiments, and testing the therapeutic function of the cross-linked nhECM cardiac patch using small or large animal model. For nhECM hydrogel, future developments will be to investigate the application of stem cells in nhECM hydrogel, which is more clinically relevant. The stem cell encapsulation, cell-nhECM hydrogel interaction, cell differentiation, repairing/remolding, and angiogenesis potential would be topics worthy of

investigation. Moreover, as we mentioned above, hydrogels for MI treatment might experience functional challenge due to its low mechanical stiffness and strength. Other challenges are the inability to carrying electrical signals and scalable production with high reliability. Those challenges could be studied and addressed by the development of hybrid techniques that increase strength and conductivity via nanoparticle inclusion. Lastly, the safety and therapeutic efficacy of nhECM-based hydrogel will be tested using small animal model (rat), as well as large animal model (pig).

REFERENCES

[1] E. J. Benjamin *et al.*, "Heart Disease and Stroke Statistics-2019 Update: A Report From the American Heart Association," *Circulation,* vol. 139, no. 10, pp. e56-e528, Mar 5 2019, doi: 10.1161/CIR.0000000000000659.

[2] C. D. Fryar, T. C. Chen, and X. Li, "Prevalence of uncontrolled risk factors for cardiovascular disease: United States, 1999-2010," (in eng), *NCHS Data Brief,* no. 103, pp. 1-8, Aug 2012.

[3] W. Raab, "The Nonvascular Metabolic Myocardial Vulnerability Factor in "Coronary Heart Disease": Fundamentals of Pathogenesis, Treatment, and Prevention," *Am Heart J,* vol. 66, pp. 685-706, 1963.

[4] G. Baroldi, "Acute coronary occlusion as a cause of myocardial infarct and sudden coronary heart death," *Am J Cardiol,* vol. 16, no. 6, pp. 859-880, 1965.

[5] G. Baroldi, "Coronary heart disease: significance of the morphologic lesions," *Am Heart J* vol. 85, pp. 1-5, 1973.

[6] F. Shaffer, R. McCraty, and C. L. Zerr, "A healthy heart is not a metronome: an integrative review of the heart's anatomy and heart rate variability," (in eng), *Front Psychol,* vol. 5, p. 1040, 2014, doi: 10.3389/fpsyg.2014.01040.

[7] W. C. Stanley, F. A. Recchia, and G. D. Lopaschuk, "Myocardial substrate metabolism in the normal and failing heart," (in eng), *Physiol Rev,* vol. 85, no. 3, pp. 1093-129, Jul 2005, doi: 10.1152/physrev.00006.2004.

[8] A. B. Aurora *et al.*, "Macrophages are required for neonatal heart regeneration," (in eng), *J Clin Invest,* vol. 124, no. 3, pp. 1382-92, Mar 2014, doi: 10.1172/jci72181.

[9] V. Deshmukh, J. Wang, and J. F. Martin, "Leading progress in heart regeneration and repair," (in eng), *Curr Opin Cell Biol,* vol. 61, pp. 79-85, Dec 2019, doi: 10.1016/j.ceb.2019.07.005.

[10] F. X. Galdos, Y. Guo, S. L. Paige, N. J. VanDusen, S. M. Wu, and W. T. Pu, "Cardiac Regeneration: Lessons From Development," (in eng), *Circ Res,* vol. 120, no. 6, pp. 941-959, Mar 17 2017, doi: 10.1161/circresaha.116.309040.

[11] M. Günthel, P. Barnett, and V. M. Christoffels, "Development, Proliferation, and Growth of the Mammalian Heart," (in eng), *Mol Ther,* vol. 26, no. 7, pp. 1599-1609, Jul 5 2018, doi: 10.1016/j.ymthe.2018.05.022.

[12] M. W. Bloom *et al.*, "Heart failure with reduced ejection fraction," *Nature Reviews Disease Primers,* vol. 3, no. 1, p. 17058, 2017/08/24 2017, doi: 10.1038/nrdp.2017.58.

[13] L. R. Erhardt, Unge, G. & Boman, G, "Formation of coronary arterial thrombi in relation to onset of necrosis in acute myocardial infarction in man. A clinical and autoradiographic study. ," *Am Heart J,* vol. 91, pp. 592-598, 1976.

[14] D. D. M. Reichenbach, N.S., " Myocardial cell necrosis and sudden death in humans. Circulation 52,

III60-62.," *Circulation,* vol. 52, pp. III60-III62., 1975.

[15] M. D. Silver, Anderson, T.W., Vand Dreumel, A.A. & Hutson, R.E, "Letter: Nutritional muscular

dystrophy and human myocardial infarction " *Lancet,* vol. 2, pp. 912-913, 1973.

[16] J. Narula, Haider, N., Virmani, R., DiSalvo, T.G., Kolodgie, F.D., Hajjar, R.J., Schmidt, U., Semigran, M.J., and G. W. K. Dec, B.A, "Apoptosis in myocytes in end-stage heart failure," *N Engl J Med,* vol. 335, pp. 1182-1189, 1996.

[17] E. D. Robin, "Special report: dysoxia. Abnormal tissue oxygen utilization," *Arch Intern Med,* vol. 137, pp. 905-910, 1977.

[18] J. P. Cleutjens, Blankesteijn, W.M., Daemen, M.J. & Smits, J.F. and [pii]). "The infarcted myocardium: simply dead

tissue, or a lively target for therapeutic interventions.," *Cardiovasc Res,* vol. 44, pp. 232-241, 1999, doi: doi:S0008-6363(99)00212-6.

[19] T. De Celle, Cleutjens, J.P., Blankesteijn, W.M., Debets, J.J., Smits, J.F. & Janssen, B.J. , "Long-term

structural and functional consequences of cardiac ischaemia-reperfusion injury in vivo in mice.," *Exp Physiol,* vol. 89, pp. 605-616, 2004.

[20] V. Sampaio-Pinto *et al.*, "Neonatal Apex Resection Triggers Cardiomyocyte Proliferation, Neovascularization and Functional Recovery Despite Local Fibrosis," (in eng), *Stem Cell Reports,* vol. 10, no. 3, pp. 860-874, Mar 13 2018, doi: 10.1016/j.stemcr.2018.01.042.

[21] M. Isomi, T. Sadahiro, and M. Ieda, "Progress and Challenge of Cardiac Regeneration to Treat Heart Failure," (in eng), *J Cardiol,* vol. 73, no. 2, pp. 97-101, Feb 2019, doi: 10.1016/j.jjcc.2018.10.002.

[22] R. S. Baker *et al.*, "In Vivo Remodeling of an Extracellular Matrix Cardiac Patch in an Ovine Model," (in eng), *Asaio j,* vol. 65, no. 7, pp. 744-752, Sep/Oct 2019, doi: 10.1097/mat.0000000000000864.

[23] D. Bejleri *et al.*, "A Bioprinted Cardiac Patch Composed of Cardiac-Specific Extracellular Matrix and Progenitor Cells for Heart Repair," (in eng), *Adv Healthc Mater,* vol. 7, no. 23, p. e1800672, Dec 2018, doi: 10.1002/adhm.201800672.

[24] J. Chen *et al.*, "Chitosan/silk fibroin modified nanofibrous patches with mesenchymal stem cells prevent heart remodeling post-myocardial infarction in rats," (in eng), *Acta Biomater,* vol. 80, pp. 154-168, Oct 15 2018, doi: 10.1016/j.actbio.2018.09.013.

[25] C. P. Jackman *et al.*, "Engineered cardiac tissue patch maintains structural and electrical properties after epicardial implantation," (in eng), *Biomaterials,* vol. 159, pp. 48-58, Mar 2018, doi: 10.1016/j.biomaterials.2018.01.002.

[26] D. Bejleri and M. E. Davis, "Decellularized Extracellular Matrix Materials for Cardiac Repair and Regeneration," (in eng), *Adv Healthc Mater,* vol. 8, no. 5, p. e1801217, Mar 2019, doi: 10.1002/adhm.201801217.

[27] J. H. Traverse *et al.*, "First-in-Man Study of a Cardiac Extracellular Matrix Hydrogel in Early and Late Myocardial Infarction Patients," (in eng), *JACC Basic Transl Sci,* vol. 4, no. 6, pp. 659-669, Oct 2019, doi: 10.1016/j.jacbts.2019.07.012.

[28] J. W. Wassenaar *et al.*, "Evidence for Mechanisms Underlying the Functional Benefits of a Myocardial Matrix Hydrogel for Post-MI Treatment," (in eng), *J Am Coll Cardiol,* vol. 67, no. 9, pp. 1074-1086, 2016, doi: 10.1016/j.jacc.2015.12.035.

[29] E. R. Porrello *et al.*, "Transient regenerative potential of the neonatal mouse heart," (in eng), *Science,* vol. 331, no. 6020, pp. 1078-80, Feb 25 2011, doi: 10.1126/science.1200708.

[30] K. D. Poss, L. G. Wilson, and M. T. Keating, "Heart regeneration in zebrafish," (in eng), *Science,* vol. 298, no. 5601, pp. 2188-90, Dec 13 2002, doi: 10.1126/science.1077857.

[31] Z. Wang *et al.*, "Mechanistic basis of neonatal heart regeneration revealed by transcriptome and histone modification profiling," (in eng), *Proc Natl Acad Sci U S A,* vol. 116, no. 37, pp. 18455-18465, Sep 10 2019, doi: 10.1073/pnas.1905824116.

[32] M. Xin, E. N. Olson, and R. Bassel-Duby, "Mending broken hearts: cardiac development as a basis for adult heart regeneration and repair," (in eng), *Nat Rev Mol Cell Biol,* vol. 14, no. 8, pp. 529-41, Aug 2013, doi: 10.1038/nrm3619.

[33] S. A. Jesty *et al.*, "c-kit+ precursors support postinfarction myogenesis in the neonatal, but not adult, heart," (in eng), *Proc Natl Acad Sci U S A,* vol. 109, no. 33, pp. 13380-5, Aug 14 2012, doi: 10.1073/pnas.1208114109.

[34] C. Jopling, E. Sleep, M. Raya, M. Martí, A. Raya, and J. C. Izpisúa Belmonte, "Zebrafish heart regeneration occurs by cardiomyocyte dedifferentiation and proliferation," (in eng), *Nature,* vol. 464, no. 7288, pp. 606-9, Mar 25 2010, doi: 10.1038/nature08899.

[35] E. Tzahor and K. D. Poss, "Cardiac regeneration strategies: Staying young at heart," (in eng), *Science,* vol. 356, no. 6342, pp. 1035-1039, Jun 9 2017, doi: 10.1126/science.aam5894.

[36] B. J. Haubner *et al.*, "Complete cardiac regeneration in a mouse model of myocardial infarction," (in eng), *Aging (Albany NY),* vol. 4, no. 12, pp. 966-77, Dec 2012, doi: 10.18632/aging.100526.

[37] C. Williams, K. P. Quinn, I. Georgakoudi, and L. D. Black, 3rd, "Young developmental age cardiac extracellular matrix promotes the expansion of neonatal cardiomyocytes in

vitro," (in eng), *Acta Biomater,* vol. 10, no. 1, pp. 194-204, Jan 2014, doi: 10.1016/j.actbio.2013.08.037.

[38] Z. Wang, D. W. Long, Y. Huang, W. C. W. Chen, K. Kim, and Y. Wang, "Decellularized neonatal cardiac extracellular matrix prevents widespread ventricular remodeling in adult mammals after myocardial infarction," (in eng), *Acta Biomater,* vol. 87, pp. 140-151, Mar 15 2019, doi: 10.1016/j.actbio.2019.01.062.

[39] Y. Eitan, U. Sarig, N. Dahan, and M. Machluf, "Acellular cardiac extracellular matrix as a scaffold for tissue engineering: in vitro cell support, remodeling, and biocompatibility," (in eng), *Tissue Eng Part C Methods,* vol. 16, no. 4, pp. 671-83, Aug 2010, doi: 10.1089/ten.TEC.2009.0111.

[40] J. M. Muncie and V. M. Weaver, "The Physical and Biochemical Properties of the Extracellular Matrix Regulate Cell Fate," (in eng), *Current topics in developmental biology,* vol. 130, pp. 1-37, 2018, doi: 10.1016/bs.ctdb.2018.02.002.

[41] H. C. Ott *et al.*, "Perfusion-decellularized matrix: using nature's platform to engineer a bioartificial heart," (in eng), *Nat Med,* vol. 14, no. 2, pp. 213-21, Feb 2008, doi: 10.1038/nm1684.

[42] A. J. Engler, S. Sen, H. L. Sweeney, and D. E. Discher, "Matrix elasticity directs stem cell lineage specification," (in eng), *Cell,* vol. 126, no. 4, pp. 677-89, Aug 25 2006, doi: 10.1016/j.cell.2006.06.044.

[43] F. Ahmad *et al.*, "Biomechanical properties and microstructure of neonatal porcine ventricles," (in eng), *J Mech Behav Biomed Mater,* vol. 88, pp. 18-28, Dec 2018, doi: 10.1016/j.jmbbm.2018.07.038.

[44] N. Bhardwaj and S. C. Kundu, "Electrospinning: a fascinating fiber fabrication technique," (in eng), *Biotechnol Adv,* vol. 28, no. 3, pp. 325-47, May-Jun 2010, doi: 10.1016/j.biotechadv.2010.01.004.

[45] R. Arumugam, E. S. Srinadhu, B. Subramanian, and S. Nallani, "β-PVDF based electrospun nanofibers – A promising material for developing cardiac patches," *Medical Hypotheses,* vol. 122, pp. 31-34, 2019/01/01/ 2019, doi: https://doi.org/10.1016/j.mehy.2018.10.005.

[46] B. Schoen *et al.*, "Electrospun Extracellular Matrix: Paving the Way to Tailor-Made Natural Scaffolds for Cardiac Tissue Regeneration," *Advanced Functional Materials,* vol. 27, no. 34, p. 1700427, 2017, doi: https://doi.org/10.1002/adfm.201700427.

[47] M. Kitsara, O. Agbulut, D. Kontziampasis, Y. Chen, and P. Menasché, "Fibers for hearts: A critical review on electrospinning for cardiac tissue engineering," (in eng), *Acta Biomater,* vol. 48, pp. 20-40, Jan 15 2017, doi: 10.1016/j.actbio.2016.11.014.

[48] X. Yan, M. Yu, S. Ramakrishna, S. J. Russell, and Y. Z. Long, "Advances in portable electrospinning devices for in situ delivery of personalized wound care," (in eng), *Nanoscale,* vol. 11, no. 41, pp. 19166-19178, Oct 25 2019, doi: 10.1039/c9nr02802a.

[49] S. Heydarkhan-Hagvall *et al.*, "Three-dimensional electrospun ECM-based hybrid scaffolds for cardiovascular tissue engineering," (in eng), *Biomaterials,* vol. 29, no. 19, pp. 2907-14, Jul 2008, doi: 10.1016/j.biomaterials.2008.03.034.

[50] B. Peña *et al.*, "Injectable Hydrogels for Cardiac Tissue Engineering," (in eng), *Macromol Biosci,* vol. 18, no. 6, p. e1800079, Jun 2018, doi: 10.1002/mabi.201800079.

[51] J. M. Singelyn, J. A. DeQuach, S. B. Seif-Naraghi, R. B. Littlefield, P. J. Schup-Magoffin, and K. L. Christman, "Naturally derived myocardial matrix as an injectable scaffold for cardiac tissue engineering," (in eng), *Biomaterials,* vol. 30, no. 29, pp. 5409-16, Oct 2009, doi: 10.1016/j.biomaterials.2009.06.045.

[52] A. M. Rosales and K. S. Anseth, "The design of reversible hydrogels to capture extracellular matrix dynamics," (in eng), *Nat Rev Mater,* vol. 1, 2016, doi: 10.1038/natrevmats.2015.12.

[53] Y. Zhang, W. Fan, K. Wang, H. Wei, R. Zhang, and Y. Wu, "Novel preparation of Au nanoparticles loaded Laponite nanoparticles/ECM injectable hydrogel on cardiac differentiation of resident cardiac stem cells to cardiomyocytes," (in eng), *J Photochem Photobiol B,* vol. 192, pp. 49-54, Mar 2019, doi: 10.1016/j.jphotobiol.2018.12.022.

[54] K. Huang *et al.*, "An off-the-shelf artificial cardiac patch improves cardiac repair after myocardial infarction in rats and pigs," (in eng), *Sci Transl Med,* vol. 12, no. 538, Apr 8 2020, doi: 10.1126/scitranslmed.aat9683.

[55] N. Li *et al.*, "Stem cells cardiac patch from decellularized umbilical artery improved heart function after myocardium infarction," (in eng), *Biomed Mater Eng,* vol. 28, no. s1, pp. S87-s94, 2017, doi: 10.3233/bme-171628.

[56] T. Hao *et al.*, "Injectable Fullerenol/Alginate Hydrogel for Suppression of Oxidative Stress Damage in Brown Adipose-Derived Stem Cells and Cardiac Repair," (in eng), *ACS Nano,* vol. 11, no. 6, pp. 5474-5488, Jun 27 2017, doi: 10.1021/acsnano.7b00221.

[57] K. M. French *et al.*, "A naturally derived cardiac extracellular matrix enhances cardiac progenitor cell behavior in vitro," (in eng), *Acta Biomater,* vol. 8, no. 12, pp. 4357-64, Dec 2012, doi: 10.1016/j.actbio.2012.07.033.

[58] S. Uriel *et al.*, "Extraction and assembly of tissue-derived gels for cell culture and tissue engineering," (in eng), *Tissue Eng Part C Methods,* vol. 15, no. 3, pp. 309-21, Sep 2009, doi: 10.1089/ten.tec.2008.0309.

[59] J. M. Singelyn *et al.*, "Catheter-deliverable hydrogel derived from decellularized ventricular extracellular matrix increases endogenous cardiomyocytes and preserves cardiac function post-myocardial infarction," (in eng), *J Am Coll Cardiol,* vol. 59, no. 8, pp. 751-63, Feb 21 2012, doi: 10.1016/j.jacc.2011.10.888.

[60] Y. Duan, Z. Liu, J. O'Neill, L. Q. Wan, D. O. Freytes, and G. Vunjak-Novakovic, "Hybrid gel composed of native heart matrix and collagen induces cardiac differentiation of human embryonic stem cells without supplemental growth factors," (in eng), *J*

Cardiovasc Transl Res, vol. 4, no. 5, pp. 605-15, Oct 2011, doi: 10.1007/s12265-011-9304-0.

[61] R. W. Farndale, D. J. Buttle, and A. J. Barrett, "Improved quantitation and discrimination of sulphated glycosaminoglycans by use of dimethylmethylene blue," (in eng), *Biochim Biophys Acta,* vol. 883, no. 2, pp. 173-7, Sep 4 1986, doi: 10.1016/0304-4165(86)90306-5.

[62] B. Wang *et al.*, "Structural and biomechanical characterizations of porcine myocardial extracellular matrix," (in eng), *J Mater Sci Mater Med,* vol. 23, no. 8, pp. 1835-47, Aug 2012, doi: 10.1007/s10856-012-4660-0.

[63] J. S. Wendel, L. Ye, P. Zhang, R. T. Tranquillo, and J. J. Zhang, "Functional consequences of a tissue-engineered myocardial patch for cardiac repair in a rat infarct model," (in eng), *Tissue Eng Part A,* vol. 20, no. 7-8, pp. 1325-35, Apr 2014, doi: 10.1089/ten.TEA.2013.0312.

[64] U. Sarig *et al.*, "Natural myocardial ECM patch drives cardiac progenitor based restoration even after scarring," (in eng), *Acta Biomater,* vol. 44, pp. 209-20, Oct 15 2016, doi: 10.1016/j.actbio.2016.08.031.

[65] Z. Mosala Nezhad *et al.*, "CorMatrix valved conduit in a porcine model: long-term remodelling and biomechanical characterization†," *Interactive CardioVascular and Thoracic Surgery,* vol. 24, no. 1, pp. 90-98, 2016, doi: 10.1093/icvts/ivw314.

[66] V. Sood, A. Heider, R. Rabah, M. S. Si, and R. G. Ohye, "Evaluation of Explanted CorMatrix TYKE Extracardiac Patches in Infants with Congenital Heart Disease," (in eng), *Ann Thorac Surg,* Oct 21 2020, doi: 10.1016/j.athoracsur.2020.06.151.

[67] A. H. Zaidi *et al.*, "Preliminary experience with porcine intestinal submucosa (CorMatrix) for valve reconstruction in congenital heart disease: histologic evaluation of explanted valves," *The Journal of thoracic and cardiovascular surgery,* vol. 148, no. 5, pp. 2216-2225. e1, 2014. [Online]. Available: https://www.jtcvs.org/article/S0022-5223(14)00289-X/pdf.

[68] A. K. Gaharwar, M. Nikkhah, S. Sant, and A. Khademhosseini, "Anisotropic poly (glycerol sebacate)-poly (ϵ-caprolactone) electrospun fibers promote endothelial cell guidance," (in eng), *Biofabrication,* vol. 7, no. 1, p. 015001, Dec 17 2014, doi: 10.1088/1758-5090/7/1/015001.

[69] N. Kumar *et al.*, "Scalable Biomimetic Coaxial Aligned Nanofiber Cardiac Patch: A Potential Model for "Clinical Trials in a Dish"," (in eng), *Front Bioeng Biotechnol,* vol. 8, p. 567842, 2020, doi: 10.3389/fbioe.2020.567842.

[70] G. Zhao, X. Zhang, T. J. Lu, and F. Xu, "Recent Advances in Electrospun Nanofibrous Scaffolds for Cardiac Tissue Engineering," *Advanced Functional Materials,* vol. 25, no. 36, pp. 5726-5738, 2015, doi: https://doi.org/10.1002/adfm.201502142.

[71] S. Roy *et al.*, "A novel approach for fabricating highly tunable and fluffy bioinspired 3D poly(vinyl alcohol) (PVA) fiber scaffolds," (in eng), *Nanoscale,* vol. 9, no. 21, pp. 7081-7093, Jun 1 2017, doi: 10.1039/c7nr00503b.

[72] C. P. Barnes, C. W. Pemble, D. D. Brand, D. G. Simpson, and G. L. Bowlin, "Cross-linking electrospun type II collagen tissue engineering scaffolds with carbodiimide in ethanol," (in eng), *Tissue Eng,* vol. 13, no. 7, pp. 1593-605, Jul 2007, doi: 10.1089/ten.2006.0292.

[73] M. Mekhail, K. K. H. Wong, D. T. Padavan, Y. Wu, D. B. O'Gorman, and W. Wan, "Genipin-Cross-linked Electrospun Collagen Fibers," *Journal of Biomaterials Science, Polymer Edition,* vol. 22, no. 17, pp. 2241-2259, 2011/01/01 2011, doi: 10.1163/092050610X538209.

[74] A. R. Sadeghi-Avalshahr, M. Khorsand-Ghayeni, S. Nokhasteh, A. M. Molavi, and H. Naderi-Meshkin, "Synthesis and characterization of PLGA/collagen composite scaffolds as skin substitute produced by electrospinning through two different approaches," (in eng), *J Mater Sci Mater Med,* vol. 28, no. 1, p. 14, Jan 2017, doi: 10.1007/s10856-016-5789-z.

[75] Y. Dror, T. Ziv, V. Makarov, H. Wolf, A. Admon, and E. Zussman, "Nanofibers made of globular proteins," (in eng), *Biomacromolecules,* vol. 9, no. 10, pp. 2749-54, Oct 2008, doi: 10.1021/bm8005243.

[76] B. M. Young *et al.*, "Electrospun decellularized lung matrix scaffold for airway smooth muscle culture," *ACS Biomaterials Science & Engineering,* vol. 3, no. 12, pp. 3480-3492, 2017.

[77] C. Yang, "Enhanced physicochemical properties of collagen by using EDC/NHS-crosslinking," *Bulletin of Materials Science,* vol. 35, no. 5, pp. 913-918, 2012/10/01 2012, doi: 10.1007/s12034-012-0376-5.

[78] K. Výborný *et al.*, "Genipin and EDC crosslinking of extracellular matrix hydrogel derived from human umbilical cord for neural tissue repair," (in eng), *Sci Rep,* vol. 9, no. 1, p. 10674, Jul 23 2019, doi: 10.1038/s41598-019-47059-x.

[79] S. Akhshabi, E. Biazar, V. Singh, S. H. Keshel, and N. Geetha, "The effect of the carbodiimide cross-linker on the structural and biocompatibility properties of collagen-chondroitin sulfate electrospun mat," (in eng), *Int J Nanomedicine,* vol. 13, pp. 4405-4416, 2018, doi: 10.2147/ijn.S165739.

[80] C. E. Campiglio, S. Ponzini, P. De Stefano, G. Ortoleva, L. Vignati, and L. Draghi, "Cross-Linking Optimization for Electrospun Gelatin: Challenge of Preserving Fiber Topography," (in eng), *Polymers (Basel),* vol. 12, no. 11, Oct 25 2020, doi: 10.3390/polym12112472.

[81] K. E. Park, S. Y. Jung, S. J. Lee, B. M. Min, and W. H. Park, "Biomimetic nanofibrous scaffolds: preparation and characterization of chitin/silk fibroin blend nanofibers," (in eng), *Int J Biol Macromol,* vol. 38, no. 3-5, pp. 165-73, May 30 2006, doi: 10.1016/j.ijbiomac.2006.03.003.

[82] K. S. Rho *et al.*, "Electrospinning of collagen nanofibers: effects on the behavior of normal human keratinocytes and early-stage wound healing," (in eng), *Biomaterials,* vol. 27, no. 8, pp. 1452-61, Mar 2006, doi: 10.1016/j.biomaterials.2005.08.004.

[83] X. Luo *et al.*, "Study on structure, mechanical property and cell cytocompatibility of electrospun collagen nanofibers crosslinked by common agents," (in eng), *Int J Biol Macromol,* vol. 113, pp. 476-486, Jul 1 2018, doi: 10.1016/j.ijbiomac.2018.01.179.

[84] F. Yang, C. Xu, M. Kotaki, S. Wang, and S. Ramakrishna, "Characterization of neural stem cells on electrospun poly (L-lactic acid) nanofibrous scaffold," *Journal of Biomaterials Science, Polymer Edition,* vol. 15, no. 12, pp. 1483-1497, 2004.

[85] E. Hoveizi, M. Nabiuni, K. Parivar, S. Rajabi-Zeleti, and S. Tavakol, "Functionalisation and surface modification of electrospun polylactic acid scaffold for tissue engineering," (in eng), *Cell Biol Int,* vol. 38, no. 1, pp. 41-9, Jan 2014, doi: 10.1002/cbin.10178.

[86] W. C. Claycomb *et al.*, "HL-1 cells: a cardiac muscle cell line that contracts and retains phenotypic characteristics of the adult cardiomyocyte," (in eng), *Proc Natl Acad Sci U S A,* vol. 95, no. 6, pp. 2979-84, Mar 17 1998, doi: 10.1073/pnas.95.6.2979.

[87] T. Riaz *et al.*, "FTIR analysis of natural and synthetic collagen," *Applied Spectroscopy Reviews,* vol. 53, no. 9, pp. 703-746, 2018/10/21 2018, doi: 10.1080/05704928.2018.1426595.

[88] I. Tzoumani *et al.*, "Modification of Collagen Derivatives with Water-Soluble Polymers for the Development of Cross-Linked Hydrogels for Controlled Release," (in eng), *Materials (Basel),* vol. 12, no. 24, Dec 6 2019, doi: 10.3390/ma12244067.

[89] L. L. Fernandes, C. X. Resende, D. S. Tavares, G. A. Soares, L. O. Castro, and J. M. Granjeiro, "Cytocompatibility of chitosan and collagen-chitosan scaffolds for tissue engineering," *Polímeros,* vol. 21, pp. 1-6, 2011. [Online]. Available: http://www.scielo.br/scielo.php?script=sci_arttext&pid=S0104-14282011000100003&nrm=iso.

[90] B. de Campos Vidal and M. L. S. Mello, "Collagen type I amide I band infrared spectroscopy," *Micron,* vol. 42, no. 3, pp. 283-289, 2011/04/01/ 2011, doi: https://doi.org/10.1016/j.micron.2010.09.010.

[91] A. Sionkowska, M. Wisniewski, J. Skopinska, C. J. Kennedy, and T. J. Wess, "Molecular interactions in collagen and chitosan blends," (in eng), *Biomaterials,* vol. 25, no. 5, pp. 795-801, Feb 2004, doi: 10.1016/s0142-9612(03)00595-7.

[92] M. Jackson, L. P. Choo, P. H. Watson, W. C. Halliday, and H. H. Mantsch, "Beware of connective tissue proteins: assignment and implications of collagen absorptions in infrared spectra of human tissues," (in eng), *Biochim Biophys Acta,* vol. 1270, no. 1, pp. 1-6, Jan 25 1995, doi: 10.1016/0925-4439(94)00056-v.

[93] O. S. Rabotyagova, P. Cebe, and D. L. Kaplan, "Collagen Structural Hierarchy and Susceptibility to Degradation by Ultraviolet Radiation," (in eng), *Materials science &*

engineering. C, Materials for biological applications, vol. 28, no. 8, pp. 1420-1429, 2008, doi: 10.1016/j.msec.2008.03.012.

[94] Z. S. S. Júnior *et al.*, "Effect of papain-based gel on type I collagen - spectroscopy applied for microstructural analysis," *Scientific Reports,* vol. 5, no. 1, p. 11448, 2015/06/23 2015, doi: 10.1038/srep11448.

[95] S. Göktepe, O. J. Abilez, K. K. Parker, and E. Kuhl, "A multiscale model for eccentric and concentric cardiac growth through sarcomerogenesis," (in eng), *J Theor Biol,* vol. 265, no. 3, pp. 433-42, Aug 7 2010, doi: 10.1016/j.jtbi.2010.04.023.

[96] T. Hoshino, H. Fujiwara, C. Kawai, and Y. Hamashima, "Myocardial fiber diameter and regional distribution in the ventricular wall of normal adult hearts, hypertensive hearts and hearts with hypertrophic cardiomyopathy," (in eng), *Circulation,* vol. 67, no. 5, pp. 1109-16, May 1983, doi: 10.1161/01.cir.67.5.1109.

[97] C. R. Gazoti Debessa, L. B. Mesiano Maifrino, and R. Rodrigues de Souza, "Age related changes of the collagen network of the human heart," *Mechanisms of Ageing and Development,* vol. 122, no. 10, pp. 1049-1058, 2001/07/31/ 2001, doi: https://doi.org/10.1016/S0047-6374(01)00238-X.

[98] T. Borg and J. Caulfield, "The collagen matrix of the heart," in *Federation proceedings*, 1981, vol. 40, no. 7, pp. 2037-2041.

[99] S. M. Weis, J. L. Emery, K. D. Becker, D. J. McBride, Jr., J. H. Omens, and A. D. McCulloch, "Myocardial mechanics and collagen structure in the osteogenesis imperfecta murine (oim)," (in eng), *Circ Res,* vol. 87, no. 8, pp. 663-9, Oct 13 2000, doi: 10.1161/01.res.87.8.663.

[100] T. J. Keane *et al.*, "Preparation and characterization of a biologic scaffold and hydrogel derived from colonic mucosa," (in eng), *J Biomed Mater Res B Appl Biomater,* vol. 105, no. 2, pp. 291-306, Feb 2017, doi: 10.1002/jbm.b.33556.

[101] J. Wu *et al.*, "An injectable extracellular matrix derived hydrogel for meniscus repair and regeneration," (in eng), *Acta Biomater,* vol. 16, pp. 49-59, Apr 2015, doi: 10.1016/j.actbio.2015.01.027.

[102] M. Norouzi, B. Nazari, and D. W. Miller, "Injectable hydrogel-based drug delivery systems for local cancer therapy," (in eng), *Drug Discov Today,* vol. 21, no. 11, pp. 1835-1849, Nov 2016, doi: 10.1016/j.drudis.2016.07.006.

[103] S. Datta *et al.*, "Decellularized bone matrix/oleoyl chitosan derived supramolecular injectable hydrogel promotes efficient bone integration," (in eng), *Mater Sci Eng C Mater Biol Appl,* vol. 119, p. 111604, Feb 2021, doi: 10.1016/j.msec.2020.111604.

[104] Y. Zhao *et al.*, "An Injectable Strong Hydrogel for Bone Reconstruction," (in eng), *Adv Healthc Mater,* vol. 8, no. 17, p. e1900709, Sep 2019, doi: 10.1002/adhm.201900709.

[105] M. E. Jeffords, J. Wu, M. Shah, Y. Hong, and G. Zhang, "Tailoring material properties of cardiac matrix hydrogels to induce endothelial differentiation of human mesenchymal

stem cells," (in eng), *ACS Appl Mater Interfaces,* vol. 7, no. 20, pp. 11053-61, May 27 2015, doi: 10.1021/acsami.5b03195.

[106] D. O. Freytes, J. Martin, S. S. Velankar, A. S. Lee, and S. F. Badylak, "Preparation and rheological characterization of a gel form of the porcine urinary bladder matrix," (in eng), *Biomaterials,* vol. 29, no. 11, pp. 1630-7, Apr 2008, doi: 10.1016/j.biomaterials.2007.12.014.

[107] M. Baghalishahi, S. H. Efthekhar-Vaghefi, A. Piryaei, S. N. Nematolahi-Mahani, H. R. Mollaei, and Y. Sadeghi, "Cardiac extracellular matrix hydrogel together with or without inducer cocktail improves human adipose tissue-derived stem cells differentiation into cardiomyocyte-like cells," (in eng), *Biochem Biophys Res Commun,* vol. 502, no. 2, pp. 215-225, Jul 12 2018, doi: 10.1016/j.bbrc.2018.05.147.

[108] S. Ramadan, N. Paul, and H. E. Naguib, "Standardized static and dynamic evaluation of myocardial tissue properties," (in eng), *Biomed Mater,* vol. 12, no. 2, p. 025013, Mar 20 2017, doi: 10.1088/1748-605X/aa57a5.

[109] G. N. Grover, N. Rao, and K. L. Christman, "Myocardial matrix-polyethylene glycol hybrid hydrogels for tissue engineering," (in eng), *Nanotechnology,* vol. 25, no. 1, p. 014011, Jan 10 2014, doi: 10.1088/0957-4484/25/1/014011.

[110] T. D. Johnson, S. Y. Lin, and K. L. Christman, "Tailoring material properties of a nanofibrous extracellular matrix derived hydrogel," (in eng), *Nanotechnology,* vol. 22, no. 49, p. 494015, Dec 9 2011, doi: 10.1088/0957-4484/22/49/494015.

[111] M. T. Wolf *et al.*, "A hydrogel derived from decellularized dermal extracellular matrix," (in eng), *Biomaterials,* vol. 33, no. 29, pp. 7028-38, Oct 2012, doi: 10.1016/j.biomaterials.2012.06.051.

[112] P. Nezhad-Mokhtari, M. Akrami-Hasan-Kohal, and M. Ghorbani, "An injectable chitosan-based hydrogel scaffold containing gold nanoparticles for tissue engineering applications," (in eng), *Int J Biol Macromol,* vol. 154, pp. 198-205, Jul 1 2020, doi: 10.1016/j.ijbiomac.2020.03.112.